NOAA Technical Report NOS OES 005

TAMPA BAY OCEANOGRAPHY PROJECT: DEVELOPMENT AND APPLICATION OF THE NUMERICAL CIRCULATION MODEL

Silver Spring, Maryland
August 1994

noaa National Oceanic and Atmospheric Administration

U.S. DEPARTMENT OF COMMERCE
National Ocean Service
Office of Ocean and Earth Sciences
Marine Analysis and Interpretation Division
Coastal and Estuarine Oceanography Branch

NOAA Technical Report NOS OES 005

TAMPA BAY OCEANOGRAPHY PROJECT: DEVELOPMENT AND APPLICATION OF THE NUMERICAL CIRCULATION MODEL

Kurt W. Hess
August 1994

noaa National Oceanic and Atmospheric Administration

U.S. DEPARTMENT OF COMMERCE
Ronald H. Brown, Secretary

National Oceanic and Atmospheric Administration
D. James Baker, Under Secretary

National Ocean Service
W. Stanley Wilson
Assistant Administrator

Office of Ocean and Earth Sciences
Melbourne G. Briscoe

Marine Analysis and Interpretation Division

Coastal and Estuarine Oceanography Branch
Bruce Parker

NOTICE

Mention of a commercial company or product does not constitute an endorsement by NOAA. Use for publicity or advertising purposes of information from this publication concerning proprietary products or the tests of such products is not authorized.

TABLE OF CONTENTS

LIST OF FIGURES

LIST OF TABLES

LIST OF ACRONYMS AND ABBREVIATIONS

ADCP	Acoustic Doppler Current Profiler
ASCII	American Standard Code for Information Interchange
BASIS	Bay Area Scientific Information Symposium
CEOB	Coastal and Estuarine Oceanography Branch
cfs	Cubic Feet per Second
cpd	cycles per day
CT	Conductivity-Temperature
CTD	Conductivity-Temperature-Depth
DOI	Department of the Interior
FL	Florida
HP	Hewlett-Packard
HCEPC	Hillsborough County Environmental Protection Commission
LORAN	Long Range Navigation
NCDC	National Climatic Data Center
NOAA	National Oceanic and Atmospheric Administration
NODC	National Oceanographic Data Center
NOS	National Ocean Service
MAID	Marine Analysis and Interpretation Division
MEC	Maximum Ebb Current
MFC	Maximum Flood Current
MLLW	Mean Lower Low Water
MSL	Mean Sea Level
OES	Office of Ocean and Earth Sciences
OLLD	Ocean and Lake Levels Division
PORTS	Physical Oceanographic Real-Time System
ppt	part per thousand
psu	practical salinity unit
rms	root mean square
QA	Quality Assurance
QC	Quality Control
SSB	Sunshine Skyway Bridge
SBE	Slack Before Ebb
SBF	Slack Before Flood
SWFWMD	Southwest Florida Water Management District
TOP	Tampa Bay Oceanography Project
TPA	Tampa International Airport
USCG	United States Coast Guard
USGS	United States Geological Survey
UT	Universal Time

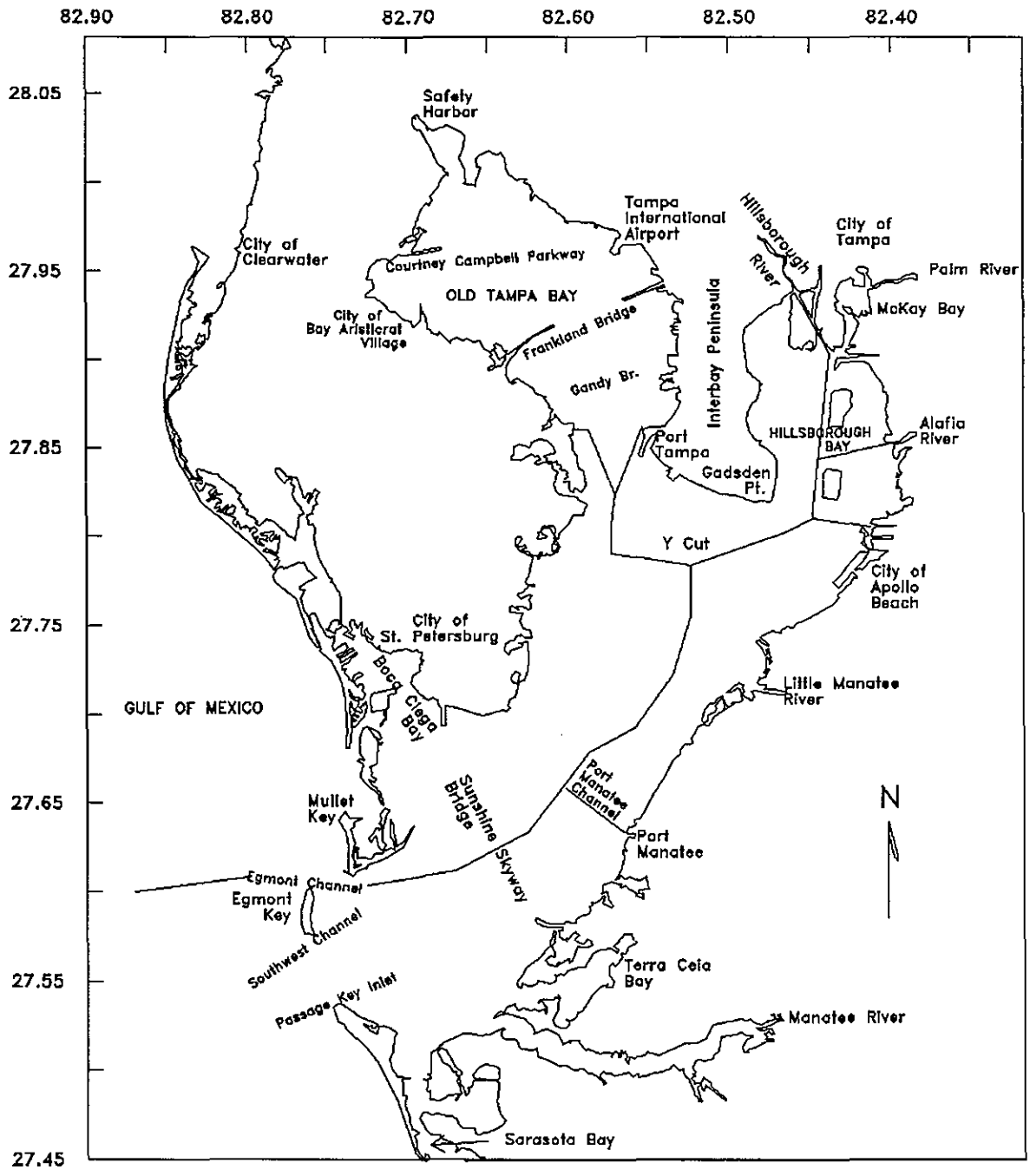

Tampa Bay area base map showing locations mentioned in this report.

ABSTRACT

The National Ocean Service, as part of the Tampa Bay Oceanography Project, has developed a three-dimensional circulation model for the Bay and has used an extensive observational data set (including water level, current, salinity, and temperature) for model calibration and validation. The model is based on the Princeton University ocean model code and has a sigma coordinate with seven levels in the vertical and orthogonal curvilinear coordinates in the horizontal with 1200 water cells. The model equations are listed and the grid is described. The model code has been modified to include a flooding and drying algorithm and a detailed atmospheric heat flux formulation.

Modeled and observed water levels and currents have been compared to give an objective assessment of model performance during calibration, and to compare calibration run output to validation run output. Statistics for comparing water levels and currents are introduced, including root mean squared (rms) differences between time series values, mean tidal extrema ratios and mean time lags, and rms differences in times and amplitudes of tidal extrema. Methods for combining results from many stations are discussed, and objective parameters were defined to assess model skill. Water level phases were found to be quite sensitive to total water depths. For the Tampa Bay model, rms hourly water level differences are 3.5 cm, and tidal rms extrema differences are 4.9 cm and 25 min. For currents, rms 10-minute differences are 10.1 cm/s and rms extrema differences are 13.2 cm/s and 37 min.

The model was assessed for skill in simulating salinities and temperatures; rms differences between hourly observations and modeled values over approximately a 7-month period (averaged for 12 stations) were 1.10 psu and 0.88°C, respectively. Mean differences for the same period were 0.46 psu and 0.35°C. Salinities were sensitive to uncertainties in freshwater inflow and temperatures were sensitive to the bulk heat transfer coefficient.

The development of the tidal current atlas is discussed. Mixed tides are accounted for by dividing currents into three categories: semidiurnal flood, semidiurnal ebb, and diurnal flood. Mean currents in these categories then form a set of basis currents. Hourly currents are predicted by adjusting the basis currents in the atlas for the time and speed of current at the Sunshine Skyway Bridge from daily predictions in the NOS tidal current tables. Computer simulation of the atlas based on this approach indicated that a mean error of 11.9 cm/s would occur when comparing atlas-predicted currents to those observed.

1. INTRODUCTION

1.1. THE TAMPA BAY OCEANOGRAPHY PROJECT

The National Oceanic and Atmospheric Administration's (NOAA's) National Ocean Service (NOS) has nearly completed the Tampa Bay Oceanography Project (TOP). The project plan (NOS, 1990) and annual progress reports (Hess, 1990 and 1992) contain important details of TOP. The Project consists of three major components:

- an intensive, 15-month survey of currents, water levels, water temperature, salinity, and winds in Tampa Bay, Florida;
- installation of the nation's first fully integrated Physical Oceanographic Real-Time System (PORTS), including information on currents, water levels, and winds critical for safe navigation; and
- development and application of a three-dimensional circulation model.

The circulation survey was designed to gather oceanographic data sufficient to gain insight to the dynamical processes of the Bay, to update the tide and current tables, and to calibrate and validate the numerical circulation model. The survey began in early June 1990, and included 42 fixed current meter stations, 16 water level stations, five meteorological instrument stations, and three moored conductivity-temperature arrays. Except for the real-time system, all instruments were removed by mid-September 1991. Details of the survey are described in the Circulation Survey Report (Nowadly, 1992) and results of the data analysis were published in the Physical Oceanographic Synthesis Report (Zervas, 1993). An overview of the data collection program appears in Appendix A.

The installation of the Nation's first fully-integrated PORTS began in Tampa Bay with a prototype in September 1990. During the course of the TOP survey, PORTS was developed and became fully operational in October 1991, with information available both as a single-call, voice-response telephone message and as either a text message or a data file via modem. This system, which is now in continuous operation, was the first of its kind in the world (Frey, 1991; Appell et al., 1991; Bethem and Frey, 1991; Nichols, 1993). PORTS consists of ADCP current meters located at the Sunshine Skyway and the mouth of Old Tampa Bay, a meteorological station located near Cut B and Manatee Channel, and water level and wind sensors located at Port Tampa, St. Petersburg, Port Manatee, and the McKay Bay entrance (see the base map on page vi for locations). Data available in real time from the PORTS include currents at all ADCP locations, winds and water levels from the corresponding sensors, and a nowcast of currents at the intersection of the navigation channel and the Port Manatee Channel (Williams et al., 1993). Ongoing maintenance and operation of the PORTS is made possible through a cooperative agreement with the Greater Tampa Bay Marine Advisory Council.

The third component of TOP is the development and application of the numerical circulation model, and is discussed in detail in the following Section. The model has been used for interpretation of observational data (Zervas, 1993) and is intended to be used to produce the tide and current atlas (see Section 6).

1.2. THE NUMERICAL CIRCULATION MODEL

A version of the Princeton three-dimensional numerical circulation model (Blumberg and Mellor, 1987; Mellor, 1993) has been applied to the Bay to understand the local oceanography, to study the tides and currents throughout the Bay, and to develop the tide and tidal current forecast atlas. The Princeton model has been under development and refinement for nearly 10 years and has been widely applied to many estuarine and coastal regions, so it has become a standard tool in the oceanographic research community. Unlike other codes, this one is freely available to the public and has therefore benefitted from examination by a variety of users. The model uses a terrain-following vertical sigma coordinate and orthogonal curvilinear coordinates in the horizontal to depict currents, salinities, and temperatures over depth and at numerous locations throughout the Bay.

The model is a powerful tool for understanding the Bay's dynamics. The model can be used to perform experiments that isolate the Bay's response to specific forcing (tides, winds, or buoyancy) or to characterize regions (high velocities, large phase lags). It can be used to estimate the Bay's natural period. The model will provide a theoretical basis for unifying data from short-term observational programs and the conceptual knowledge of the important physical processes in the Bay. It can also assist in designing future observational networks. Finally, the model (when validated) could assist estuarine management by providing circulation data for water quality models.

A numerical circulation model of the Bay can improve navigational safety in several ways. It can interpolate tidal water level response characteristics between shoreline gages and throughout the Bay, including the navigation channels, to enhance the spatial coverage of predictions. Model results will be used to construct a current and water level forecast atlas and to provide additional information to help correlate modeled currents to those observed by the PORTS.

The circulation model can fulfill its promise only after it has been validated against observational data. No specific standards for accuracy for modeling presently exist, but prediction standards have been developed and these will serve as a benchmark for the model. The model will first undergo sensitivity testing to determine the model's response under a variety of forcing. Then, calibration is carried out by altering certain inputs to obtain optimum model performance. Finally, a validation procedure will compare the model's computed values to data to gage accuracy.

1.3. OCEANOGRAPHIC CHARACTERIZATION OF TAMPA BAY

Tampa Bay, located on the west coast of Florida, is the largest estuary in that state. The y-shaped Bay extends 39 kilometers from the mouth at Egmont Key to the southern tip of the Interbay Peninsula, where 13-kilometer-long Hillsborough Bay meets 26-kilometer-long Old Tampa Bay. The surface area of the Bay is about 1,031 square kilometers (Clark and MacAuley, 1989) and the mean depth is 4 meters, although the main Bay shipping channel is dredged to a nominal 13 to 14 meters.

Tampa Bay is subject to the tides of the adjacent Gulf of Mexico, which are mixed diurnal and semidiurnal. Mean ranges throughout the Bay are typically on the order of 0.7 meters. The phase lag is approximately 2.7 hours from the entrance to upper Hillsborough Bay and 4 hours from the Gulf to upper Old Tampa Bay, due to the shallowness of the estuary. Because the tides are mixed, the diurnal inequality, or difference between successive highs or lows, is likely to be large. Following Defant (1958), the ratio

$$r = \frac{K_1 + O_1}{M_2 + S_2} = 1.42 \tag{1.1}$$

at St. Petersburg indicates that the tide is mixed but strongly semidiurnal. The inequality between successive ebb currents can be so large that at the times of maximum lunar declination the second ebb can disappear completely. The presence of mixed tides will make the development of the tidal atlas more difficult, because present tidal current charts apply only for tides that are predominantly semidiurnal. Monthly variations in the tide are coupled to both the moon's declinational cycle (tropic tides) and the perigee-apogee cycle (spring-neap tides). A standard least-squares harmonic analysis (Zetler, 1982) of year-long tidal records that yields amplitudes of 37 constituents at St. Petersburg indicates that the shallow water tides and the overtides are relatively small.

Strong meteorological forcing can significantly affect daily currents and water level variations in Tampa Bay due to the Bay's shallowness and the small astronomical tidal range. Extreme wind and storm surge conditions have occurred during the passage of hurricanes. Strong winds are likely to be associated with summertime localized thunderstorms and with wintertime frontal passages, and moderate winds will occur during daily landbreeze-seabreeze situations.

The Bay's climate is subtropical, with rainfall the heaviest during summer months of frequent convective thunderstorm activity (Flannery, 1989). During the late winter, cold fronts moving down the Florida peninsula bring less frequent but longer duration rain showers. Due to the limited drainage area, mean annual freshwater inflow (from gaged rivers) is small, averaging only 35 m^3/s. Peak flow in the annual cycle occurs in August-September, with a secondary peak in February-March. Since freshwater inflow is small, salinity stratification is weak, although there can be large horizontal density gradients in the upper Bay due to the presence of several rivers concentrated on the eastern shore of the Bay. Therefore, buoyancy-driven currents may be significant.

Oceanographic studies of Tampa Bay have been conducted by NOAA, U.S. Geological Survey (USGS), Department Of Interior (DOI), and local state agencies and universities. The major studies are briefly described here. Dragovich and Sykes (1967) reported on a physical and chemical oceanographic survey of Tampa Bay and the adjacent shelf (out to about 45 nautical miles) carried out from 1958 to 1961 by DOI. They depicted monthly sections of temperature, salinity, density, inorganic phosphorus, total phosphorous, nitrogen, and copper along the occupied transects. The data showed a strong annual cycle in the temperature data but little variation in the salinity.

Dinardi (1978) described an extensive circulation survey of the Bay carried out by the National Ocean Survey (NOS's predecessor) in 1963. These data have been used for the NOAA Tidal Current Tables and the Tidal Current Charts for Tampa Bay. The most recent NOS bathymetric surveys of the Bay occurred in 1957-58.

Goodwin and Michaelis (1976) reported on a water level study carried out by USGS during 1971-1973. During the study period, the maximum tide at St. Petersburg was recorded at 1.5 meters during Hurricane Agnes and the minimum tide was recorded at 0.9 meters below mean sea level.

Boler (1992) described the ongoing data collection program of the Hillsborough County Environmental Protection Commission (HCEPC). Although directed at measuring water quality variables, the HCEPC surveys salinity and temperature on a regular basis, as well as meteorological and river discharge data. The data showed significant lateral variation in the salinity in the upper Bay.

1.4. PREVIOUS MODELING STUDIES OF TAMPA BAY

All of the early simulations of Tampa Bay used two-dimensional, vertically-integrated numerical models. Ross (see Goodwin, 1987, and Spaulding et al., 1988) has carried out several numerical modeling studies of tidal residual circulation and water quality in Tampa Bay. He and his associates used vertically-averaged horizontal momentum equations that ignored horizontal shear stresses and density gradients. The solution technique was determined by Spaulding et al. (1988) to be fully explicit, much like the Reid and Bodine (1968) model. The residual (time-averaged) circulation was determined to be an important component in flushing the Bay.

Goodwin and Ross (1984) made comparisons of tidal amplitudes, residual tidal circulation, and storm surges on Tampa Bay using their respective vertically-averaged numerical models. They estimated changes in circulation likely to occur after the completion of pier protection islands near the New Sunshine Skyway Bridge. While the overall circulation in the Bay was not altered significantly, there were noticeable changes in current vectors near the bridge.

Goodwin (1977, 1980, 1987, 1991) made highly detailed numerical simulation of currents to simulate the effects of dredging to the flushing of the Tampa Bay and Hillsborough Bay. He used a two-dimensional, vertically-integrated, semi-implicit numerical model (Leendertse, 1967) with a grid cell size as small as 500 meters to produce relatively accurate estimates of the tidal currents. Goodwin (1987) achieved an average standard error of 3 centimeters between modeled and observed half-hourly water levels at 11 locations, although only 1.5 days of data were used. He also achieved an average standard error of 3 cm/s for a 40-hour period when comparing currents measured at a distance above the bottom equal to 40 percent of the total water depth and the model's vertically averaged currents. These studies implied the importance of residual circulation, especially in the effects of gyres, in flushing the Bay.

Shaffer et al. (1986) described the National Weather Service's SLOSH storm surge modeling program for the U.S. East and Gulf coasts. Model basins included one developed for Tampa Bay. The vertically-integrated surge model (Jelesnianski et al., 1984) operates on a polar grid that covers the central portion of the southwest Florida coast with a grid cell size of 4 kilometers, and has higher resolution (cell size approximately 1 kilometer) inside the Bay. This model did not, however, simulate astronomical tidal variations.

With the advent of faster computers has come the feasibility of running fully three-dimensional numerical models that overcome the limitations of the early generation of two-dimensional models. Unlike tidal currents, buoyancy- and wind-driven currents vary significantly (and even change direction) with depth, making the vertical variations necessary to completely describe them. In addition, momentum, mass, and pollutant mixing processes depend significantly on density stratification. Finally, a vertically-integrated scheme will alias a three-dimensional flow into a two-dimensional one and will thus distort the distribution of currents.

Galperin et al. (1991) describe initial results from three-dimensional modeling of the bay with the Blumberg and Mellor (1987) model formulation. They found that, for the barotropic case, net currents were about 2-3 cm/s. For the baroclinic case, however, the timed-averaged, two-layered estuarine (buoyancy-driven) circulation was strong and could reach values as large as 10 cm/s. Winds could also have a profound effect on the three-dimensional circulation and hence on the salinity structure. In a following study, Galperin et al. (1992) looked at the system of gyres that are thought to exist and found that the location and number of gyres produced by a model is profoundly different depending on whether a two-dimension barotropic or a three-dimensional baroclinic model is used.

Peene and Sheng (1992) modeled Sarasota and Tampa Bays with the Sheng (1983) model and compared model currents in each estuary with their own and NOS data. Their skill at matching observed water levels was better than for currents. They also modeled the storm surge from tropical storm Marco which passed west of the Florida coast on October 11, 1990; it is difficult to interpret their results because the surge was relatively small (less than 20 cm) and the authors did not subtract out the tidal signal when showing comparisons.

1.5. ORGANIZATION OF THIS REPORT

This report describes the testing and application of the NOS Tampa Bay model. Section 2 lists the circulation model equations in the curvilinear, sigma coordinates and defines the turbulence closure scheme and the generic boundary conditions. The model grid and the bathymetry are discussed, as well as the extension of the model code to account for cell flooding and drying.

Section 3 describes the boundaries on the west Florida shelf and the rivers, explains the mathematical boundary conditions, and details the observational data needed to run the model. Model initialization, which depends on the boundary conditions, is also explained.

Section 4 describes the calibration and validation of the computed water levels and currents. First, the principles of validation are discussed. Then, statistics and skill parameters for comparing time series are developed. Next, the model is calibrated by adjusting the horizontal viscosity and the roughness height. Calibration and validation results are compared using the Chi-squared statistic. Then the model is recalibrated by adjusting depths and the roughness height to match the tidal constituents amplitudes and phases. A final estimate of model accuracy is then made and the results compared to those from other model studies.

In Section 5, the validation of salinity and temperature are discussed, including the effect of increasing river discharge and modifying latent and sensible heat fluxes. Objective comparisons between observed and predicted salinity and temperature are made and the results are compared to those from other model studies.

Section 6 describes experiments performed to develop the proposed atlas, including grouping currents into semidiurnal flood, semidiurnal ebb, and diurnal flood. Objective comparisons between observed and predicted currents are made.

Section 7 lists the major findings and summarizes the entire effort and is followed by the references and acknowledgements.

Appendix A describes the TOP circulation survey and instrument locations, Appendix B gives details of the atmospheric heat exchange, Appendix C shows an example of the model gird file, and Appendix D derives a formula for estimating the rms difference between two tidal series in terms of the constituents. Appendix E summarizes the comparison statistics and the results of the validation run described in Hess and Bosley (1992).

2. MODEL FORMULATION

To meet the Tampa Bay modeling project's goals, the numerical model must be capable of fulfilling the following requirements: simulate tidal, wind, density, and shelf-induced currents in Tampa Bay at small time scales (minutes) for long time periods (up to 12 months); resolve currents in the navigation and port channels, and other locations important for navigation; and meet NOS quality assurance (QA) working standards for accuracy (see Section 4.1). Necessary model characteristics include:

1. velocities, salinities, and temperatures that are three-dimensional and time-dependent;
2. a free-surface;
3. non-linear horizontal advection;
4. horizontal and vertical density gradients;
5. variable grid spacing to resolve narrow channels; and
6. grid configuration allowing representation of thin barriers such as causeways.

Three spatial dimensions are required to simulate the vertical shear produced by bottom and wind stresses and by horizontal density gradients, to resolve horizontal differences between the deep channels and the shallow side embayments, and to represent accurately the significant horizontal and vertical salinity and temperature gradients that were observed by NOS in Tampa Bay during the survey. Resolution of currents over the vertical is a requirement for navigation under strong wind and tidal conditions, and is necessary for accurate modeling of bottom stress. Vertical variations in water density generally occur near freshwater discharge locations, such as river entrances, and in deeper water under conditions of intense heating. Presently-available turbulence theory that provides methods of estimating vertical diffusive momentum and mass fluxes also requires information on the vertical variation of density and horizontal currents.

The Princeton three-dimensional numerical circulation model (Blumberg and Mellor, 1987) was chosen as the formulation best suited to meet the above requirements. This model includes a dimensionless sigma vertical coordinate, a level 2-1/2 turbulence closure representation, and an orthogonal curvilinear horizontal coordinate system. The code is structured to take advantage of high-speed vector processing. Similar models were considered, but were found to be limited in some critical way: the MECCA model (Hess, 1989) is limited to square grid cells and the Sheng model (Sheng and Choi, 1992) has a non-time varying turbulent closure scheme. In addition, because the Princeton model has been publicly available, it has been used by numerous investigators and has undergone constant improvement over the years. Dr. George Mellor, of NOAA's Geophysical Fluid Dynamics Laboratory, has been available for advice.

Occasional problems arising from the use of sigma coordinates have been noted in the literature. Haney (1991) reported that potential errors in the horizontal pressure gradient are alleviated by using uniform sigma intervals, reducing cell spacing in regions of large bottom slopes, subtracting the mean water density from the local density, and using a carefully-selected finite difference expression. At any rate, this potential problem is a concern only where density forcing is the dominant horizontal force; horizontal density forcing is small compared to surface slope and bottom friction forcing in an estuary like Tampa Bay. Another potential problem is

improperly large vertical diffusion when bottom slopes are large: this was corrected by altering the diffusion terms (Mellor and Blumberg, 1985). A final problem of the exchange through advection of lighter, lower layers in shallow water with adjacent denser, lower layers in deep water can be alleviated by using more horizontal grid cells (Sheng, Lee, and Wang, 1990).

2.1. MODEL EQUATIONS

The model solves the equations of fluid motion (momentum balance, mass conservation, equation of state, salinity and temperature conservation, and hydrostatic balance) at all cells in the three-dimensional grid. The equations in three-dimensional Cartesian space are recast in generalized horizontal orthogonal curvilinear coordinates, and further transformed using a vertical dimensionless sigma coordinate. Details of the derivation are given in Blumberg and Mellor (1987) and Blumberg and Herring (1987) and will not be repeated here. Additional important information appears in Mellor (1993) and Schmalz (1994).

The full set of equations is as follows. Here u, v, and w are the x, y, and z components of velocity, t is time, S is salinity, θ is potential temperature, ρ is water density (Mellor, 1991), ρ_o is a reference water density (1000 kg/m^3), f is the Coriolis parameter, g is gravitational acceleration, P is pressure, P_a is atmospheric pressure, η is the departure of water elevation from mean sea level at z = 0, H is water depth at mean sea level, K_m and K_h are the vertical eddy mixing coefficients for momentum and heat/salt, respectively, A_m and A_h are the horizontal eddy mixing coefficients for momentum and heat/salt, respectively, and h_1 and h_2 are metrics (corresponding to grid dimensions ΔX and ΔY) (all units are SI). In the temperature conservation equation (Eq. 2.5), R_θ is the heating due to short wave radiation (see Appendix B).

Sigma coordinate:

$$\sigma = \frac{z - \eta}{H + \eta} = \frac{z - \eta}{D} \tag{2.1}$$

Continuity:

$$h_1 h_2 \frac{\partial \eta}{\partial t} + \frac{\partial}{\partial x}(h_2 u D) + \frac{\partial}{\partial y}(h_1 v D) + h_1 h_2 \frac{\partial \omega}{\partial \sigma} = 0 \tag{2.2a}$$

Vertically-integrated continuity:

$$h_1 h_2 \frac{\partial \eta}{\partial t} + \frac{\partial}{\partial x}\left(h_2 D \int_{-1}^{o} u d\sigma\right) + \frac{\partial}{\partial y}\left(h_1 D \int_{-1}^{o} v d\sigma\right) = 0 \tag{2.2b}$$

X-direction momentum:

$$\frac{\partial(h_1h_2Du)}{\partial t} + \frac{\partial}{\partial x}(h_2Du^2) + \frac{\partial}{\partial y}(h_1Duv) + h_1h_2\frac{\partial(\omega u)}{\partial \sigma} - Dv(f - \frac{u}{h_1}\frac{\partial h_1}{\partial y} + \frac{v}{h_2}\frac{\partial h_2}{\partial x})$$

$$= -h_2(gD\frac{\partial \eta}{\partial x} + \frac{1}{\rho_o}\frac{\partial P_a}{\partial x}) - \frac{gD^2h_2}{\rho_o}\int_\sigma^o [\frac{\partial \rho}{\partial x} - \frac{\sigma}{D}\frac{\partial D}{\partial x}\frac{\partial \rho}{\partial \sigma}]d\sigma + \frac{\partial}{\partial x}[A_mD(\frac{h_2}{h_1}\frac{\partial u}{\partial x})]$$

$$+ \frac{\partial}{\partial y}[A_mD(\frac{h_1}{h_2}\frac{\partial u}{\partial y} + \frac{\partial v}{\partial x})] + \frac{h_1h_2}{D}\frac{\partial}{\partial \sigma}(K_m\frac{\partial u}{\partial \sigma}) \qquad (2.3)$$

Y-direction momentum:

$$\frac{\partial(h_1h_2Dv)}{\partial t} + \frac{\partial}{\partial x}(h_2Duv) + \frac{\partial}{\partial y}(h_1Du^2) + h_1h_2\frac{\partial(\omega v)}{\partial \sigma} + Du(f - \frac{u}{h_1}\frac{\partial h_1}{\partial y} + \frac{v}{h_2}\frac{\partial h_2}{\partial x})$$

$$= -h_2(gD\frac{\partial \eta}{\partial y} + \frac{1}{\rho_o}\frac{\partial P_a}{\partial y}) - \frac{gD^2h_1}{\rho_o}\int_\sigma^o [\frac{\partial \rho}{\partial y} - \frac{\sigma}{D}\frac{\partial D}{\partial y}\frac{\partial \rho}{\partial \sigma}]d\sigma + \frac{\partial}{\partial y}[A_mD(\frac{h_1}{h_2}\frac{\partial v}{\partial y})]$$

$$+ \frac{\partial}{\partial x}[A_mD(\frac{h_2}{h_1}\frac{\partial v}{\partial x} + \frac{\partial u}{\partial y})] + \frac{h_1h_2}{D}\frac{\partial}{\partial \sigma}(K_m\frac{\partial v}{\partial \sigma}) \qquad (2.4)$$

Conservation of heat:

$$\frac{\partial(h_1h_2D\theta)}{\partial t} + \frac{\partial}{\partial x}(h_2Du\theta) + \frac{\partial}{\partial y}(h_1Dv\theta) + h_1h_2\frac{\partial(\omega\theta)}{\partial \sigma} \qquad (2.5)$$

$$= \frac{\partial}{\partial x}(A_hD\frac{h_2}{h_1}\frac{\partial \theta}{\partial x}) + \frac{\partial}{\partial y}(A_hD\frac{h_1}{h_2}\frac{\partial \theta}{\partial y}) + \frac{h_1h_2}{D}\frac{\partial}{\partial \sigma}(K_h\frac{\partial \theta}{\partial \sigma}) + h_1h_2DR_\theta$$

Conservation of salt:

$$\frac{\partial(h_1h_2DS)}{\partial t} + \frac{\partial}{\partial x}(h_2DuS) + \frac{\partial}{\partial y}(h_1DvS) + h_1h_2\frac{\partial(\omega S)}{\partial \sigma} \qquad (2.6)$$

$$= \frac{\partial}{\partial x}(A_hD\frac{h_2}{h_1}\frac{\partial S}{\partial x}) + \frac{\partial}{\partial y}(A_hD\frac{h_1}{h_2}\frac{\partial S}{\partial y}) + \frac{h_1h_2}{D}\frac{\partial}{\partial \sigma}(K_h\frac{\partial S}{\partial \sigma})$$

Conservation of turbulent kinetic energy:

$$h_1h_2\frac{\partial(Dq^2)}{\partial t} + \frac{\partial}{\partial x}(h_2Duq^2) + \frac{\partial}{\partial y}(h_1Dvq^2) + h_1h_2\frac{\partial(\omega q^2)}{\partial \sigma} \tag{2.7}$$

$$= \frac{\partial}{\partial x}(A_hD\frac{h_2}{h_1}\frac{\partial q^2}{\partial x}) + \frac{\partial}{\partial y}(A_hD\frac{h_1}{h_2}\frac{\partial q^2}{\partial y}) + \frac{h_1h_2}{D}\frac{\partial}{\partial \sigma}(K_q\frac{\partial q^2}{\partial \sigma})$$

$$+ h_1h_2\{\frac{2K_m}{D}[(\frac{\partial u}{\partial \sigma})^2 + (\frac{\partial v}{\partial \sigma})^2] + \frac{2g}{\rho_o}K_h\frac{\partial \rho}{\partial \sigma} - \frac{2Dq^3}{B_1\lambda}\}$$

Conservation of turbulent macroscale:

$$h_1h_2\frac{\partial(Dq^2\lambda)}{\partial t} + \frac{\partial}{\partial x}(h_2Duq^2\lambda) + \frac{\partial}{\partial y}(h_1Dvq^2\lambda) + h_1h_2\frac{\partial(\omega q^2\lambda)}{\partial \sigma} \tag{2.8}$$

$$= \frac{\partial}{\partial x}(A_hD\frac{h_2}{h_1}\frac{\partial q^2\lambda}{\partial x}) + \frac{\partial}{\partial y}(A_hD\frac{h_1}{h_2}\frac{\partial q^2\lambda}{\partial y}) + \frac{h_1h_2}{D}\frac{\partial}{\partial \sigma}(K_q\frac{\partial q^2\lambda}{\partial \sigma})$$

$$+ h_1h_2\{\frac{\lambda E_1K_m}{D}[(\frac{\partial u}{\partial \sigma})^2 + (\frac{\partial v}{\partial \sigma})^2] + \frac{\lambda E_1g}{\rho_o}K_h\frac{\partial \rho}{\partial \sigma} - \frac{q^3D}{B_1}[1 + E_2(\frac{\lambda}{\kappa L})^2]\}$$

where L is a scale length

$$L^{-1} = (\eta - z)^{-1} + (H + z)^{-1} \tag{2.9}$$

Equation of state:

$$\rho(S, \theta, P) = \rho_1(S, \theta) + 10^5\frac{P}{C^2}(1 - 2\frac{P}{C^2}) \tag{2.10}$$

where C is approximately the speed of sound

$$C = 1449.1 + 0.0821P + 4.55\theta - 0.045\theta^2 + 1.34(S - 35.0) \tag{2.11}$$

and P is pressure in bars

$$P = 0.01\left[P_a - gD\int_{\sigma}^{o}\rho\, d\sigma\right] \tag{2.12}$$

and

$$\rho_1 = 999.842594 + 6.793952x10^{-2}\theta - 9.095290x10^{-3}\theta^2 + 1.001685x10^{-4}\theta^3$$

$$- 1.120083x10^{-6}\theta^4 + 6.536332x10^{-9}\theta^5 + (0.824493 - 4.0899x10^{-3}\theta$$

$$+ 7.6438x10^{-5}\theta^2 - 8.2467x10^{-7}\theta^3 + 5.387555x10^{-9}\theta^4)S + (-5.72466x10^{-3}$$

$$+ 1.0227x10^{-4}\theta - 1.6546x10^{-6}\theta^2)S^{1.5} + 4.8314x10^{-4}S^2 \tag{2.13}$$

The Coriolis parameter is

$$f = 2\Omega\sin(\phi) \tag{2.14}$$

where ϕ is latitude.

The vertical and horizontal mixing coefficients are expressed as follows.

Horizontal mixing coefficients:

$$A_m = C_H h_1 h_2[(\frac{\partial u}{\partial x})^2 + \frac{1}{2}(\frac{\partial v}{\partial x} + \frac{\partial u}{\partial y})^2 + (\frac{\partial v}{\partial y})^2]^{1/2} \tag{2.15}$$

$$A_h = \frac{A_m}{N_p} \tag{2.16}$$

where $C_H = 0.03$ and the Prandtl number $N_p = 1.0$.

Vertical mixing coefficients:

$$K_m = S_m q\lambda \tag{2.17}$$

$$K_h = S_h q\lambda \tag{2.18}$$

$$K_q = 0.2q\lambda \tag{2.19}$$

where

$$S_h[1 - (3A_2B_2 + 18A_1A_2)G_h] = A_2[1 - 6\frac{A_1}{B_1}] \tag{2.20}$$

$$S_m[1 - 9A_1A_2G_h] - S_h[(18A_1^2 + 9A_1A_2)G_h] = A_1(1 - 3C_1 - 6\frac{A_1}{B_1}) \tag{2.21}$$

$$G_h = \frac{\lambda^2}{q^2}\frac{g}{\rho_o}(\frac{1}{D}\frac{\partial \rho}{\partial \sigma}) \tag{2.22}$$

and

$$(A_1,A_2,B_1,B_2,C_1,E_1,E_2) = (0.92,\ 0.74,\ 16.6,\ 10.1,\ 0.08,\ 1.8,\ 1.33) \tag{2.23}$$

2.2. BOUNDARY CONDITIONS

Lateral Boundary Conditions

At land boundaries, momentum, mass, and heat flux normal to the land are zero. At open ocean boundaries, either the water level or the external-mode velocity is explicitly specified. The internal-mode velocity is determined by an Orlanski (1976) radiation boundary condition

$$\frac{\partial u}{\partial t} + (\frac{\Delta \rho}{\rho_o} g D)^{1/2}\frac{\partial u}{\partial x} = 0 \tag{2.24}$$

where $\Delta\rho$ is the difference between the top and bottom densities. Further discussion of the open (ocean and river) boundary conditions appears in Section 3.

Surface Boundary Conditions

Momentum is added at the water surface by winds and the atmosphere adds (or removes) heat and water. Surface stresses are transferred to the internal mode velocities by

$$(K_m\frac{\partial u}{\partial z})|_s = \frac{\tau_{sx}}{\rho_s} \tag{2.25}$$

$$(K_m\frac{\partial v}{\partial z})|_s = \frac{\tau_{sy}}{\rho_s} \tag{2.26}$$

where the subscript "s" means the surface. Net evaporation (or negative precipitation) is Π

(m/s) and there is no salt flux across the interface. Downward heat flux across the upper surface, Q_s, is modeled as the long-wave downward radiation (see Appendix B).

$$(K_h \frac{\partial S}{\partial z})|_s = S_s \Pi \tag{2.27}$$

$$(K_h \frac{\partial \theta}{\partial z})|_s = Q_s \tag{2.28}$$

The surface conditions on turbulent kinetic energy, q^2, and the product $q^2\lambda$ are

$$q^2|_s = B_1^{2/3} u_{*s}^2 \tag{2.29}$$

$$q^2\lambda|_s = 0 \tag{2.30}$$

where B_1 is defined in Eq. 2.24 and the surface friction velocity, u_{*s}, is

$$u_{*s}^2 = (\frac{\tau_{sx}}{\rho_s})^2 + (\frac{\tau_{sy}}{\rho_s})^2 \tag{2.31}$$

Bottom Boundary Conditions

Bottom stresses are related to the internal mode velocities by

$$\begin{aligned} (K_m \frac{\partial u}{\partial z})|_b &= \frac{\tau_{bx}}{\rho_b} \\ (K_m \frac{\partial v}{\partial z})|_b &= \frac{\tau_{by}}{\rho_b} \end{aligned} \tag{2.32}$$

where the subscript "b" denotes the bottom. The velocity matching condition (incorporating a bottom logarithmic velocity profile) is also required to compute the bottom drag coefficient

$$C_b = [\frac{1}{\kappa} \ln(\frac{H + z_b}{z_o})]^{-2} \tag{2.33}$$

where z_b is the depth of the modeled velocity at the level closest to the bottom, κ is von Karman's constant (0.40), and z_o is the roughness height. The salt and heat flux across the bottom are

$$(K_h \frac{\partial S}{\partial z})|_b = 0 \tag{2.34}$$

$$(K_h \frac{\partial \theta}{\partial z})|_b = Q_b \tag{2.35}$$

where Q_b is the downward heat flux across the bottom (assumed here to be zero). The bottom conditions on turbulent kinetic energy, q^2, and the product $q^2\lambda$ are

$$q^2|_b = B_1^{2/3} u_{*b}^2 \tag{2.36}$$

$$q^2\lambda|_b = 0 \tag{2.37}$$

where

$$u_{*b}^2 = (\frac{\tau_{bx}}{\rho_o})^2 + (\frac{\tau_{by}}{\rho_o})^2 \tag{2.38}$$

2.3. THE MODEL GRID

The Tampa Bay model runs on an orthogonal curvilinear grid closely fitted to the Bay's lateral boundaries (Figure 2.1). A 2400-cell, orthogonal curvilinear mesh was generated using techniques explained in Blumberg and Herring (1987). The actual mesh was generated by HydroQual, Inc., using NOAA Sea Grant funds from the University of South Florida study headed by Dr. Boris Galperin. Grid cells are closely spaced in regions where higher resolution is needed, such as near the navigation channel, passages across causeways, and entrances to sub-basins. The grid configuration includes the two large spoil islands in Hillsborough Bay, the Hillsborough River, and McKay Bay. Cell spacing varies from 300 meters to 2000 meters. Each cell has a depth value obtained from bathymetric data for Tampa Bay available from NOAA's National Geophysical Data Center in gridded (15-second interval) format. Bathymetry generated from these data is shown in Figure 2.2. The present grid replaced two earlier test versions (Hess, 1990); a square-cell grid and a curvilinear grid generated in CEOB (Hess, unpublished).

A substantial number of cells cover the Florida shelf region west of the Bay entrance. This placement of the boundaries allows for internal dynamics to dominate the simulation of currents and the density field in the bathymetrically complex entrance region around Egmont Key, rather than increase uncertainty by specifying the boundary condition in an oversimplified manner and risk imposing a dynamic inconsistency. The grid has another connection to the shelf through Pass a Grille Channel but is not connected to Boca Ciega Bay north of the Pinellas Byway. At present there is no connection to Sarasota Bay.

The grid covers most of the water area of Tampa Bay, but cannot resolve all the small features along the shore. The grid is detailed enough to represent the following features explicitly:

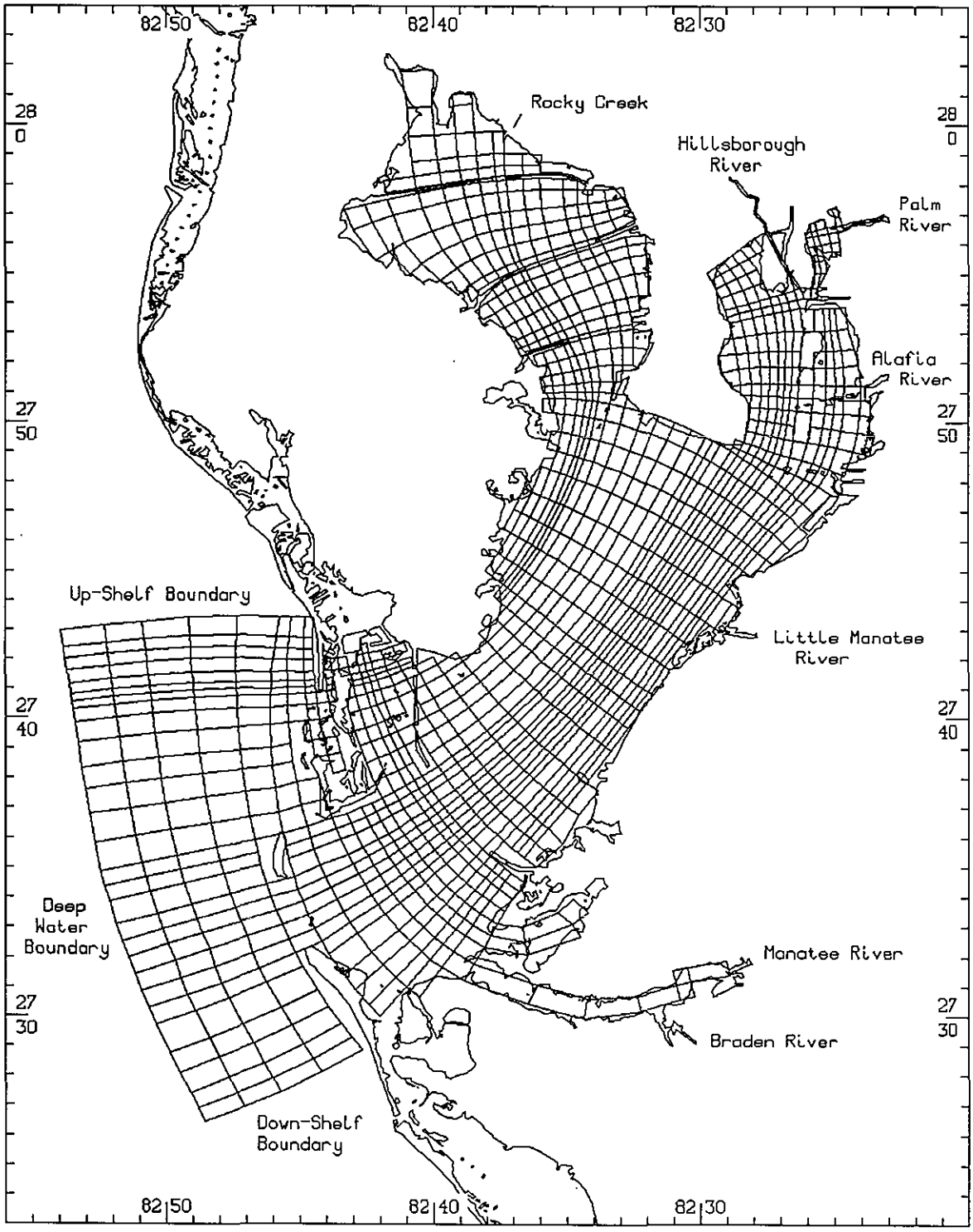

Figure 2.1. Tampa Bay curvilinear orthogonal grid, west Florida shelf boundaries, and seven rivers.

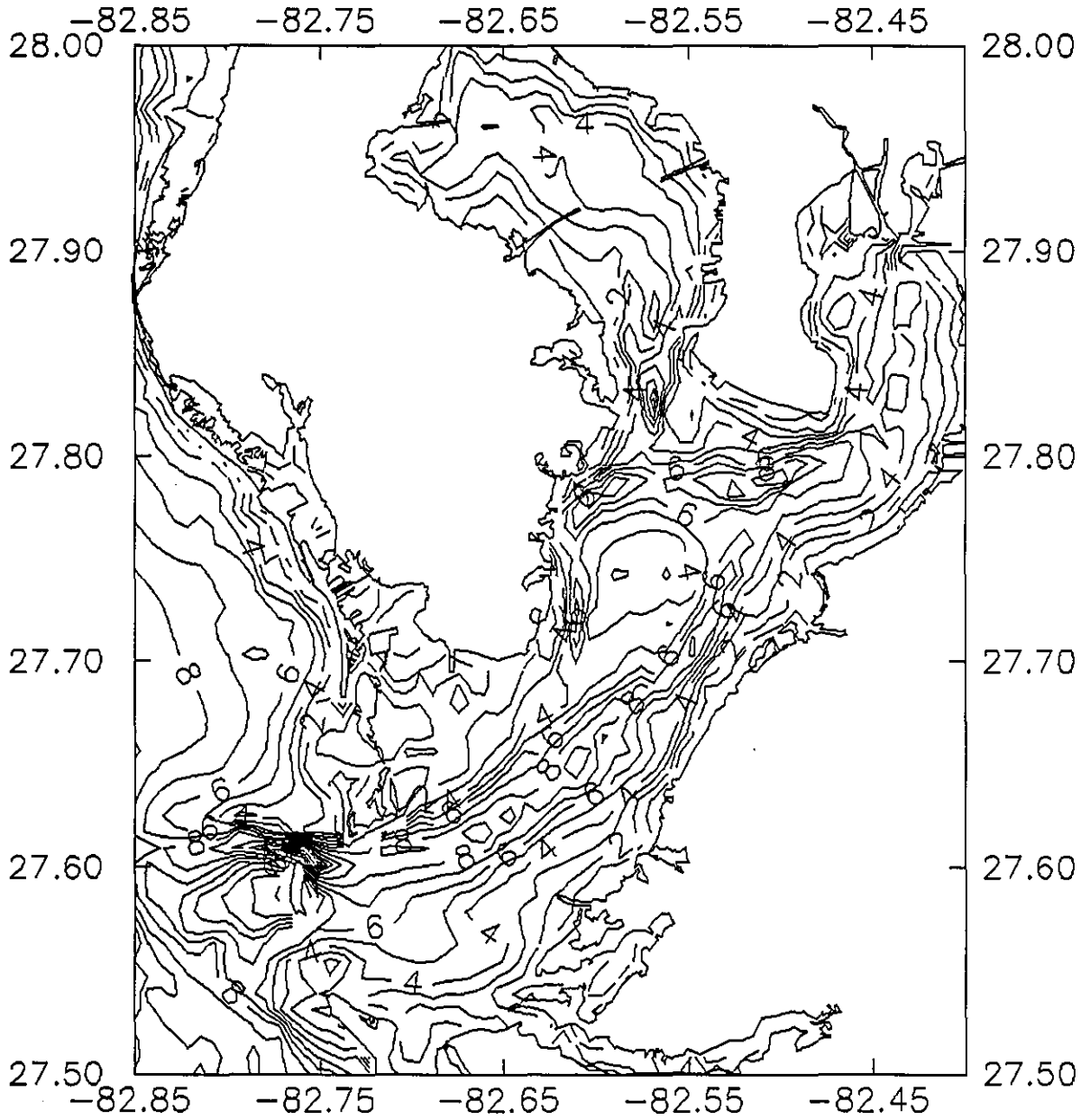

Figure 2.2. Isobaths contoured at 1-meter intervals.

Hillsborough River, Tampa Bypass Canal, and Manatee River. Additional rivers were included by adding a single cell along the perimeter: Rocky Creek, Alafia River, and Little Manatee.

At each cell (denoted by indices I and J) there is a length (h_1) in the x direction, DX, a length (h_2) in the y direction, DY, a msl depth, H, a cell rotation angle, Ψ, a latitude used in computing the Coriolis acceleration, ϕ, and a roughness height, z_o. The local y-direction in each cell is related to north by a rotation angle, Ψ (counterclockwise from north to the y axis).

A portion of the grid file appears in Appendix C. In the vertical, there are eight sigma levels of uniform thickness: σ = (0.0, -.14, -.28, -.43, -.57, -.71, -.86, -1.00). This is considered sufficient to resolve the moderate density stratification observed. Considering cell lengths and depths, the model is run with an external-mode time step of 24 s and an internal mode time step of 120 s. A 24-h simulation requires 8 minutes on an SGI 380-4DX computer.

The numerical model simulation requires driving forces (water levels, river discharges, winds) that are applied at the open boundaries on the grid. These forces are represented by time series of values. The open boundaries on the west Florida shelf are denoted as the deep water, the up-shelf, and the down-shelf boundaries (Figure 2.1), and each cell along the boundary requires a water level value and salinity and temperature values at all vertical levels at each model time step. The river boundaries require discharge, salinity, and temperature values. The wind is applied at the surface of all cells. At the closed boundaries there is zero momentum, salt transfer, and heat transfer. These requirements are discussed in detail in the next Section.

2.4. ADDITIONAL MODEL FEATURES

The model code was originally adapted from the Long Island Sound version (Schmalz, 1994). Several new features of the model and grid application to Tampa Bay have been added and these are discussed below.

Cell Emergence and Submergence

Shallow water areas are subject to emergence, or having the water depth approach zero, as area-wide water levels decrease. Once exposed, the same areas are subject to submergence as the water level rises. In the present model, this phenomenon is simulated by a reduction of inter-cell flow and the method of solution follows some of the ideas presented by Roig and King (1992). As water level drops, emerging vegetation and natural bathymetric variation (mud flats, channels, etc.) combine to reduce the pathways for water to depart, leaving less net cell width available for water transport. When total water depth falls below some critical value (on the order of centimeters), all exiting transport ceases as the net width becomes zero and the cell, which still contains some water, becomes dynamically passive; no water leaves or enters the cell. Flow will only recommence when the elevation of the water surface in an adjacent cell rises above the elevation of the water surface in the passive cell; then the net width rises above zero and water enters the passive cell. Passive cell water depth must be sufficiently large that applied forces do not produce infinitely large accelerations.

The mathematical representation is as follows. Let Q_i represent the volume flux in the x direction (used in the continuity equation) between cell i-1 and cell i, where U_i is the vertically-averaged velocity, D_i is the total water depth in cell i, Δ_Y is the width of the cell in the direction normal to x, and W_i is the effective width factor which is dimensionless and not greater than unity.

$$Q_i = U_i \Delta_Y W_i \frac{1}{2}(D_i + D_{i-1}) \tag{2.39}$$

The width reduction factor, which is a function of total cell water depth, D, is defined here as

$$\begin{aligned} W_i &= 1 && \text{for } D > d_2 \\ &= \frac{D - d_1}{d_2 - d_1} && \text{for } d_2 > D > d_1 \\ &= 0 && \text{for } D < d_1 \end{aligned} \tag{2.40}$$

where D is the upstream cell water depth and d_1 and d_2 are the scale depths. W_i is calculated at each external-mode time step. The W factor must be used for all horizontal fluxes (mass, momentum, salinity, temperature, and turbulence variables) and for wind stress.

For Tampa Bay, d_1 (average water depth for a "dry" cell) and d_2 (vegetation height scale) were chosen to be 2 cm and 30 cm, respectively. About five cells were shallow enough that emergence occurred during some of the simulations when winds exceeded 20 kts. These cells were located in the shallowest portions of Boca Ciega Bay west of the Sunshine Skyway Bridge.

Curvilinear Grid Option

The model can be run in either the rectilinear or curvilinear mode. Additional computations are performed when the grid is curvilinear rather than rectilinear and are included in a modified Coriolis term (see Eqs 2.3 and 2.4):

$$f - \frac{u}{h_1}\frac{\partial h_1}{\partial y} + \frac{v}{h_2}\frac{\partial h_2}{\partial x} \tag{2.41}$$

The second two terms in Eq. 2.41 are computed when the variable ICURV is set to 1; for a rectilinear grid they are zero and need not be calculated.

Barriers

Barriers between water cells are introduced in the grid file by setting DUM and/or DVM to zero (see Appendix C). The barriers are used to represent sub-grid scale features such as causeways and small islands that are not overtopped but remain fixed once they are set at the beginning of the run.

Spatially-Varying Bottom Roughness

Bottom friction is parameterized by a roughness height z_o (Eq. 2.34) which varies with location in the Bay. In shallow areas, sea grasses and pilings tend to increase bottom roughness, while in deep areas there are no grasses. Regional adjustments were also made during the calibration phase. The final array of roughnesses (see Section 4.5) appears in Figure 2.3.

$$\frac{\partial \xi}{\partial t} + \frac{\partial}{\partial x}(hu) + \frac{\partial}{\partial y}(hv) = 0$$

$$\frac{\partial \xi}{\partial t} + \frac{\partial}{\partial x}(W(h)\, hu) + \frac{\partial}{\partial y}(W(h)\, hv) = 0$$

drying function.

← question of:

1) time scale to stay dry?

2) potentially leaving wet cells behind.

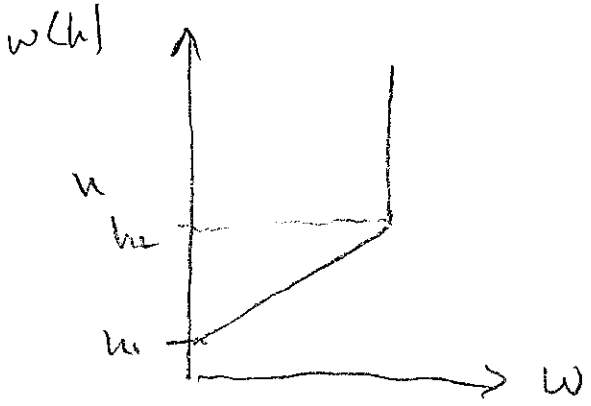

60	.	.	.	.	.	.	.	.	.	.	.	.	.	.	.	.	.	.	.	.	.	.	.	.	.	.	.	.	.	.	.	.	.	.	.	.	.	.	.	.
59	.	.	.	.	20	.	20	.	.	.	.	.	.	.	.	.	.	.	.	.	.	.	.	.	.	.	.	.	.	.	.	.	.	.	.	.	.	.	.	.
58	.	.	.	.	20	.	20	.	.	.	.	.	.	.	.	.	.	.	.	.	.	.	.	.	.	.	.	.	.	.	.	.	.	.	.	.	.	.	.	.
57	.	.	.	.	20	20	20	20	20	.	20	.	.	.	.	.	.	.	.	.	.	.	.	.	.	.	.	.	.	.	.	.	.	.	.	.	.	.	.	.
56	.	.	.	.	20	20	20	20	20	20	20	.	.	.	.	.	.	.	.	.	.	.	.	.	.	.	.	.	.	.	.	.	.	.	.	.	.	.	.	.
55	.	.	.	20	20	20	20	20	20	20	20	.	.	.	.	.	.	.	.	.	.	.	.	.	.	.	.	.	20	.	.	.	.	.	20	.	.	.	.	.
54	.	.	.	.	.	.	.	.	20	.	.	.	.	.	.	.	.	.	.	.	.	.	.	.	.	.	.	.	20	.	.	20	20	.	20	.	.	.	.	.
53	.	20	20	20	20	20	20	20	20	20	20	20	20	.	.	.	.	.	.	.	.	.	.	.	.	.	.	.	20	.	20	20	20	20	20	20	20	20	20	.
52	.	20	20	20	20	20	20	20	20	20	20	20	20	20	20	20	.	.	.	.	.	.	.	.	.	.	.	.	20	.	20	20	20	20	.	.	.	.	.	.
51	.	.	20	20	20	20	20	20	20	20	20	20	20	20	20	20	.	.	.	.	.	20	20	20	20	20	20	.	20	.	20	.	20	20	.	.	.	.	.	.
50	.	.	.	20	20	20	20	20	20	20	20	20	20	20	20	20	.	.	.	.	.	20	20	20	20	.	.	.	20	.	20	.	.	.	.	.	.	.	.	.
49	.	.	.	20	20	20	20	20	20	20	20	20	20	20	20	20	.	.	.	.	.	20	20	20	20	.	.	.	20	.	20	20	.	.	.	.	.	.	.	.
48	.	.	.	.	20	20	20	20	20	20	20	20	20	20	.	.	.	.	.	.	.	20	20	20	20	.	.	.	20	.	20	.	.	.	.	.	.	.	.	.
47	.	.	.	.	.	.	.	.	.	20	20	20	20	20	.	.	.	.	.	.	.	20	20	20	20	20	20	20	20	20	20	.	.	.	.	.	.	.	.	.
46	.	.	.	.	.	20	20	20	20	20	20	20	20	20	20	20	.	.	.	.	.	20	20	20	20	20	20	20	.	.	.	.	.	.	.	.	.	.	.	.
45	.	.	.	20	20	20	20	20	20	20	20	20	20	20	20	20	.	.	.	.	.	20	20	20	20	20	20	20	20	20	20	20	20	.	.	.	.	.	.	.
44	.	.	.	.	20	20	20	20	20	20	20	20	20	20	20	20	.	.	.	.	20	20	20	20	20	20	20	20	.	.	20	20	20	.	.	.	.	.	.	.
43	.	.	.	.	20	20	20	20	20	20	20	20	20	20	20	20	.	.	.	.	20	20	20	20	20	20	20	20	.	20	20	20	20	.	.	.	.	.	.	.
42	.	.	.	.	20	20	20	20	20	20	20	20	20	20	20	.	.	.	.	.	20	20	20	20	20	20	20	20	20	20	20	20	20	20	.	.	.	.	.	.
41	.	.	.	.	20	20	20	20	20	20	20	20	20	20	.	.	.	.	.	.	.	20	20	20	20	20	20	20	20	20	20	20	20	.	.	.	.	.	.	.
40	.	.	.	.	.	.	.	.	.	20	20	20	20	20	.	.	.	.	.	.	.	.	20	20	20	20	20	20	20	20	20	20	20	20	.	.	.	.	.	.
39	.	.	.	.	.	20	20	20	20	20	20	20	20	20	20	.	.	.	.	.	.	.	20	20	20	20	20	20	.	20	20	20	20	20	.	.	.	.	.	.
38	.	.	.	.	.	.	20	20	20	20	20	20	20	20	20	.	.	.	.	.	.	.	20	20	20	20	20	20	.	20	20	20	20	20	20	.	.	.	.	.
37	.	.	.	.	.	20	20	20	20	20	20	20	20	.	.	.	.	.	.	.	.	.	20	20	20	20	20	20	20	20	20	20	20	.	.	.	.	.	.	.
36	.	.	.	.	.	20	20	20	20	20	20	20	.	.	.	.	.	.	.	.	.	20	20	20	20	20	20	20	20	20	20	20	.	.	.	.	.	.	.	.
35	.	.	.	.	.	.	20	20	20	20	20	20	20	.	.	.	.	.	.	.	.	20	20	20	20	20	20	20	20	20	20	20	20	.	.	.	.	.	.	.
34	.	.	.	.	.	20	20	20	20	20	20	20	20	20	20	20	20	20	20	20	20	20	20	20	20	20	20	20	20	20	20	20	20	.	.	.	.	.	.	.
33	.	.	.	.	.	.	.	20	20	20	20	20	20	20	20	20	20	20	20	20	20	20	20	20	20	20	20	20	20	20	20	20	20	20	.	.	.	.	.	.
32	.	.	.	.	.	.	20	20	20	20	20	20	20	20	20	20	20	20	20	20	20	20	20	20	20	20	20	20	20	20	20	20	20	20	.	.	.	.	.	.
31	.	.	.	.	.	.	.	20	20	20	20	5	20	20	20	20	20	20	20	20	20	20	20	20	20	20	20	20	20	20	20	20	20	.	.	.	.	.	.	.
30	.	.	.	.	.	.	20	20	20	20	20	20	20	20	20	20	20	20	20	20	20	20	20	20	20	20	20	20	20	20	20	20	.	.	.	.	.	.	.	.
29	.	.	.	.	.	20	20	20	20	20	20	20	50	50	50	20	20	20	20	20	20	20	20	20	20	20	20	20	20	20	20	20	20	20	.	.	.	.	.	.
28	.	.	.	.	.	20	20	20	20	20	20	20	50	50	50	20	20	20	20	20	20	20	20	20	20	20	20	20	20	20	20	20	.	.	.	.	.	.	.	.
27	.	.	.	.	.	.	20	20	20	20	20	20	50	50	50	20	20	20	20	20	20	20	20	20	20	20	20	20	20	20	20	.	.	.	.	.	.	.	.	.
26	.	.	.	.	.	.	20	20	20	20	20	20	20	20	20	20	20	20	20	20	20	20	20	20	20	20	20	20	20	20	20	20	.	.	.	.	.	.	.	.
25	.	.	.	.	.	.	.	.	.	20	20	20	20	20	20	20	20	20	20	20	20	20	20	20	20	20	20	20	20	20	20	20	.	.	.	.	.	.	.	.
24	.	.	.	.	.	.	.	.	.	.	.	.	20	20	20	20	20	20	20	20	20	20	20	20	20	20	20	20	20	20	20	20	.	.	.	.	.	.	.	.
23	.	.	.	.	.	.	.	.	.	.	.	.	20	20	20	20	20	50	50	50	20	20	20	20	20	20	20	20	20	20	20	20	.	.	.	.	.	.	.	.
22	.	.	.	.	.	.	.	.	.	.	.	.	.	20	20	20	20	50	50	50	20	20	20	20	20	20	20	20	20	20	20	20	.	.	.	.	.	.	.	.
21	.	.	.	.	.	.	.	.	.	.	.	.	20	20	20	20	20	50	50	50	20	20	20	20	20	20	20	20	20	20	20	20	20	.	.	.	.	.	.	.
20	.	.	.	.	.	.	.	.	.	.	.	20	20	20	20	20	20	20	20	20	20	20	20	20	20	20	20	20	20	20	20	20	20	20	.	.	.	.	.	.
19	.	.	.	.	.	.	.	20	.	20	20	20	.	20	20	20	20	20	20	20	20	20	20	20	20	20	20	20	20	20	20	20	20	.	.	.	.	.	.	.
18	.	.	.	.	.	.	.	20	.	20	20	20	20	.	.	20	20	20	20	20	20	20	20	20	20	20	20	20	20	20	20	20	20	.	.	.	.	.	.	.
17	.	.	.	.	.	.	.	20	20	20	20	20	20	20	.	20	.	.	20	20	20	20	20	20	20	20	20	20	20	.	.	.	.	.	.	.	.	.	.	.
16	.	.	.	.	.	.	20	20	20	20	20	20	20	20	20	20	20	20	20	20	20	20	20	20	20	20	20	20	20	20	20	20	20	.	.	.	.	.	.	.
15	.	.	.	.	.	.	.	20	20	20	20	20	20	20	20	20	20	20	20	20	20	20	20	20	20	20	20	20	20	20	20	20	20	.	.	.	.	.	.	.
14	.	.	.	.	.	.	.	.	20	20	20	20	20	20	20	20	20	20	20	20	20	20	20	20	20	20	20	20	20	20	20	20	20	.	.	.	.	.	.	.
13	.	.	.	.	.	.	.	20	20	.	.	.	20	20	20	20	20	20	20	20	20	20	20	20	20	20	20	20	20	20	20	20	20	.	.	.	.	.	.	.
12	.	.	.	.	.	.	.	20	.	.	.	.	.	.	.	.	.	.	20	20	20	20	20	20	20	20	20	20	20	20	20	20	20	20	20	20	.	.	.	.
11	.	.	.	.	.	.	.	20	20	20	20	20	.	.	.	.	.	.	20	20	20	20	20	20	20	20	20	20	20	20	20	20	20	20	20	.	.	.	.	.
10	.	.	.	.	.	.	.	.	.	.	.	20	20	.	20	20	.	.	20	20	20	20	20	20	20	20	20	20	20	20	20	20	.	.	.	.	.	20	20	.
9	.	.	.	.	20	20	20	20	20	20	20	20	20	20	20	.	.	.	20	20	20	20	20	20	20	20	20	20	20	20	20	20	20	20	20	20	20	20	.	.
8	.	.	.	.	20	20	20	20	20	20	20	20	20	.	.	.	20	20	20	20	20	20	20	20	20	20	20	20	20	20	20	20	.	.	.	.	.	.	.	.
7	.	.	.	.	20	20	20	20	20	20	20	20	20	20	20	20	20	20	20	20	20	20	20	20	20	20	20	20	20	20	20	.	.	.	.	.	.	.	.	.
6	.	.	.	.	20	20	20	20	20	20	20	20	20	20	20	20	20	20	.	.	.	5	5	5	20	20	.	.	.	.	.	.	.	.	.	.	.	.	.	.
5	.	.	.	.	20	20	20	20	20	20	20	20	20	20	20	20	20	20	20	20	20	5	5	5	20	20	20	20	20	20	20	20	.	.	.	.	.	.	.	.
4	.	.	.	.	20	20	20	20	20	20	20	20	20	20	20	20	20	20	20	20	20	5	5	5	20	20	20	20	20	20	20	20	.	.	.	.	.	.	.	.
3	.	.	.	.	20	20	20	20	20	20	20	20	20	20	20	20	20	20	20	20	20	20	20	20	20	20	20	20	20	20	20	20	.	.	.	.	.	.	.	.
2	.	.	.	.	.	20	20	20	20	20	20	20	20	20	20	20	20	20	20	20	20	20	20	20	20	20	20	20	20	20	20	.	.	.	.	.	.	.	.	.
J=1	.	.	.	.	.	.	.	.	.	.	.	.	.	.	.	.	.	.	.	.	.	.	.	.	.	.	.	.	.	.	.	.	.	.	.	.	.	.	.	.
I=	1	2	3	4	5	6	7	8	9	10	11	12	13	14	15	16	17	18	19	20	21	22	23	24	25	26	27	28	29	30	31	32	33	34	35	36	37	38	39	40

Figure 2.3. Cell roughness height z_0 (mm) times 10.

3. BOUNDARY CONDITIONS, OBSERVATIONAL DATA, AND INITIALIZATION

To obtain the mathematical solution, at the boundaries for each time step the numerical model requires specification of the values of the dependent variables (water level, current, salinity, and temperature) or their first derivatives in the direction normal to the boundary. These values are obtained (a) directly from the data by interpolation, (b) by specifying a physical condition, such as a flux, to relate the required variable to another variable (such as wind velocity) which has been observed, or (c) by evaluating an analytic expression whose constants have been derived from data. Through these variables the driving forces (tidal and nontidal water levels, winds, and river discharges) are imposed. The present study simulates conditions that occurred during the survey (June 1990 to September 1991), so observational data is available to drive the model.

In the present model, the open boundaries on the west Florida shelf are denoted as the deep water, the up-shelf, and the down-shelf boundaries (Figure 2.1), and each cell along the boundary requires a water level value and salinity and temperature values at all vertical levels at each model time step. The river boundaries require discharge, salinity, and temperature values. The wind is applied at the surface of all cells. At the closed boundaries there is no transfer of momentum, salt, or heat. Since each geographical type of boundary requires a different set of data, the boundaries are discussed in turn. Once the boundary conditions were set, it was relatively easy to develop the initial conditions for this basin.

3.1. FLORIDA SHELF BOUNDARIES

The Florida shelf open boundaries consist of the deep water, up-shelf, and down-shelf boundaries. Each cell requires specification of (1) a water level or a velocity and (2) a density. These are prescribed as follows.

Water Level

Water levels at the deep-water, up-shelf, and down-shelf boundaries are expressed as

$$\eta(t) = \eta_a(t) + \eta_r(t) \tag{3.1}$$

where η is the total water level, η_a is the astronomical tide, and η_r is the nontidal residual due to shelf effects, river runoff, and atmospheric influences. This water level condition can be supplied by either a time series of observed values or by an analytic expression as follows. The astronomical tide is expressed in terms of constituents (Schureman, 1958), as

$$\eta_a(t) = \sum_{n=1}^{37} f_n A_n \cos(\omega_n t + E_n - k_n) \tag{3.2}$$

where, for each constituent n, f is the lunar node factor, A is the amplitude, ω is the angular speed, E is the equilibrium angle, and k is the local epoch. The constituents obtained for C-1, which were used in the tidal simulations, are shown in Table 3.1.

Table 3.1. Astronomical tidal water level constituents obtained from pressure records at C-1.

n	NAME	A (m)	k (deg)	n	NAME	A (m)	k (deg)
1	M2	0.183	332.3	2	S2	0.080	333.9
3	N2	0.042	340.9	4	K1	0.178	301.2
5	M4	0.006	115.1	6	O1	0.137	292.3
7	M6	0.002	34.7	8	MK3	0.000	0.0
9	S4	0.003	207.8	10	MN4	0.000	0.0
11	NU2	0.008	339.8	12	S6	0.001	278.0
13	MU2	0.000	0.0	14	2N	0.005	349.5
15	OO	0.005	310.0	16	LAM2	0.001	333.0
17	S1	0.000	0.0	18	M1	0.009	296.8
19	J1	0.010	305.6	20	MM	0.000	0.0
21	SSA	0.000	0.0	22	SA	0.000	0.0
23	MSF	0.000	0.0	24	MF	0.000	0.0
25	RHO1	0.005	288.5	26	Q1	0.026	287.9
27	T2	0.004	333.8	28	R2	0.000	333.9
29	2Q	0.003	283.5	30	P1	0.040	300.6
31	2SM	0.000	0.0	32	M3	0.000	0.0
33	L2	0.006	335.5	34	2MK3	0.000	0.0
35	K2	0.021	334.0	36	M8	0.001	155.0
37	MS4	0.000	0.0				

Two other boundary conditions were tested. A second water level boundary condition, used only in testing, is that of a zero slope normal to the boundary, i.e.,

$$\frac{\partial \eta}{\partial x_n} = 0 \tag{3.3}$$

where x_n is the outward normal direction. This condition forces the flow to be parallel to the boundary. Tests show that the use of this condition at the up-shelf and down-shelf boundaries has little effect on the interior solution. A third boundary condition used in the present study is a radiation condition. Derived from the linearized Riemann invariant (Wurtele et al., 1971), the condition is expressed in terms of water levels by

$$\eta - (\eta_a + \eta_r) = \frac{U_n D}{[g(D + \eta)]^{1/2}} \tag{3.4}$$

where U_n is the outward normal barotropic velocity. This condition was required in the salinity and temperature simulations to prevent an instability at the up-shelf boundary, indicating that it allowed northward-propagating disturbances (such as Kelvin waves) generated inside the grid to pass out of the grid.

Observed water levels were recorded at 14 locations inside Tampa Bay and at two coastal locations outside the Bay. Those data, which have been quality-controlled and are available at hourly intervals, were used for model calibration and validation. A time series of observational

values taken during the TOP survey is available from a pressure transducer fixed to either the bottom-mounted ADCP unit or the CTD mooring at C-1 (see Appendix A), located approximately 8 kilometers west of the entrance to Tampa Bay. Total water pressure values and computed water depths at 10-minute intervals are available for the periods June 6 to December 28, 1990; March 12 to May 28, 1991; and July 11 to September 28, 1991. The ADCP software computed a depth value by subtracting a fixed, standard atmospheric pressure value from the total measured pressure due to water and air and dividing by the product of gravitational acceleration and water density. The water density was computed from a bottom measurement of water temperature. The final water level value was then computed from the ADCP total water depth by subtracting the atmospheric variation (in equivalent depth units) and de-meaning the remainder.

Estimates of tidal water level constituents on the west Florida shelf (Schwiderski, 1980) indicate that the tide wave on the West Florida shelf propagates normal to the isobaths, which are approximately parallel to the shore line in the Tampa Bay region, and has little north-south amplitude gradient. Therefore, the amplitudes and phases of astronomical tidal constituents at C-1 should be valid for all cells along at the deep water boundary.

Current

External mode and internal mode velocities directed normal to the boundary are set equal to the values in adjacent cells within the computational grid, i.e.,

$$\frac{\partial U}{\partial x_n} = \frac{\partial V}{\partial x_n} = 0 \tag{3.5}$$

where x_n is the outward normal. Internal mode velocities are set using the Orlanski radiation condition (Eq. 2.24).

Density

The salinity and temperature boundary condition can be specified in one of three ways: using observational data, applying a zero-slope condition, or applying a flux condition. The second condition is

$$\frac{\partial S}{\partial x_n} = \frac{\partial \theta}{\partial x_n} = 0 \tag{3.6}$$

where x_n is the outward normal. Therefore, the salinity and temperature are set to the values in the adjacent non-boundary cell within the grid. This condition was used at the up- and the down-shelf boundaries.

In the third type of boundary condition, salinity and temperature at each level are determined by advection equations with upstream differencing, which are simplified forms of the conservation equations (Eqs. 2.5 and 2.6). These are

$$\frac{\partial S}{\partial t} + u_n \frac{\partial S}{\partial x_n} = \frac{\partial \theta}{\partial t} + u_n \frac{\partial \theta}{\partial x_n} = 0 \qquad (3.7)$$

where u_n is the current speed in the upstream direction. During ebb, when water is flowing out of the grid, salinity and temperature are determined from values in adjacent cells in the interior field. During flood, when water is flowing into the grid from the outside, the salinity and temperature are determined by the deep water, or oceanic, values. The oceanic conditions (S_{ocean} and θ_{ocean}) are conceptualized as being slowly-changing (relative to the tidal period).

Observational data for salinity and temperature on the shelf during TOP show that stratification was practically non-existent throughout the year (Figure 3.1). Salinities throughout the water column were rather steady over the time of the survey and ranged from 34 to 36 psu. Temperatures showed a strong annual cycle with a maximum in the late summer of 32°C and a winter minimum of 18°C. Shelf salinity and temperature data from Dragovich and Sykes (1967) also show the same annual patterns and little stratification.

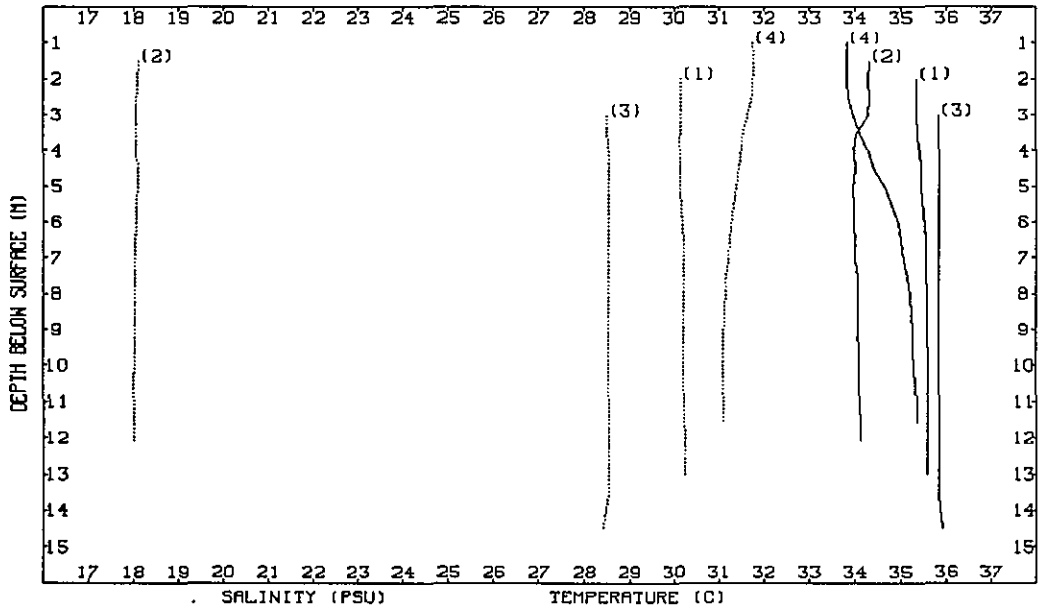

Figure 3.1. Vertical profiles of salinity (solid lines) and temperature (dotted lines) from CTD casts at C-1, 10 km outside the entrance to Tampa Bay. Times of observation are (1) August 17, 1990; (2) March 1, 1991; (3) June 4, 1991; and (4) August 17, 1991.

A long series of salinity and temperature measurements at two levels at the shelf station S-1 were collected during TOP. Plots of bottom salinity and temperature collected are shown in Figure 3.2. Time series of depth-varying ocean boundary salinities and temperatures were generated by:

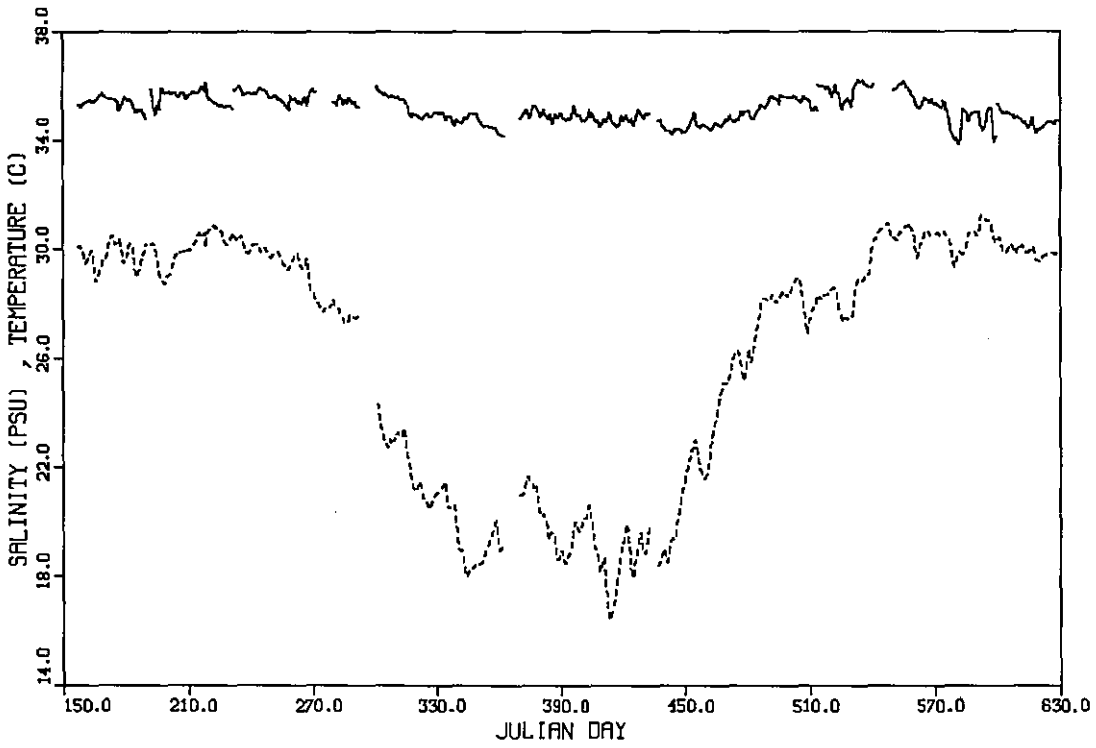

Figure 3.2. Near-bottom salinity (solid line) and temperature (dotted line) at C-1 during 1990 and 1991.

$$S_{ocean}(z,t) = \overline{S}_{observed}(t) + \delta_s(z) \tag{3.8a}$$

$$\theta_{ocean}(z,t) = \overline{\theta}_{observed}(t) + \delta_\theta(z) \tag{3.8b}$$

where observed values refer to bottom measurements at C-1, the overbar denotes interpolation from monthly averages, and δ_s and δ_θ are adjustments for depth as defined in Table 3.2. These values were chosen to give a realistic (i.e., weakly stratified) density profile. Monthly averages were used to eliminate small time-scale variations and to fill in data gaps. Vertical interpolation of these values was used to generate the values needed at other depths.

3.2. RIVER BOUNDARIES

River input to Tampa Bay, while relatively small compared to that in other estuaries, is large enough to create significant horizontal density gradients and hence to drive an estuarine circulation.

Table 3.2. Temperature and salinity adjustment functions, δ, added to the 10-meter values to obtain values at other depths.

Depth (m)	Florida Shelf δ_θ (°C)	Florida Shelf δ_S (psu)	Hillsborough Bay δ_S^h (psu)
0	0.2	-0.2	-1.0
5	0.1	-0.1	-0.2
10	0.0	0.0	0.0
100	0.0	0.0	0.0

River Discharge

The river boundary is conceptualized as a single cell with water entering as a water falls. The additional water level change due to discharge (as opposed to tides, etc.) is computed from

$$\frac{\partial \eta}{\partial t} = \frac{Q_R}{A} \quad or \quad \eta(t + \Delta t) - \eta(t) \equiv \Delta\eta = \frac{Q_R}{A}\Delta t \tag{3.9}$$

where Q_R is the discharge (m^3/s) and A is the cell area in the horizontal plane.

Daily averaged river discharge data were obtained for the major tributaries (Alafia, Bullfrog Creek, Braden River, Hillsborough River, Lake Tarpon Canal, Little Manatee River, Manatee River, Rocky Creek, Sulphur Springs, Sweetwater Creek, and Tampa Bypass Canal) from the USGS in Tampa and for the Tampa Bypass Canal from the Southwest Florida Water Management District. The monthly mean discharges for these rivers are plotted in Figure 3.3 and show the sub-tropical cycle with peaks in the summer. Discharge in 1991 was considerably higher than in 1990.

The location of the gaging stations is shown in Figure A.2 (Appendix A). For modeling convenience, some of the tributaries were combined into the effective rivers shown in Figure 2.1: Lake Tarpon Outfall and Sweetwater Creeks with Rocky Creek, Sulphur Springs with Hillsborough River, and Bullfrog Creek with Alafia River.

The total amount of fresh water entering the Bay is larger than that measured at the gaging stations (Flannery, 1989). There are numerous, small streams that are ungaged, and many of the major tributaries that are measured have their gages a considerable distance upstream, beyond tidal influences, and therefore leave out a substantial part of the watershed. The long-term annual mean of the eleven waterways is 35 m^3/s, but estimated total flow from Flannery (1989) was 57 m^3/s and from Goodwin (1987) was 54 m^3/s. Thus the total fresh water inflow may be 60% larger than that from the major tributaries.

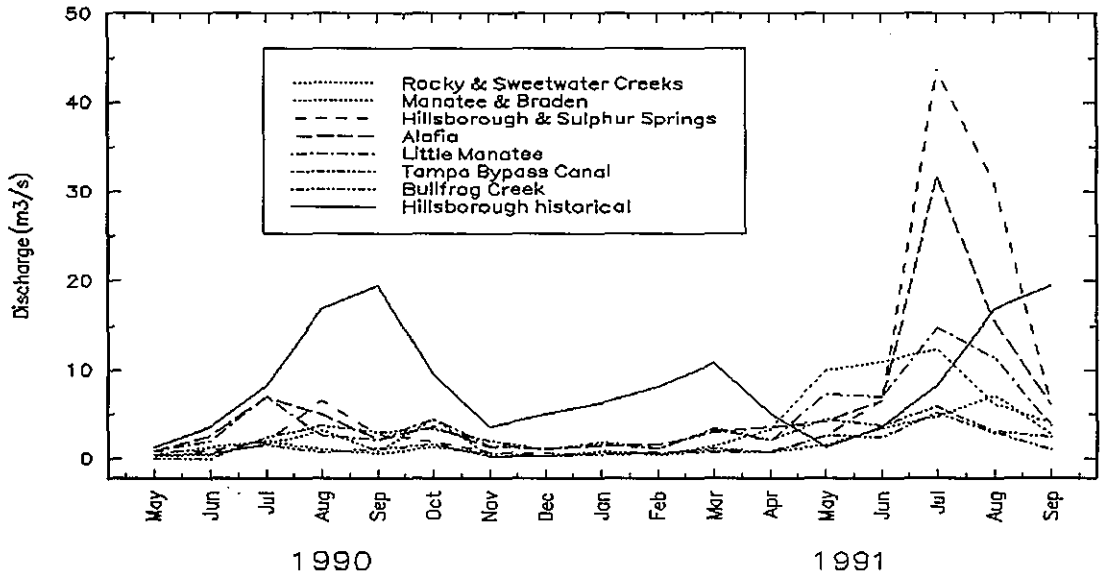

Figure 3.3. Mean monthly discharge for eleven Tampa Bay waterways. Three small waterways in the proximity of large rivers were combined with those rivers. The heavy solid line indicates the historical mean discharge for the Hillsborough River. The annual and interannual signals are similar for all the waterways.

River Density

The boundary conditions for salinity and temperature are based on the conservation principle that change within the boundary cell is equal to flux across the cell surface. This is expressed as:

$$\frac{\partial DS}{\partial t} = \frac{Q_R S_R}{A} \quad or \quad \Delta S = \frac{\Delta\eta}{D}(S_R - S) \tag{3.10}$$

$$\frac{\partial D\theta}{\partial t} = \frac{Q_R \theta_R}{A} \quad or \quad \Delta\theta = \frac{\Delta\eta}{D}(\theta_R - \theta) \tag{3.11}$$

where D is total water depth and $\Delta\eta$ is determined from Eq. 3.9.

River salinity, S_R, is zero. River water temperature, θ_R, is taken (for convenience) to be equal to θ_{ocean}; since temperatures throughout the Bay are strongly determined by atmospheric heat flux, the river temperature does not need to be determined precisely.

3.3. THE AIR-SEA BOUNDARY

Momentum flux is added to the water across the surface by winds, and the atmosphere adds (or removes) heat and water. Winds at the real-time site M-2 were used to estimate the wind stress for the entire Bay. Surface stress as a function of wind speed is parameterized by

$$\frac{\tau_{sx}}{\rho_a} = C_w W_x (W_x^2 + W_y^2)^{1/2} \tag{3.12a}$$

$$\frac{\tau_{sy}}{\rho_a} = C_w W_y (W_x^2 + W_y^2)^{1/2} \tag{3.12b}$$

where W_x and W_y are components of the wind speed at 10 meters and the air density, ρ_a, is taken to be 1.225 kg/m^3. The drag coefficient formulation is taken from Large and Pond (1981); C_w, is a function of wind speed at 10 meters above the water, W_{10}, and is

$$C_w = C_1 + C_2 W_{10} = C_1 + C_2 (W_x^2 + W_y^2)^{1/2} \tag{3.13}$$

where

$$C_1 = 0.0012 \qquad C_2 = 0.0 \qquad \text{for } W_{10} \leq 11.0 \text{ m/s} \tag{3.14a}$$

$$C_1 = 0.00049 \qquad C_2 = 0.000065 \qquad \text{for } W_{10} > 11.0 \text{ m/s} \tag{3.14b}$$

The heat flux across the surface is expressed as a function of air temperature, water temperature, wind speed, solar radiation, and several other variables. Details of the calculation are given in Appendix B. Net precipitation and evaporation are neglected when computing surface salinity.

Wind data were collected at five locations on the Bay and the NOAA data collected at Tampa International Airport were also available. A data file using 10-minute values at M-2 was filtered to produce a time series of 3-hourly values of wind speed, wind direction, and air temperature. Periods of missing data were filled in with data from the airport.

3.4. MODEL INITIALIZATION

At the start of a model run, all values of the time-varying variables must be initialized. Water level and velocity are set to zero. Temperature is set as follows. A value of temperature for any time at a depth of 10 m for the Florida shelf, $\overline{\theta}_{ocean}$, is computed by linear interpolation in time from a set of monthly mean values. For any other depth, the temperature is computed by vertical interpolation using Eq. 3.8b and the values of δ_θ given in Table 3.2. All cells and levels are initialized by setting the cell temperature equal to the ocean temperature at the same depth.

For salinity, values for any time at a depth of 10 m for the Florida shelf, $\overline{S}_{ocean}$, and for Hillsborough Bay, $\overline{S}_{HB}$, are computed by linear interpolation from a set of monthly mean values from S-1 and S-4, respectively. For any other depth, there is a Hillsborough Bay value, S_{HB}, as determined from vertical interpolation using Eq. 3.16 and the values in Table 3.2 as follows

$$S_{HB}(z,t) = \overline{S}_{S\text{-}4}(t) + \delta_s^h(z) \tag{3.15}$$

The salinity at any horizontal location at the same depth is determined by using (1) the ocean value if cell index J is less than 7, (2) the Hillsborough Bay value if the cell index J is greater than 34, or (3) a linear interpolation between the two values for any other cell index values. The pattern of salinity so generated resembles the distribution shown by Boler (1992).

During the first 24 hours of simulation time, boundary water levels and winds are ramped up linearly from zero to their full values. Horizontal density gradients are set to zero during the first 24 hours, and ramped up linearly from zero to their full values during the second 24 hours. Values of all variables are saved at the end of a run so they may be used for initialization at the start of a subsequent simulation.

4. EVALUATION OF MODELED WATER LEVELS AND CURRENTS

This Section describes the sensitivity analysis, calibration, and validation of the model for simulating currents and water levels. Terms are defined and the overall strategy is explained. Although the time-varying density field is included in the simulations, discussion of the calibration for salinity and temperature is deferred to Section 5.

4.1. MODEL EVALUATION

Terminology

The model evaluation process is broadly defined in this report to include the sensitivity analysis and the calibration and validation phases, each of which may not be distinct because steps in the process are usually repeated. In some sense the process is never complete since more data and knowledge continually become available. In Tampa Bay, tidal currents predominate so the evaluation is focused on them. Of secondary importance are the non-tidal currents driven by shelf events, winds, and buoyancy forces, so evaluation will include them only when feasible. For the evaluation process, the model is run with a time-varying density to produce realistic stratification for turbulence generation and dissipation, but the accuracy of the salinity and temperature simulation is addressed in the next Section. The following paragraphs discuss the steps in the model evaluation process and use terminology recommended by the American Society for Testing and Materials (ASTM, 1992).

First, it is assumed that the model is verified, i.e., that in the limit of small time step and grid size the finite difference equations approach the differential equations they were designed to represent.

During the sensitivity analysis, the important model parameters are varied over their expected range to see how the computed solution changes. These parameters, called the adjustable constants, include the grid configuration, bathymetry, time step size, and bottom friction variables. The aim is to gather knowledge on how the modeled solution behaves so the calibration process becomes more efficient. The model is considered to be sensitive if, for a given forcing condition, a small change in a parameter produces a large change in output.

During the calibration phase, certain model parameters are adjusted so the computed solution produces the best match to the observed data. Differences between the data and model output are quantified, and the calibration process continues until (a) predetermined criteria for accuracy are reached, (b) the results are otherwise judged to be acceptable, or (c), if the desired level of accuracy is not reached, the model must be either significantly revised or abandoned altogether. Since Tampa Bay's dominant currents are tidally driven, it is desirable to select calibration and validation data, depending on the results of the field survey, for periods both when wind and other forcings are negligible and when they are strong. Several distinct time periods may be used for the calibration and verification process.

NOS has proposed standards for accuracy for its predictions of water levels and currents (Williams et al., 1989). These values (Table 4.1) reflect the needs of the navigation community. Tampa Bay tides, which have a mean range of 0.7 m, are small by comparison to the standards and the criteria are easily met by the model. Note that these standards rely on statistical analysis of predictions at discrete locations; there is no attempt to validate by comparison of spatial distributions (i.e., patterns) of variables.

Table 4.1. Proposed NOS standards for tidal prediction. For all comparisons of predicted and observed values (for at least 30 days of data), 90 percent of the differences of the following variables should be smaller than the given limit.

	Variable	Limit
For tides	1. amplitude at high water/low water	15 cm
	2. time of high water/low water	15 min
For currents	3. amplitude of maximum flood/ebb current	32 cm/s
	4. time of maximum flood/ebb current	30 min
	5. time of slack before flood/ebb	15 min

During the validation phase, the adjustable constants are fixed at their calibration values, and the model is rerun for other time periods or conditions that are different from those used for the calibration phase. Differences between observational data and model outputs are quantified and compared to the criteria for calibration accuracy. The model is considered to be validated for the specific scenario if the validation accuracy is equivalent to the calibration accuracy. In practice, however, validation accuracy will usually be somewhat less than calibration accuracy since the model has been tuned to the calibration data.

Strategy

Generally, evaluation focuses on observed total water level and current signals, as in Hess and Bosley (1992). However, during the time periods of the calibration and validation discussed by them, only eleven of the 14 water level gages were in operation and only seven of the 29 current meters (which returned useful data) were in operation. In addition, the locations of the instruments was not representative of the whole Bay; four of the current meters (C-2, C-3, C-4, and C-5) were located along the main natural channel for nearly the entire survey, while three current meters (C-20, C-21, and C-23) were located near the entrance of Tampa Bay for at most two months near the beginning of the survey. Therefore, the validation using that set of current meters does not necessarily give a representative assessment of accuracy for the whole Bay. Correction of this shortcoming would require numerous simulations of the entire 15 months for

which data were collected and is therefore too computer intensive to be accomplished in a reasonable time.

One way to reduce computational requirements is to calibrate the model using observed tidal constituents (as was done by Hess [1993]) since they do not vary significantly throughout the year. Modeled constituents can be obtained from harmonic analysis of model output time series. Validation can then be made using the total water level and current signals.

The model was set up to run in the following way. River discharges and variable salinity are included in the tidal simulations, since tidal currents are strongly influenced by vertical momentum mixing, which is in turn a function of the density distribution. River flow data consist of daily values equal to the annual means. Salinity at the oceans was set using annual average values and a vertical distribution as described in Section 3.1. and the salinity of the rivers was zero. Bottom friction is represented by initially setting $z_o = 0.3$ cm everywhere and horizontal viscosity was set according to Eq. 2.15. Winds were set to zero and temperatures were set to isothermal conditions.

4.2. TIDAL CONSTITUENT ANALYSIS

Harmonic Analysis

The astronomical tide is represented as the sum of several tidal constituents (c.f. Eq. 3.4), most of which have periods near 12 and 24 hours. The standard NOS Fourier harmonic analysis (Dennis and Long, 1971) gives a characteristic amplitude and phase for each of 24 constituents. In Tampa Bay, as in most other U.S. coastal areas, the primary constituents are the M_2, S_2, K_1, and O_1, where the number in the subscript represents the approximate number of cycles per day. In the northeast U.S., the M_2 and S_2 constituents are much larger than K_1 and O_1, giving characteristic semidiurnal tides. In the Gulf of Mexico, the amplitudes of the four are similar, giving mixed (partly diurnal and partly semidiurnal) tides. It is the interaction of the diurnal constituents O_1 and K_1 with the semidiurnal terms M_2 and S_2 that produce the diurnal inequality (tropic tides). A record length of 29 days is required to separate the 24 primary constituents. Ten of the constituents are determined directly from the data, while the remaining 14 are calculated from the first 10. Tests performed as part of this evaluation showed that when the analysis method is applied to a time series generated with 24 known constituents, the four major constituents are accurately recovered to within 0.2 cm in amplitude and 2° in phase. For the following discussion, currents were analyzed along their principal direction.

Constituent Comparison Techniques

An objective method of comparing observed and computed constituents is necessary for assessing model accuracy. For a limited number of constituents (four), an index of the total tidal amplitude, $\underline{A}$, from a vector sum of the amplitudes of each of the constituents, A_i, is as follows:

$$\underline{A} = \left[\sum_{i=1}^{4} A_i^2 \right]^{1/2} \tag{4.1}$$

Eq. 4.1 is used to compute a value for the observational data, $\underline{A}_O$, and a value for the model, $\underline{A}_M$. The first comparison statistic is the amplitude gain,

$$G_a = \frac{\underline{A}_M}{\underline{A}_O} \tag{4.2}$$

The second comparison statistic is the estimated time lag (model behind observation) and is computed by

$$L = \frac{1}{4} \sum_{i=1}^{4} \left[\frac{({}^m\kappa_i - {}^o\kappa_i)}{\omega_i} \right] \tag{4.3}$$

where ${}^m\kappa$ is the modeled epoch, ${}^o\kappa$ the observed epoch, and ω_i is the constituent's angular speed.

A third statistic is an estimate of the overall rms error, E, calculated from the constituent amplitudes and phases. As derived in Appendix D, given a cosine series with individual amplitudes, A_i, and epochs, κ_i, and a second series with amplitudes, $A_i + \delta_i$, and epochs, $\kappa_i + \epsilon_i$, then the rms difference between the two is

$$E = \left[\frac{1}{2} \sum_{i}^{4} (Z_i A_i)^2 \right]^{1/2} \tag{4.4}$$

where

$$Z_i^2 = [1 - (1 + \frac{\delta_i}{A_i}) \cos \epsilon_i]^2 + [(1 + \frac{\delta_i}{A_i}) \sin \epsilon_i]^2 \tag{4.5}$$

4.3. SENSITIVITY ANALYSIS

Model output is dependent on initial conditions, grid configuration and resolution, friction parameters, bathymetry, time step size, and boundary conditions; during the course of model development, the effect of many of these were analyzed. For example, model output is dependent on the initial forcing and the computed solution requires an initial spin-up time to stabilize. To minimize unrealistic transient solutions (i.e., initial oscillations that usually damp out after a few days) induced by the sudden forcing of water at rest, during the model spin-up

period, forcings are gradually applied, rising from zero at time T_o to their full strengths a finite time later T_1 using the ramp function r(t),

$$\begin{aligned} r &= 0 && \text{for } t \leq T_o \\ &= \frac{t - T_o}{T_1 - T_o} && \text{for } T_o < t \leq T_1 \\ &= 1 && \text{for } T_1 < t \end{aligned} \tag{4.6}$$

For tides and winds, (T_o, T_1) are (0 h, 24 h) and for buoyancy forcing they are (24 h, 48 h). Tests show that 2 full days are needed for water levels to reduce transients to less that 1% of the total amplitude and 3 full days are needed for currents with density forcing. In one test with river inflow and buoyancy forcing, 4 days were needed for volume transport at the Sunshine Skyway to stabilize.

The grid configuration strongly influences the computed solution. Experimentation with three separate Tampa Bay grids showed that the present grid (Figure 2.1), with its higher resolution, gives better results than either of the two previous grids tested earlier in the study: a square grid having cells 1.8 kilometers on a side (Hess, 1990: Figure 6) and a curvilinear grid having cells averaging 1 kilometers (Hess, 1990: Figure 7). One reason for the higher accuracy may be that the present grid has the most resolution in the cross-estuary direction.

Friction and bathymetry also influence the solution in a systematic way. Previous studies by the author have demonstrated that increasing bottom friction reduces current and water level amplitudes throughout the estuary (but with possibly increased amplitude near the boundary where forcing is applied) with little change in phase. As for bathymetry, increasing water depths speeds the tide wave and thus reduces the phase difference between two locations. Amplitudes may or may not increase as more water is allowed through. Some adjustments of the bathymetry and bottom roughness were made during the validation, although a formal approach such as was done by Lardner et al. (1993) was not pursued.

Several experiments tested the effect of the deep water boundary conditions on the water levels. The boundary conditions were (1) a given time series of values, η(t), (2) the condition of zero water level slope normal to the boundary, and (3) a radiation condition. There was little difference in the computed solution in Tampa Bay between any of the above water level boundary conditions for the barotropic case.

4.4. CALIBRATION

The Benchmark Case

For the first calibration run, the model was forced at the deep-water boundary with a 24-constituent tide (see Table 3.1) and run for 31 days; this case is referred to as the benchmark.

Then the water level and current signals at selected locations throughout the Bay for the last 29 days of the run were harmonically analyzed. Currents were analyzed at the standard NOS prediction depth: 15 feet below MLLW, or half the total depth below MLLW, whichever is smaller.

The amplitudes, phases, and comparison statistics for four constituents for water levels at St. Petersburg (E-520) and for currents at the Sunshine Skyway (C-3) are presented in Table 4.2. The modeled water level constituents are all larger than the observed by from 0.0 to 2.7 cm. Summing the observed and the modeled amplitudes by the method of Eq. 4.1 gives the ratio (Eq. 4.2) G_a = 1.089, meaning that the modeled tide is larger than that observed. The estimated time lag (Eq. 4.3) L is -12.9 min, meaning that the model leads the observed tide.

The rms difference, E, estimated from Eq. 4.4 using the four constituents of St. Petersburg water levels, was 2.8 cm. Using all 24 constituents available for this location gave a value for error of 3.2 cm, so using the four largest constituents accounted for 88% of the total error. The rms error for the total signal for 30 days of hourly values was computed to be 4.7 cm, so the estimate E was 60% of the computed value. For the current, the value of the estimate E was 9.2 cm/s, which was 55% of the value computed from 30 days of 10-minute values.

The analysis shown in Table 4.2 was then extended to include the amplitudes and phases at 14 water level and 29 current stations by computing the G_a, L, and E values for all stations (Table 4.3). One consistency check on the output is that the epochs for the major semidiurnal constituents must be nearly equal (to within about 10°) as must be the epochs for the major

Table 4.2. Comparison of observed and modeled constituents for water levels at St. Petersburg (E-520) and currents at Sunshine Skyway (C-3). A is constituent amplitude (cm or cm/s), k is epoch (degrees), $\underline{A}$ is the mean amplitude, G_a is the ratio of mean modeled to the mean observed amplitude, L is time lag (min), and E is rms error (cm or cm/s) for four constituents.

	M_2		S_2		K_1		O_1		$\underline{A}$	G_a	L	E
	A	k	A	k	A	k	A	k				
St. Petersburg Water Level												
Obs	16.4	53.5	5.2	64.2	15.7	335.8	14.8	329.4	27.60			
										1.089	-12.9	2.8
Mod	19.1	51.5	7.1	63.3	15.7	330.7	15.5	323.6	30.04			
Sunshine Skyway Current												
Obs	48.9	337.7	17.6	345.1	27.2	250.6	21.5	246.6	62.47			
										0.798	-0.8	9.2
Mod	39.6	338.2	14.5	351.4	19.7	250.5	17.9	242.9	49.87			

diurnal constituents; inspection shows that most of them were. At one location, C-40, the model produced a current with an unrealistically large time lag of 491 min; this error was due to the modeled principal current direction being different from the observed. The remedy used in subsequent simulations was to bilinearly interpolate the four closest velocity components to the exact location of the current meter, then vectorially add the components.

For the benchmark case, then, the mean value of the gain G_a (obtained by summing) for water levels was 1.054, the mean time lag L was -3.3 min, and the mean error E was 2.8 cm. For currents, mean gain was 1.212, mean time lag was 12.7 min, and mean error was 10.6 cm/s.

Final Calibration

Numerous additional runs (about 40) with adjustments covering a single time period were carried out in an attempt to improve model results. The first priority was to correct the tide phase. This was attempted by altering mean sea level water depths. Since the original bathymetric data were collected by NOS approximately 27 years ago, it is reasonable to expect that small changes in bottom geometry, such as deepening due to dredging and scouring and filling due to increased sedimentation and construction along the shoreline, may have occurred since then at various locations and rates. The changes to bathymetry were made by multiplication of the initial cell depth values. The best results for phase were obtained by use of the following multiplication factors: 0.9 in the lower Bay, 0.85 in the eastern middle Bay, 0.9 in Hillsborough Bay, and 1.1 in Old Tampa Bay. These changes decrease the Bay's mean depth by about 30 cm.

Additionally, the bottom roughness height z_o was varied. The best results were obtained when z_o was decreased from the original value of 0.3 cm to 0.2 cm nearly everywhere (see Figure 2.4). Experiments with a spatially-varying roughness did not give significantly improved accuracy. With the altered bathymetry and roughness, the results are significantly improved (Table 4.3). In general, water levels are large by 3.9% and the currents are too small by 8.9%. The time lags and estimated errors have been reduced. The model skill is therefore significantly better than that for the benchmark case.

4.5. VALIDATION USING THE WHOLE SIGNAL

Limited Time Series

Now that a calibration has been obtained, the next step is to validate the model using the validation time period and data discussed in Hess and Bosley (1992) (see Appendix E). This was done and the results are shown in Tables 4.4 and 4.5. The new skill scores for water levels were somewhat higher (as much as 1%) than the previous validation scores (Appendix E, Table E.1). The scores for currents were about the same as those in Table 4.3, with the score for time better by 2% but the amplitude score lower by 4%.

Part of the reason for slightly lower current amplitude score is that the model as configured in Hess and Bosley (1992) was optimized for stations in the lower Bay, while the calibration

Table 4.3. Amplitude gains (G_a), time lags (L), and estimated rms errors (E) based on four constituents for water levels and currents for the benchmark case and the final calibration case.

No.	Station	Benchmark Case G_a	Benchmark Case L	Benchmark Case E	Final Calibration G_a	Final Calibration L	Final Calibration E
			Water Levels				
1	E-364	1.028	6.3	1.5	1.038	-1.2	1.3
2	E-520	1.088	-12.9	2.8	1.026	3.7	1.6
3	E-537	1.093	-14.0	3.0	1.035	2.8	2.0
4	E-657	1.091	-27.5	5.1	1.038	-9.7	2.7
5	E-689	1.025	-3.5	1.8	1.034	-7.1	2.0
6	E-217	1.096	-10.8	2.1	1.111	-18.8	2.8
7	E-243	1.033	12.1	1.8	1.033	12.1	1.8
8	E-273	1.095	-7.7	2.1	1.107	-15.3	2.7
9	E-347	1.044	4.7	1.4	1.053	0.5	1.4
10	E-384	1.083	-6.6	2.6	1.039	-4.4	1.6
11	E-428	1.008	20.2	3.2	0.985	19.5	3.0
12	E-641	0.996	1.5	3.3	1.007	2.0	3.4
13	E-667	1.063	-13.4	4.7	1.012	4.4	3.7
14	E-738	1.018	5.5	3.4	1.028	-3.3	3.2
	MEAN	1.054	-3.3	2.8	1.039	-1.1	2.4
	MIN	0.996	-27.5	1.4	0.985	-18.8	1.3
	MAX	1.096	20.2	5.2	1.111	19.5	3.7
	SD	0.035	12.0	1.1	0.033	9.7	0.8
			Currents				
1	C- 2	0.890	-3.7	6.1	0.860	3.4	7.3
2	C- 3	0.798	-0.8	9.2	0.820	10.9	9.0
3	C- 4	0.842	-3.9	5.3	0.953	-2.8	3.4
4	C- 5	1.275	-3.4	10.9	0.949	2.7	4.2
5	C-10	1.235	-31.2	3.6	1.407	-16.8	5.1
6	C-12	0.450	-57.2	7.8	0.980	-50.1	3.1
7	C-14	1.004	-1.7	2.8	1.129	9.9	6.6
8	C-15	1.106	-17.3	4.1	1.126	0.6	5.6
9	C-20	0.688	7.7	11.9	0.737	1.5	10.3
10	C-21	0.664	-23.0	12.0	0.777	-4.2	8.1
11	C-23	0.927	-6.7	3.1	0.978	-7.6	2.5
12	C-27	0.847	101.4	1.5	0.846	11.8	1.3
13	C-30	0.581	-2.8	15.1	0.652	-7.6	12.9
14	C-31	1.179	-24.5	3.4	1.146	-10.2	2.5
15	C-32	1.332	-10.1	6.3	1.242	-11.7	4.8
16	C-33	1.304	-3.8	6.9	1.249	-0.6	5.9
17	C-34	1.348	-9.7	4.6	1.220	-10.1	3.1
18	C-36	0.885	192.8	7.1	1.475	41.0	5.0
19	C-40	1.058	491.2	43.3	1.283	16.4	7.1
20	C-41	0.600	-71.5	21.3	0.955	-6.4	5.8
21	C-42	2.799	18.5	17.0	1.412	-18.0	4.6
22	C-43	2.561	7.0	29.1	0.805	-13.7	4.8
23	C-44	1.294	-42.1	4.8	1.070	18.7	1.8
24	C-46	0.836	-11.7	2.5	1.218	3.9	2.2
25	C-50	2.409	-0.5	20.8	1.479	-20.3	7.3
26	C-51	1.307	3.2	6.8	1.367	-6.4	8.2
27	C-52	2.083	30.0	14.7	1.325	19.7	5.7
28	C-53	1.389	-70.4	12.6	0.931	-13.5	2.6
29	C-54	1.454	-88.5	11.7	1.198	-18.8	4.6
	MEAN	1.212	12.7	10.6	1.089	-2.7	5.3
	MIN	0.450	-88.5	1.4	0.652	-50.1	1.3
	MAX	2.799	491.2	43.3	1.479	41.0	12.9
	SD	0.574	103.6	8.9	0.232	16.3	2.6

Table 4.4. Results of the validation run for currents.

Station		n	R (m/s)	D_{rms} (m/s)	D′	M	G_w	A_{rms} (m/s)	L_m (hr)	L_{rms} (hr)
1	C- 2	1153	1.307	.187	0.14	28	0.677	.278	0.62	0.90
2	C- 3	1062	1.253	.137	0.11	23	0.698	.201	0.42	0.56
3	C- 4	1153	.814	.065	0.08	25	0.879	.065	0.32	0.48
4	C- 5	1153	1.101	.111	0.10	28	0.713	.167	0.39	0.54
5	C-20	1153	1.037	.141	0.14	26	0.619	.212	0.34	0.46
6	C-21	1153	.899	.138	0.15	26	0.634	.178	0.47	0.70
7	C-23	1153	.953	.071	0.07	26	0.850	.079	0.44	0.63
Global Values				.122	0.11		0.723	.170	0.43	0.61
Skill parameters				S_D = 88.6%				S_A = 84.3%	S_L = 90.1%	

Table 4.5. Results of the validation run for water levels.

Station		n	R (m)	D_{rms} (m)	D′	M	G_w	A_{rms} (m)	L_m (hr)	L_{rms} (hr)
1	E-c01	192	.414	.007	.016	26	.999	.001	-.028	.064
2	E-217	193	.425	.032	.076	24	1.058	.023	-.100	.497
3	E-243	193	.440	.040	.091	26	.942	.029	.282	.561
4	E-273	104	.506	.031	.061	9	.985	.032	-.186	.561
5	E-347	193	.434	.021	.048	24	.990	.029	-.002	.480
6	E-364	191	.411	.021	.051	24	1.000	.017	-.060	.299
7	E-384	193	.432	.028	.064	27	.925	.029	-.018	.251
8	E-428	193	.427	.023	.055	26	.959	.022	-.175	.283
9	E-520	193	.455	.032	.070	27	.910	.030	.167	.567
10	E-537	193	.518	.040	.077	27	.900	.039	.192	.482
11	E-657	193	.590	.045	.076	25	.913	.049	.305	.544
12	E-689	193	.638	.050	.078	27	.861	.054	.129	.345
Global Values:				.031	.064		.950	.029	.058	.402
Skill Parameters:				S_D = 93.60%				S_A = 94.00%	S_L = 93.53%	

includes all stations. In addition, the model code and the exact locations where the currents were saved are slightly different from those used in the previous Section.

Estimated Model Error

The accuracy of the new calibration for all station using the statistics developed in the previous Section was estimated as follows. For the currents, the mean value of the estimated rms error

for the 29 stations listed in Table 4.3 is 5.3 cm/s. For the seven stations listed in Table 4.4, mean error is 6.4 cm/s. Since D_{rms} from Table 4.4 is 12.2 cm/s, D_{rms} for all stations is estimated from a simple proportion as

$$D_{rms}|_{all} = (D_{rms} = 12.2\ cm/s)\left[\frac{E_{29\ stations} = 5.3\ cm/s}{E_{7\ stations} = 6.4\ cm/s}\right] = 10.1\ cm/s \qquad (4.7)$$

For the maximum flood/ebb amplitude error, the ratio A_{rms}/D_{rms} from Table 4.4 is 1.39. Using this ratio and D_{rms} from Table 4.4, A_{rms} for all stations is estimated to be 14.0 cm/s. The statistics for water levels were estimated the same way and the results are shown in Table 4.6.

Table 4.6. Estimated rms hourly amplitude differences and extrema amplitude differences for all stations in Tampa Bay. Inferred values are underlined.

Variable	Number of Stations	E	D_{rms}	A_{rms}
Current	7	6.4 cm/s	12.2 cm/s	17.0 cm/s
	29	5.3 cm/s	<u>10.1</u> cm/s	<u>14.0</u> cm/s
Water Level	11	2.4 cm	3.3 cm	3.2 cm
	14	2.8 cm	<u>3.9</u> cm	<u>3.7</u> cm

4.6. CONCLUSIONS

The present version of the code has been significantly improved over the one used by Hess and Bosley (1992) by (a) horizontally interpolating within the cell to better match the current meter location, (b) vertically interpolating to match the current meter depth, (c) including a variable horizontal eddy viscosity, and (d) adding certain cells to the grid to account for some sub-grid scale features (channels and passes). The simulated tide range in the new calibration is significantly better than the old; in the earlier version, the minimum tide range was predicted to be at Mullet Key, while in the new version it was predicted to be near Point Pinellas, close to where NOS observational data indicates it actually is. For these reasons, the new calibration is accepted as being an improvement over the old.

It is also apparent that for some locations the present model grid lacks spatial resolution. These locations are the narrow openings in causeways and the portions of the navigation channels. The model grid was constructed in such a way that additional rows and/or columns could be added without too much difficulty, if necessary, to improve resolution.

Overall, the model simulates water levels and currents as well as other models do. A comparison of the results from several validation studies is summarized in Table 4.7. Since the tide and current range differ widely among estuaries, mean rms differences, D_{rms}, were normalized by the mean range. For Long Island Sound, only the east-west currents were included since currents were not analyzed along the principal direction. Rms water level errors in Chesapeake Bay are relatively large due to significant phase errors at the head of the estuary (Havre de Grace).

Table 4.7. Comparison of results from several modeling studies.

		Water Level			Current		
Location	Source	D_{rms} (cm)	Range (cm)	$\frac{D_{rms}}{Range}$	D_{rms} (cm/s)	Range (cm/s)	$\frac{D_{rms}}{Range}$
Tampa Bay	This Report	3.9	56.0	0.070	10.1	60.3	0.167
Long Island Sound	Schmalz et al., 1994	7.8	125.7	0.062	18.8	90.9	0.207
Chesapeake Bay	Johnson et al., 1991	15.2	48.3	0.315	14.4	95.0	0.152
Tampa-Sarasota Bays	Peene & Sheng, 1992	4.3	53.6	0.080	19.1	108.8	0.176

5. EVALUATION OF MODELED SALINITY AND TEMPERATURE

5.1. INTRODUCTION

The goal of this Section is to validate the model for salinity and temperature. There are few published standards for accuracy, but if (for example) environmental modeling were important, perhaps maximum rms salinity errors would be on the order of 1 or 2 psu and maximum rms temperature differences on the order of 1 or 2°C. Overall, the purpose of the simulation is to reproduce the major scales of variability. As shown by the data (Figure 5.1), there are significant annual and interannual variations in Hillsborough Bay, where a long time series of

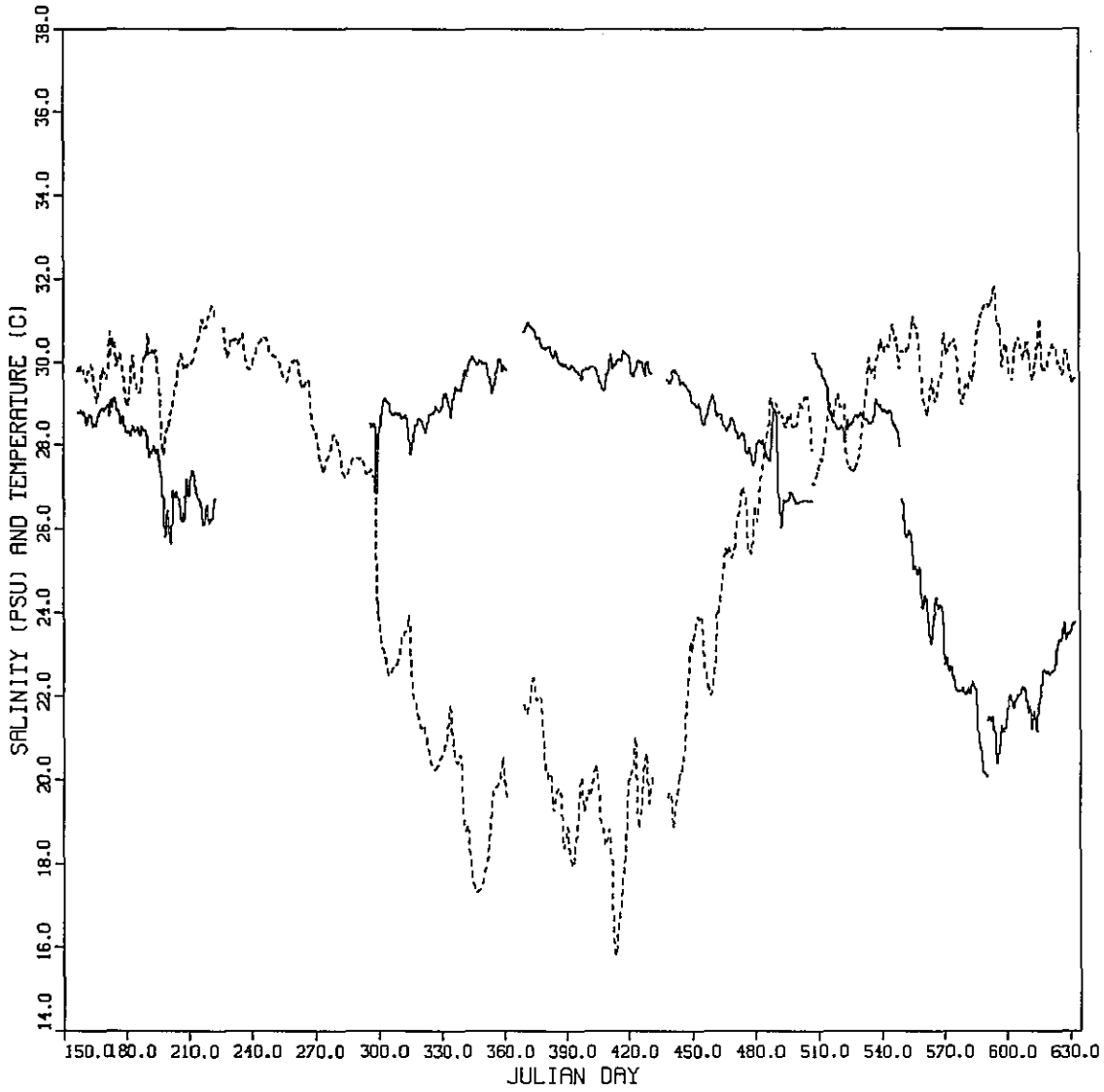

Figure 5.1. Near-bottom salinity (solid line) and temperature (dashed line) at stations representating the southern end of Hillsborough Bay starting from Julian Day 150 in 1990.

observations is available. The CTs in Hillsborough Bay at S-4 (Figure A.1) were attached to the base of the southern C Cut Channel range marker just south of the entrance to the Bay and west of the Apollo Beach pier. During several deployments they collected data at 10 min-intervals to produce a long, relatively high quality data series. Values shown were 25-h boxcar filtered to remove tidal variations. Because of some data gaps, salinity and temperature data for days 156 to 222 was taken at the CT at S-3, which was located near C-31 (Figure A.1). Temperature data for days 225 to 361 was taken from the CT at C-4. The plot (Figure 5.1) shows the salinity and temperature near the bottom for the entire survey. Days 300 to 600 contain the longest, nearly-continuous data series, so the modeling will focus on this period.

The salinity at S-4, from the 1991 measurements at 1.5 m and 4.0 m below MSL in 5.0 m of total water, is only slightly stratified (Figure 5.2). However, some problems in data quality are evident. For example, the bottom salinity in the second deployment, between days 70 and 140, appears to drop off over time, especially after day 100. During the last two deployments, from day 180 to 265, the bottom salinity appears to be about 1 psu lower than the surface salinity (abnormally low salinities are indicative of biofouling). Therefore, in the comparisons that follow, salinity from the near-surface gage will be used for the second deployment.

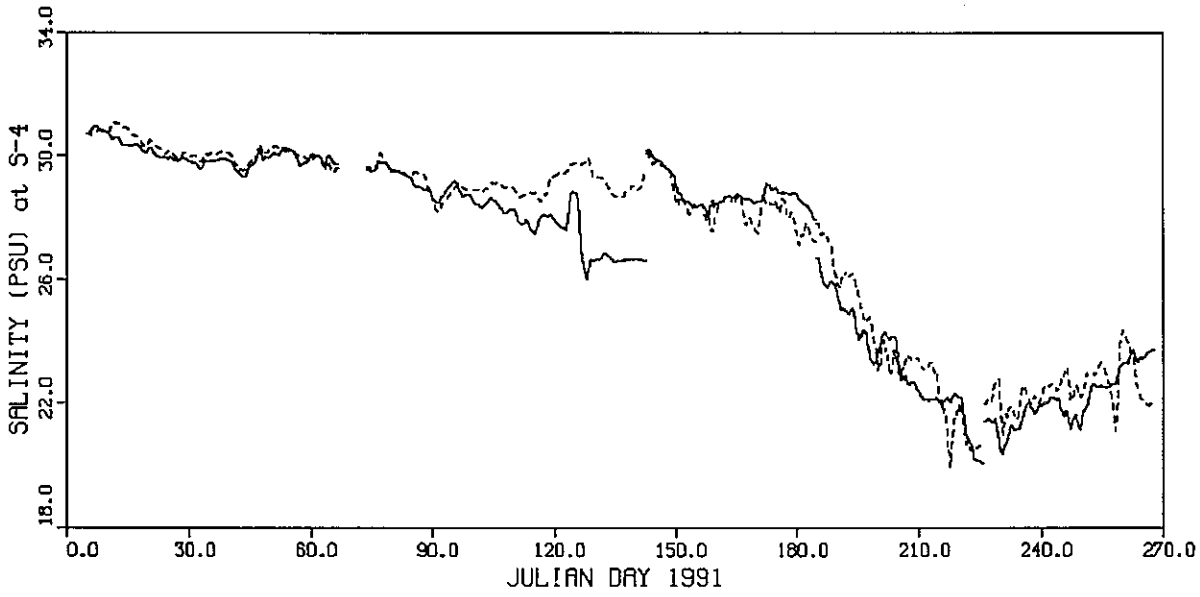

Figure 5.2. Near-bottom (solid line) and near-surface (dashed line) salinity at S-4 during 1991.

Over the course of the year, the primary factor effecting salinity in Tampa Bay is river inflow (Zervas, 1993), although changes on the west Florida shelf can have an impact. The primary factor effecting water temperature is atmospheric heat flux, which is strongly dependent on air temperature and wind speed. Figure 5.3 shows plots of river flow, air temperature, and wind speed for June 1, 1990 (Julian day 152), to September 22, 1991 (Julian day 630). For the river flow, combined daily flow from three Hillsborough Bay tributaries (the Palm River/Bypass Canal, and the

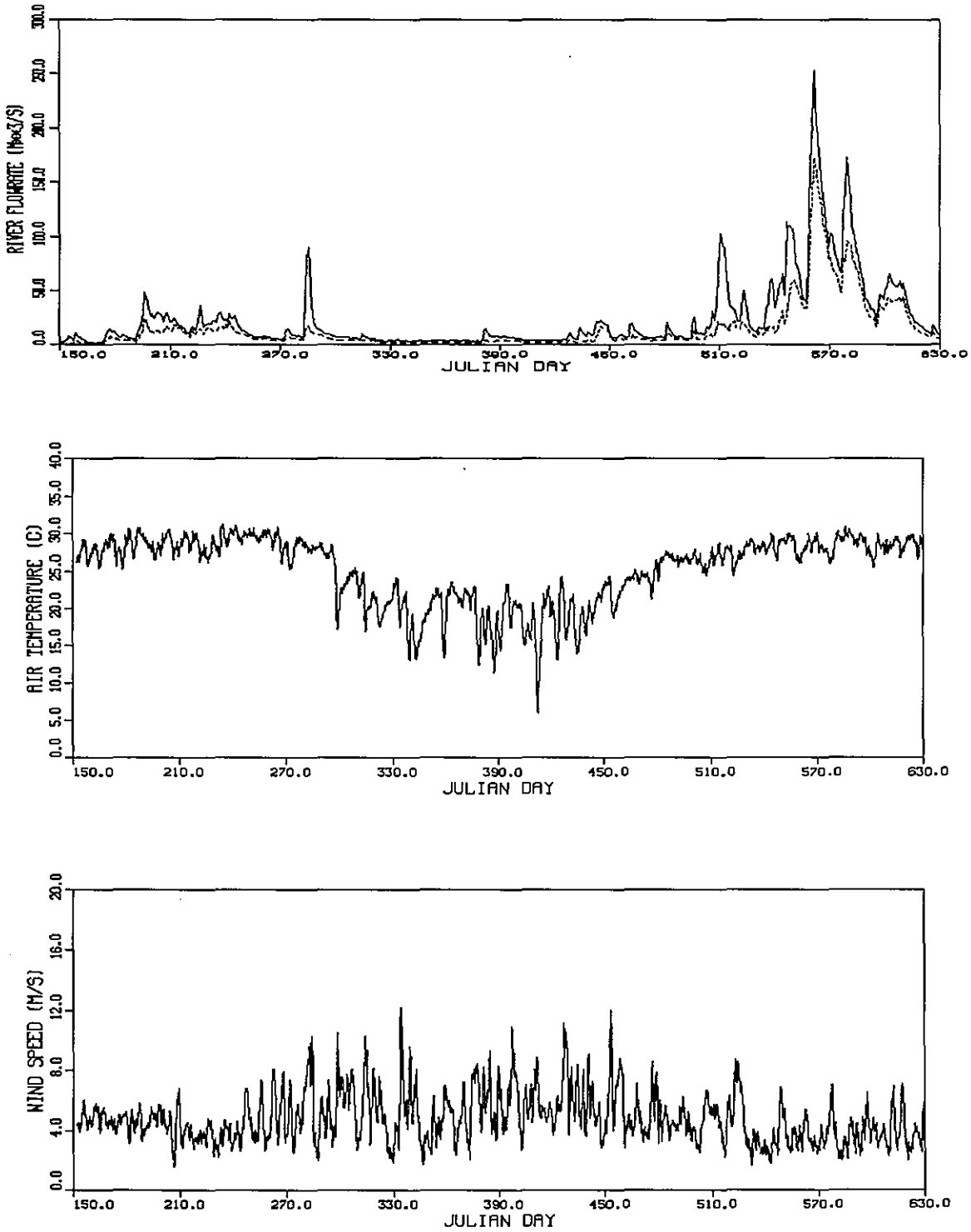

Figure 5.3. The primary Tampa Bay environmental forcing variables during 1990 and 1991: (top panel) daily total river flow rates (solid line) and the sum for Hillsborough Bay tributaries (dashed line), (middle panel) air temperature, and (bottom panel) wind speed.

Hillsborough and Alafia) are plotted, plus the total which includes four more (Rocky Creek and the Little Manatee, Manatee, and Braden Rivers).

The heat flux formulation used in these simulations is explained in Appendix B (in previous simulations, heat flux was set to zero). The main atmospheric variables determining heat flux are air temperature, wind speed, relative humidity, cloud cover, water temperature, and air pressure. Additional variables are albedo of the water and surface emissivity. Of these, air temperature and wind speed are available from observations at M-2 (or the airport) and water temperature is available from the model. The other variables were set to fixed values (see Appendix B, Eq. B.19).

5.2. EVALUATION EXPERIMENTS

The Benchmark Case

The set of model runs for the benchmark case covered the period of January 1 to mid-September, 1991, in 35-day segments; the model was run as calibrated for water level and current and with standard heat flux coefficients to produce a benchmark case. Figure 5.4 shows the results of this simulation. Hourly modeled salinities were 25-h boxcar filtered. At the beginning, modeled values rapidly approached the observed values (within 10 to 15 days), then remained within about 1 psu or less of the observed for the next few months. The modeled salinity spike of more than 1 psu around Day 89 (March 30, 1991) corresponded to a sudden increase in modeled water temperature due to the presence of warm air and strong winds. The rapid drop in modeled salinity around Day 153 (June 2, 1991) accurately simulated the observed change due to the large, rapid increase in river discharge.

Modeled and observed hourly values were compared as follows. For each modeled value, the closest observed value within 0.5 h was selected. The rms difference was computed by Eq. E.1 (Appendix E) and the mean difference, D_m, by

$$D_m = \frac{1}{n}\sum_{i=1}^{n} (\hat{y}_i - y_i) \tag{5.1}$$

where $\hat{y}_i$ is the modeled and y_i is the observed value. Additional comparison statistics are the mean absolute difference, D_a, and the relative error, ϵ_r, as defined by

$$D_a = \frac{1}{n}\sum_{i=1}^{n} |\hat{y}_i - y_i| \tag{5.2}$$

$$\epsilon_r = \frac{D_a}{\frac{1}{n}\sum_{i=1}^{n} y_i} \tag{5.3}$$

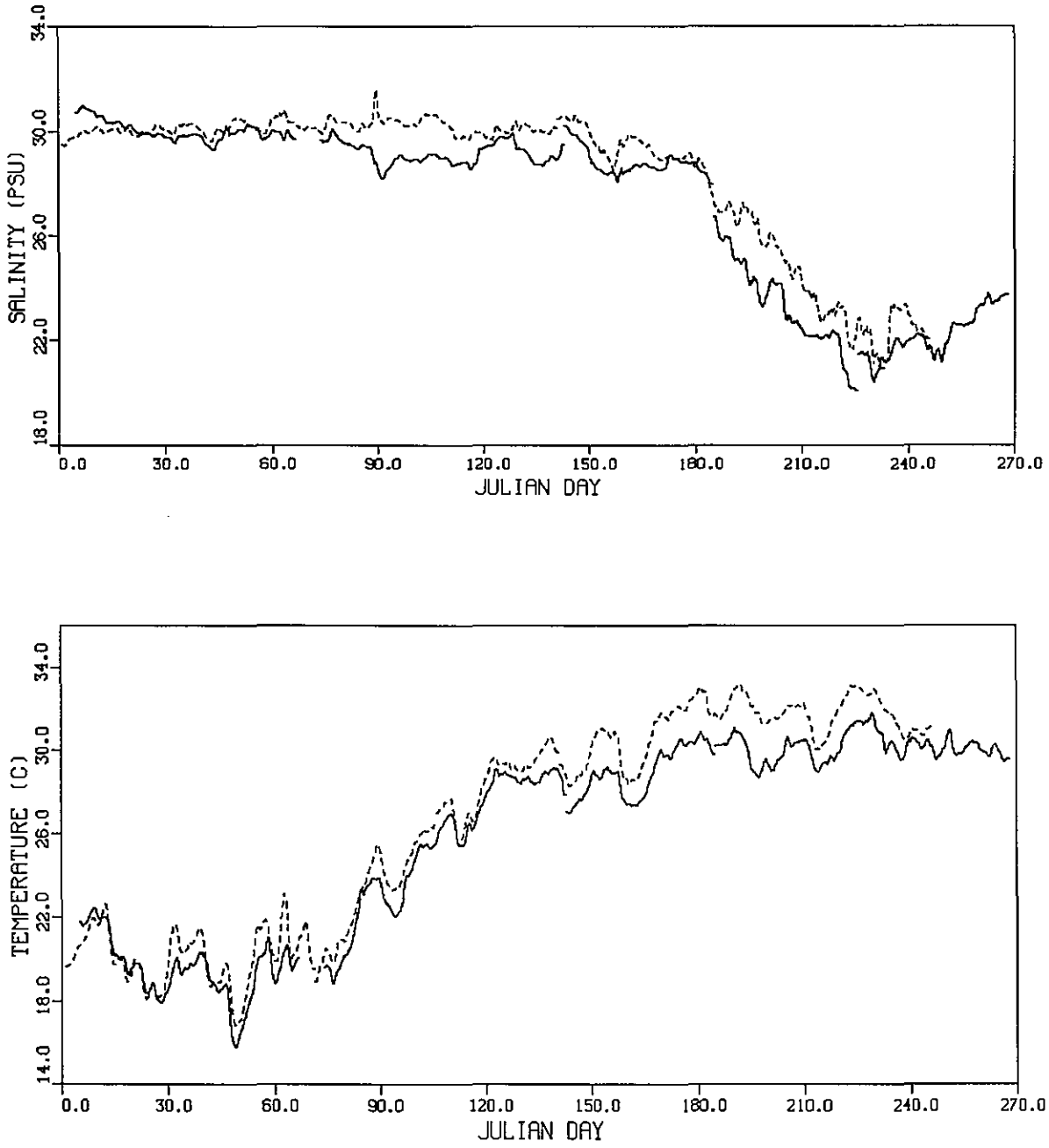

Figure 5.4. For the benchmark run, observed (solid line) and modeled (dashed line) salinities (top panel) and temperatures (bottom panel) vs. Julian days in 1991 at S-4. Data are from a CT near the bottom of the water column, south of the entrance to Hillsborough Bay during 1991.

The results are shown in Table 5.1. The mean salinity difference for the entire set of data (238 days, from Day 5 to Day 246, excluding gaps between deployments) for the benchmark run was 1.09 psu, indicating that the modeled salinity was a little high. Modeled temperatures quickly approached the observed values within 10 days, and then followed the observed to within 0.5°C or less until Day 30 when the water warmed to from 1 to 2°C above the observed and remained there for the remainder of the simulation. In 1991, the minimum modeled and observed temperature occurred at Day 50. The mean temperature difference was 1.21°C, so the modeled temperatures are somewhat too high.

Table 5.1. Mean absolute error, mean biased error, relative error, and rms differences between hourly modeled and observed salinities and temperatures at S-4 for the benchmark run. A positive mean difference indicates that the modeled value is higher than the observed. The data were from Julian days 4.75 to 246 in 1991 (data from days 176 to 195 were not used).

Variable	Hours	D_a	D_m	ϵ_r	D_{rms}
Salinity	5170	1.17	1.09	0.043	1.51
Temperature	5170	1.09	1.21	0.043	1.25

The Calibration Run

Results from the benchmark run indicate that salinity was slightly high during the time Julian day 180 to 240. High salinity is indicative of too little fresh water input. Flannery (1989) notes that on most of the tributaries the USGS discharge gages are placed far up the waterway to avoid tidal influences; therefore, significant areas of the watershed are ungaged. The annual average discharge, based on data available for the last 20 years, for the 11 rivers included in this study is 35 m^3/s (Zervas, 1993): according to Goodwin (1987), the adjusted total is 54 m^3/s (1,904 ft^3/s), or 54% higher than the unadjusted average. Therefore, for the calibration run modeled flow in each river was increased by multiplying the daily flow input value by 1.50.

Temperatures were too high by about 1°C. The plot (Figure 5.4) indicates that the water warms too much after a rise in air temperature, and does not fall enough after a drop in air temperature. Therefore, for the calibration run, the bulk heat flux coefficient, C_d, was modified from its constant value of 0.003 to

$$\begin{aligned} C_d &= 0.004 \quad for \quad T_{air} \leq T_{water} \\ C_d &= 0.001 \quad for \quad T_{air} > T_{water} \end{aligned} \tag{5.4}$$

which reduces the coefficient during times of stable thermal stratification and increases it during unstable conditions. The observed and modeled values for the calibration run are shown in Figure 5.5 and the statistical comparison is shown in Table 5.2. The mean and rms salinity differences are smaller than for the benchmark run. Temperature differences are both significantly smaller.

Table 5.2. Mean absolute error, mean biased error, relative error, and rms differences between hourly modeled and observed salinities and temperatures at S-4 for the calibration run. A positive mean difference indicates that the modeled value is higher than the observed. The data were from Julian days 4.75 to 246 in 1991 (data from days 176 to 195 were not used).

Variable	Hours	D_a	D_m	ϵ_r	D_{rms}
Salinity	5170	1.03	0.25	0.038	1.36
Temperature	5170	0.61	0.24	0.024	0.76

Validation

It was decided that the salinity from the benchmark run and the temperature from the calibration run constitute the best of each simulation. Since salinity and temperature variations are relatively independent (except possibly through evaporation), it was decided not to run additional simulations but to use the results from the previous simulations. Validation can now proceed by comparing modeled and observed time series from stations other than S-4. During 1991 there were 25 near-bottom CT stations. Because of the proximity of some stations and the lack of modeled values at others, comparisons were made at 12 stations; the results are shown in Table 5.3.

In the mean, modeled salinity was 0.46 psu above observed salinity and modeled temperature was 0.35°C above observed. Rms differences were 1.10 psu and 0.88°C, respectively. The salinity error at C-22 is the largest and is probably due to the lack of a connection to Sarasota Bay, thereby forcing relatively fresh water from the Manatee River to pool in the area rather than exiting to the south.

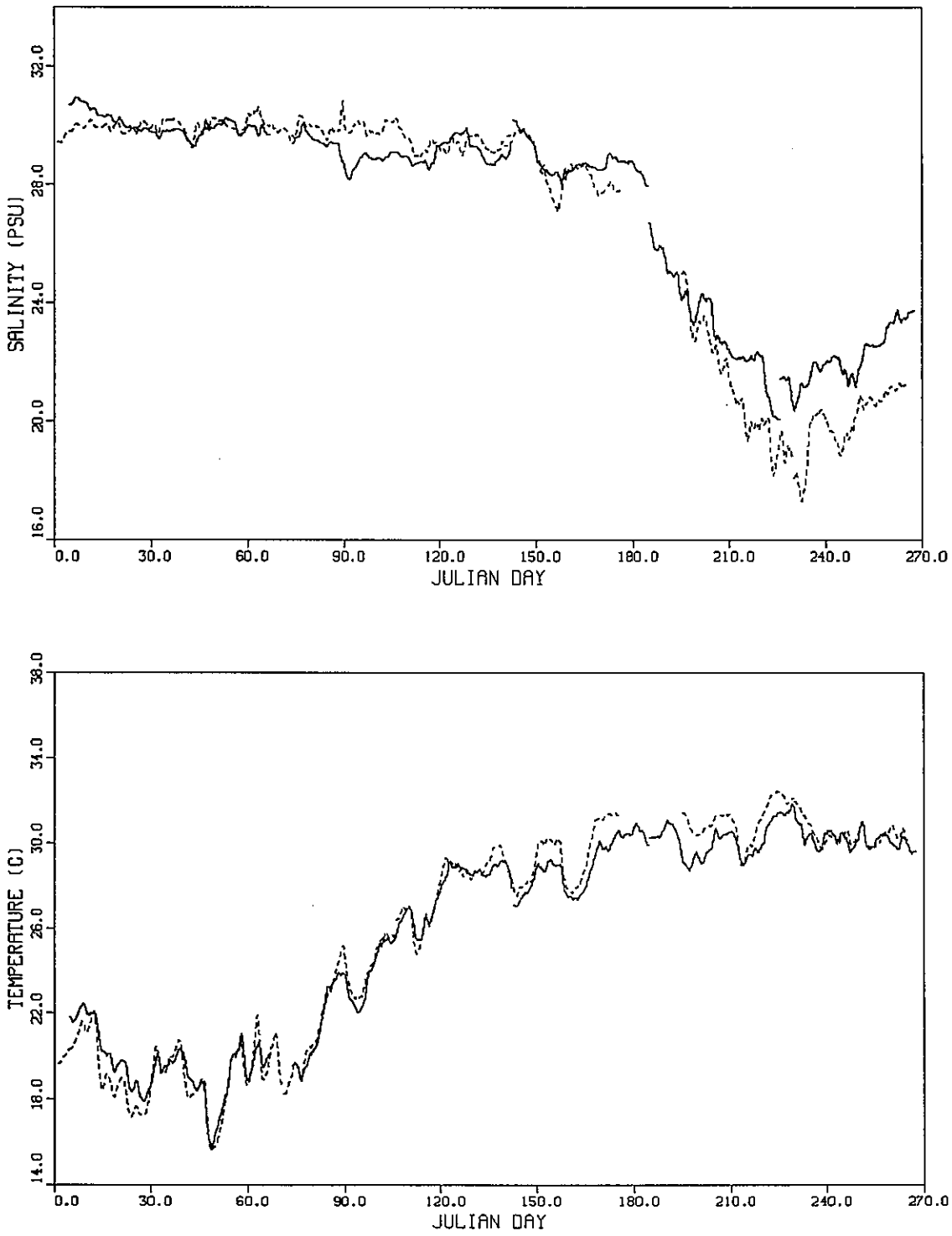

Figure 5.5. For the calibration run, observed (solid line) and modeled (dashed line) salinities (top panel) and temperatures (bottom panel) vs. Julian days in 1991 at S-4.

Table 5.3. Differences between hourly modeled and observed salinity and temperature for the validation run. Average values were obtained by weighting individual station results by the number of hours.

	Salinity					Temperature				
Sta.	Hrs	D_a	D_m	ϵ_r	D_{rms}	Hrs	D_a	D_m	ϵ_r	D_{rms}
S-2	4718	1.17	1.12	0.037	1.30	4719	0.74	0.74	0.028	0.86
C-2	4138	0.54	0.00	0.016	0.72	5734	0.76	0.28	0.030	0.92
C-4	3842	0.70	0.45	0.022	0.97	4888	0.86	0.68	0.033	0.97
C-5	5643	1.26	0.69	0.045	1.69	5718	0.94	-0.03	0.036	1.07
C-22	343	2.29	-2.29	0.070	2.37	343	1.03	1.03	0.034	1.13
C-26	341	1.52	1.16	0.057	1.68	797	0.53	0.50	0.018	0.61
C-31	625	0.89	0.63	0.031	1.09	625	0.89	-0.57	0.045	1.01
C-33	1261	0.73	-0.73	0.024	0.78	1480	0.46	-0.25	0.024	0.59
C-34	1345	1.07	1.07	0.038	1.09	1500	0.47	-0.12	0.025	0.59
C-44	1633	0.54	0.47	0.018	0.64	1676	0.62	0.60	0.025	0.70
C-46	1681	0.34	-0.15	0.012	0.40	1681	0.51	0.35	0.021	0.61
C-54	925	0.38	0.17	0.011	0.47	683	0.97	0.97	0.034	1.08
Averages		0.89	0.46	0.029	1.10		0.76	0.35	0.030	0.88

5.3. CONCLUSIONS

Overall, the salinity and temperature are simulated to a high degree of accuracy. By comparison, the Tampa Bay results are somewhat less accurate than those obtained from a model of Long Island Sound (Schmalz et al., 1994). In that study, the rms errors were found to be 0.6 psu and 0.7°C. For Galveston Bay, Berger et al. (1994) reported mean salinity errors of -1.10 ppt (i.e., model lower than observed) and a mean absolute error of 2.09 ppt (1 ppt is virtually identical to 1 psu). For the main stem of the Chesapeake Bay, Johnson et al. (1991) reported that the mean salinity error was 0.23 ppt and mean temperature error was -1.21°C. Rms errors were 1.90 ppt and 1.79°C, respectively. The errors in the tributaries were somewhat higher. These comparisons are summarized in Table 5.4.

For the Tampa Bay model, accuracy for the salinity may potentially be increased by (a) using altered river inflows (i.e., using a factor greater than 1.5) and (b) using the actual daily salinity data for the ocean boundary condition rather than values interpolated from monthly means. The accuracy for temperature may potentially be increased by (a) improving the cloudiness data and formulation; (b) further modifying the heat exchange coefficient, C_d; and (c) adding

heat flux through the bottom as a way to reduce the large variations in temperature that accompany synoptic-scale changes.

Table 5.4. Comparison of salinity and temperature errors in the Tampa Bay model and those from models of other bays. The symbol "-" means no statistic was available. Salinity statistics from Johnson et al. (1991) and Berger et al. (1994) were in ppt.

		Salinity Errors (psu)			Temperature Errors (°C)		
Location	Source	D_a	D_m	D_{rms}	D_a	D_m	D_{rms}
Tampa Bay	This report	0.89	0.46	1.10	0.76	0.35	0.88
Long Island Snd	Schmalz et al., 1994	-	-	0.67	-	-	0.77
Chesapeake Bay	Johnson et al., 1991	1.73	0.33	2.15	1.73	-1.46	1.99
Galveston Bay	Berger et al., 1994	2.09	-1.10	-	-	-	-

6. DEVELOPMENT OF A TIDAL CURRENT ATLAS

6.1. INTRODUCTION

NOS is replacing its present tidal current charts with computer-generated atlases. NOS publishes several volumes of tidal current charts for selected coastal estuaries and bays, including the *Tampa Bay Tidal Current Charts* (National Ocean Survey, 1979). The charts have a standard format that consists of a set of hourly plots of instantaneous water current vectors at numerous locations covering one typical tidal cycle and include a table for adjusting speeds for a given tide or current range. A proposed, computer-generated *Tampa Bay Current and Water Level Atlas* is under development and is patterned after the Delaware Bay atlas (Parker and Patchen, 1987) and Long Island Sound atlas (Wei, 1993). The atlas is to replace the present current charts and will have the standard paper chart format. Scale factors will be related to daily predictions, such as current speeds at the SSB. Current and water level accuracy should be related to proposed NOS prediction standards (see Table 4.1): 32 cm/s for currents and 15 cm for water levels (Williams et al., 1989). The computer-generated atlas is expected to be more accurate than the present charts because more observational stations are used, the data collected at each station are of higher accuracy and longer duration, and the numerical model was used to synthesize the observational data. Potentially, meteorological forcing could be included in the atlas and the charts could be digitized for desktop computer access.

Because the tides in Tampa Bay are mixed, the production of a paper atlas for the Bay requires a new approach and the development of new methods. Tides and currents in all U.S. estuaries for which NOS tidal current charts have been published are semidiurnal (dominated by the M_2 tidal constituent) and therefore on the average have a 12.42-hour period between successive floods or successive ebbs. However, the tidal currents in Tampa Bay are mixed (i.e., they have a strong diurnal component), so during some 12.42-hour cycles the ebbs are missing (i.e., the ebbs have a zero or negative value) (Figure 6.1). Thus there are semidiurnal cycles (flood-ebb-flood) and diurnal cycles (flood-flood-flood-ebb). Mixed currents occur at certain locations because the sum of amplitudes of the major diurnal tidal constituents (K_1 and O_1) are approximately equal to the sum of the amplitudes of the major semidiurnal constituents (M_2 and S_2). Diurnal currents are most pronounced when the moon is at maximum northern or southern declination (latitude above earth's equator). The period of this lunar variation is called the tropical month and is approximately 27.32 days. During the 70-day period analyzed in this study, 16.7% of the current cycles at SSB were diurnal. Also, in most diurnal current cycles in Tampa Bay, the first flood peak is stronger than the second. Because of the presence of the diurnal cycles, the atlas may need additional charts as well as the 13 normally shown in embayments with semidiurnal tides. Although the final atlas will have water levels, this Section focuses on techniques needed for the prediction of the astronomical tidal currents.

6.2. DESCRIPTION OF CURRENT REGIMES

The currents in Tampa Bay were analyzed to identify current regimes. The first step was to run the model for two 35-day periods (August 17 to September 21 and September 21 to October 26,

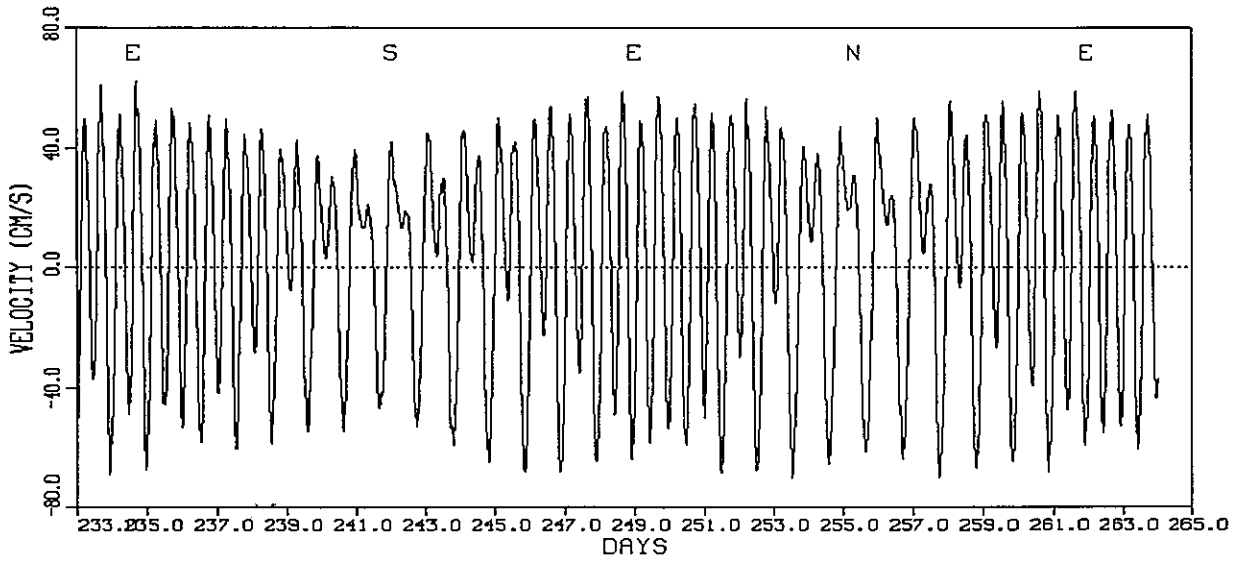

Figure 6.1. Currents at 4.6 m below MLLW at Sunshine Skyway Bridge for August 22 to September 22, 1990. Times of phase of lunar declination are shown; E is over the equator, S is maximum south declination, and N is maximum north declination.

1990); these simulations are denoted as Runs A and B. Run A covers the same time period examined by Hess and Bosley (1992) and Run B was made to gage the effect on accuracy of using a different time period. For this analysis, the model was driven by a reconstructed astronomical tide at the Florida shelf boundary, i.e., the tide was generated from constituents analyzed from 15 months of pressure-sensor records at an offshore station. The runs also included annual mean river flows for five major rivers and salinity at the shelf based on CTD measurements; water temperature was held constant and winds and atmospheric pressure effects were set to zero. The three-dimensional velocity and salinity fields were updated each 2 minutes and the computed eastward and northward components of currents at NOS prediction depth (15 feet below MLLW or half the water depth below MLLW, whichever is smaller) horizontally interpolated to coincide with Project locations were saved at 10-minute intervals to correspond with current meter records. A plot of typical flood current vectors is shown in Figure 6.2.

Based on a preliminary analysis of model-generated tidal current fields, the current regimes over 13 hours following slack before flood (SBF) are characterized as follows. During a semidiurnal tidal cycle, currents in Old Tampa Bay (OTB), which is the embayment northwest of station C-5 shown in Figure A.1, lag those on the lower Bay by 2 to 4 hours. Thus in a typical cycle flood in the lower Bay is followed a few hours later by flood in OTB and 6 hours later ebb in the lower Bay is followed by ebb in OTB. During a diurnal tidal cycle, the situation is different. As before, flood in the lower bay is followed a few hours later by flood in OTB. However, 6 hours later, although there is no true ebb in the lower bay (only a weak flood), OTB still follows

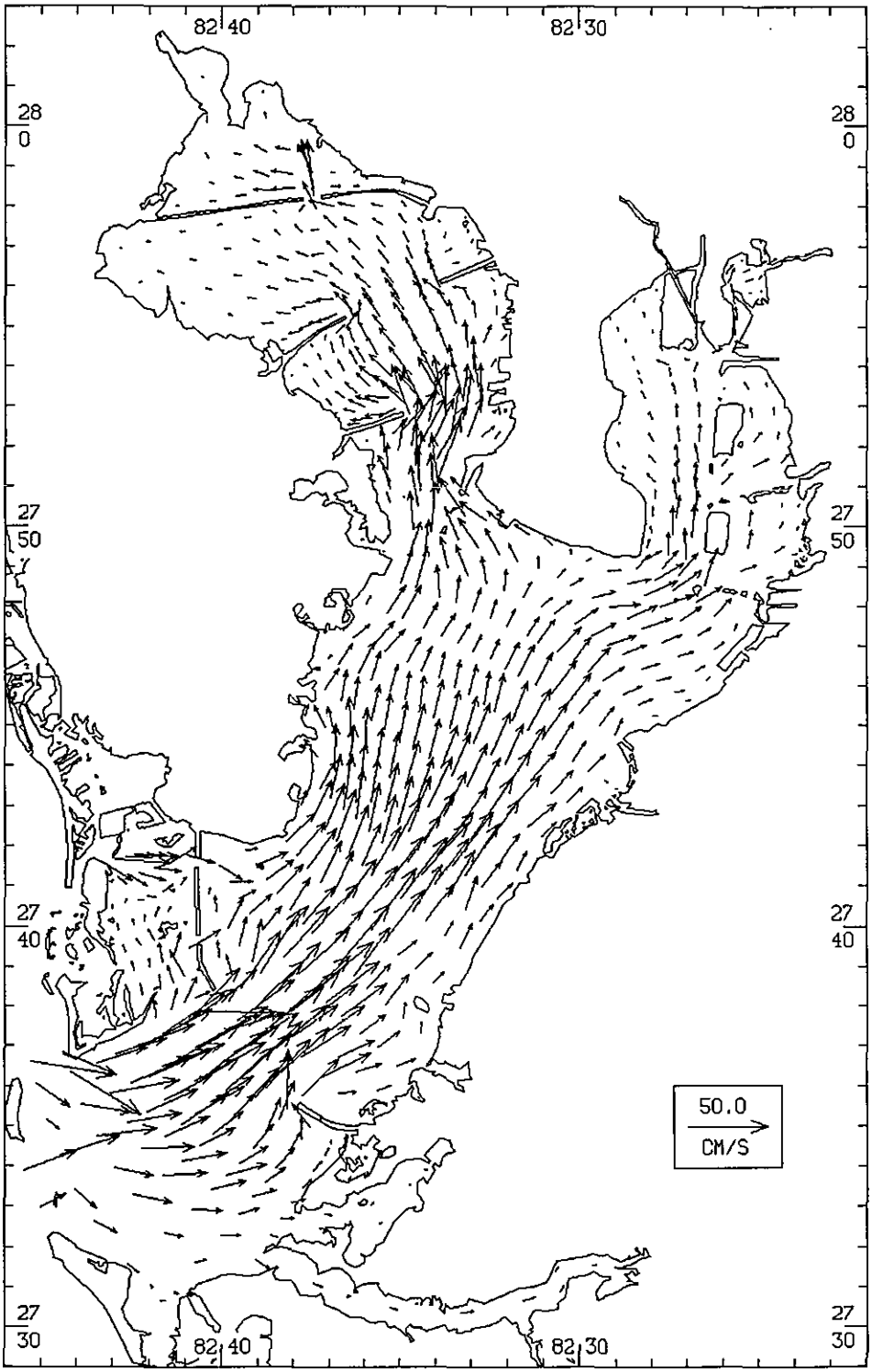

Figure 6.2. Modeled current vectors representing a time near maximum flood current in a typical semidiurnal tidal cycle at NOS prediction depth.

(for a short time) with an ebb, and then returns to flood. Thus there are two distinct evolutions of current patterns.

The method tested here used three sets of (approximately) hourly charts, one for a semidiurnal flood, one for an ebb, and one for a diurnal flood. The specific set to be used (semidiurnal or diurnal) was determined by the character of the of currents at SSB. The following Sections describe the prediction method and explain the results of tests for accuracy.

6.3. METHODS FOR ANALYSIS AND PREDICTION

Flood and Ebb Categories

Modeled currents, v_m, at SSB were analyzed for each of the two runs and divided into individual current floods and ebbs, depending on the direction of the current from one slack water, T_s, to the next, T_{s+1}. Since the currents in Tampa Bay are reversing and nearly rectilinear, only the currents along the principal component direction at each station were analyzed. Individual floods were then categorized as either semidiurnal (duration less than 12 hours) or diurnal (duration greater than 12 hours). For Run A there were 38 semidiurnal floods, 9 diurnal floods, and 47 ebbs and for Run B there were 40 semidiurnal floods, 8 diurnal floods, and 47 ebbs. Overall, therefore, 17.9% of the floods were diurnal.

Modeled currents in each flood and ebb (defined at SSB) at all stations were then time-stretched into one of two standard durations as follows. Each semidiurnal flood and each ebb was divided into six equally-spaced intervals starting at the beginning slack and ending at the following slack; only the velocities at the start of each of these six intervals were saved. The number of intervals (six) is approximately equal to the number of hours in half the M_2 tidal period. Similarly, diurnal floods were divided into 18 equal intervals, which is the approximate number of hours in a diurnal flood. Thus the standardized times that velocity was saved in each current phase was

$$\tau_{is} = T_s + (T_{s+1} - T_s)\frac{(i - 1)}{n} \qquad \text{for i = 1, 2, ...,n} \qquad (6.1)$$

where T_s is the observed time of the preceding slack at SSB, T_{s+1} is the time of the next slack, i is the time index, and n is either 6 for ebb or semidiurnal flood or 18 for diurnal flood. Mean modeled tidal currents were then found for each category by summing the values for each standardized time in the category and dividing by the total number in the category. The mean modeled tidal current is denoted by V_{ijk}, where i is the time index, j is the location, and k is the category (k=1 for semidiurnal flood, k=2 for ebb, and k=3 for diurnal flood). It is these mean currents that will be eventually depicted in the atlas. The mean tidal currents at SSB in each category for Run A are shown in Figure 6.3.

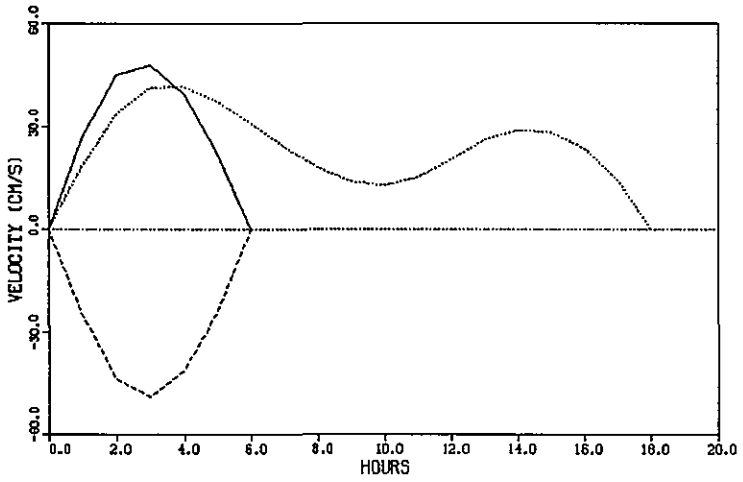

Figure 6.3. Mean tidal currents at 4.6 m below MLLW at Sunshine Skyway Bridge for the semidiurnal flood (solid line), ebb (dashed line), and diurnal flood (dotted line).

Scale Factors

The predicted currents at any time or location using the atlas currents are constructed as follows. For a selected location j, the atlas-predicted current, c_{ij}, at time index i is

$$c_{ij} = S_f V_{ijk} \tag{6.2}$$

where S_f is a scale factor that is constant over the current phase (flood or ebb). The mean velocities, V_{ijk}, are in effect a set of basis functions. S_f is computed from the predicted current speed at SSB, v_p, for that phase and the speed of the mean current as follows:

$$S_f(v_p) = \frac{\max|v_p|}{\max|V_{ijk}|} \qquad (\text{v, V, k at SSB}) \tag{6.3}$$

Here v_p represents flood and ebb speeds from the daily predictions at SSB from the NOS *Tidal Current Tables*, although during the testing for accuracy the observed current at SSB, v_o, and the modeled current, v_m, were also used. The time for which the prediction is valid, τ_{is}, corresponding to the time index, i, is computed from Eq. 6.1 and T_s are the predicted times of slack water. The major assumption implicit in the use of the single scale factor during one flood or ebb was that the factors derived for currents at SSB are equally valid throughout the entire Bay.

To summarize the analysis procedure, first the 10-minute modeled currents at SSB, v_m, were analyzed to determine the times of slack water and the category (semidiurnal flood, diurnal flood, or ebb) of the phase. Then the currents were time-stretched into a standard duration, and summed to find the mean current and the maximum and minimum speeds in each category. Then for all stations the mean currents at approximately hourly intervals, V_{ijk}, starting from

slack water at SSB in the categories were determined. To summarize the prediction procedure, at each cycle the flood and ebb ratios, S_f, were computed from Eq. 6.3 using the daily tidal current table predictions of flood and ebb speed at SSB, v_p. For any location, the (approximately) hourly mean current for that location and category was multiplied by the factor S_f to get a current prediction, c_{ij}.

6.4. ACCURACY IN RECONSTRUCTING THE MODELED CURRENT

Three tests of accuracy were performed on the atlas-predicted currents. Since the atlas basis currents were derived from the modeled currents, the first test compares the atlas-predicted current, with S_f and T_s determined from the modeled current, to the modeled current. In Section 6.5, a second test compares the atlas-predicted current, with S_f and T_s determined from the observed current, to the observed current. A third test compares the atlas-predicted current, with S_f and T_s determined from the NOS *Tidal Current Tables* daily predicted current, to the observed current.

The ability of the atlas prediction to reproduce the modeled velocity is a measures both the accuracy of using a constant S_f value for the entire flood/ebb phase and the accuracy of using a single S_f value throughout the Bay. The difference between the modeled current, v_m, and the atlas-predicted current, c, was computed as follows:

$$d_1 = v_m - c_{ij} = v_m - S_f(v_m) V_{ijk} \tag{6.4}$$

Here the factor S_f was obtained from the modeled velocity at SSB and the slack times corresponding to the beginning of either the six or the 18 intervals.

In order to illustrate the types of error that occur, plots of the modeled velocity, the atlas-predicted velocity, and the difference for a 3-day period in 1990 at SSB (C-3) are shown in Figure 6.4. At that station, the rms difference was small (1.8 cm/s for the 35 days of Run A) because it is based on the current there and consists mainly of shape errors around the peak between the mean current and the actual current. Errors at any other station are expected to be larger because, in addition to these shape differences, amplitude errors will occur due to non-linearities and timing errors will occur because slack water times at other locations will be less accurate. For example, plots of the modeled velocity, the atlas-predicted velocity, and the difference for the same 3-day period at C-5 are shown in Figure 6.5. Rms errors at this station totaled 5.1 cm/s for Run A. Both amplitude and timing errors are evident and the shape of the mean current is less representative of that in the cycles depicted, especially around 239.0 Julian days.

The rms differences for several cases are given in Table 6.1. For comparison purposes, the rms differences for the case of $S_f = 0.0$ (where the rms difference then is the rms of the total modeled current) and $S_f = 1.0$ (where the rms difference then is the deviation of the modeled current about the modeled mean current) are included. The atlas currents are expected to be most accurate at SSB since the slack times and S_f factors are derived from the time series there.

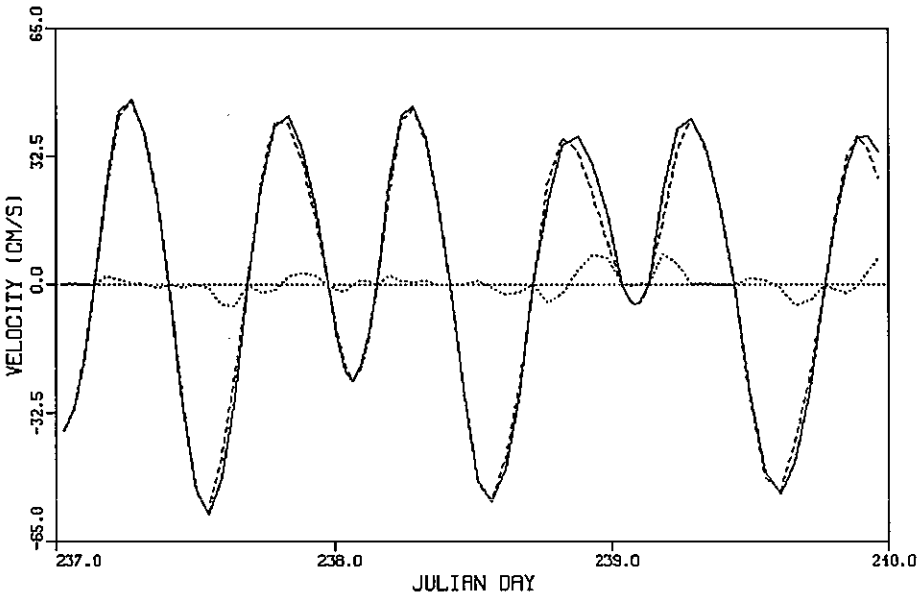

Figure 6.4. Comparison of modeled current (solid line), hourly atlas-predicted current (dashed line), and the difference d_1 (dotted line) at 4.6 m below MLLW at SSB for 3 days in 1990. Errors at this station appear to be minimal.

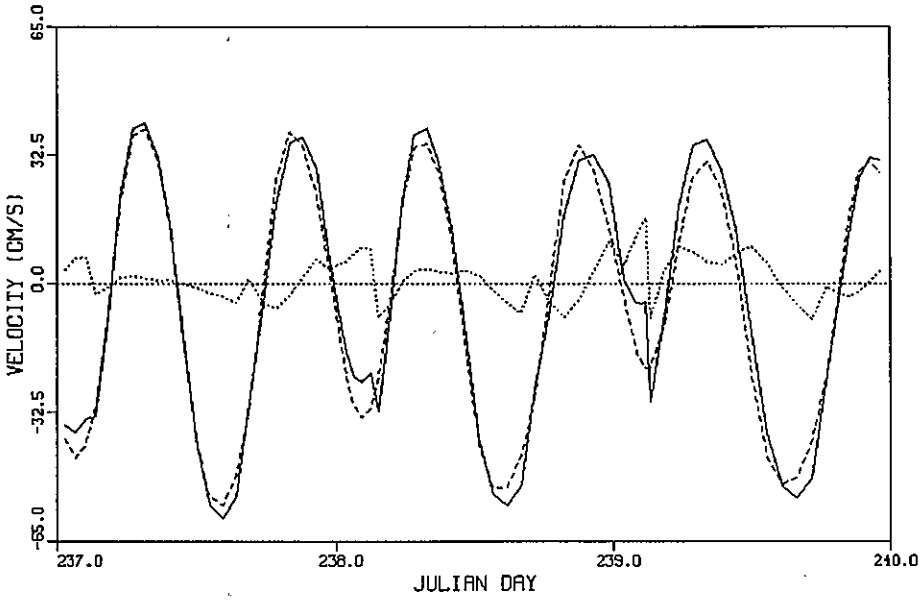

Figure 6.5. The hourly modeled current (solid line), the atlas-predicted current (dashed line), and the difference d_1 (dotted line) at C-5 for 3 days in 1990. Shape, timing, and amplitude errors are evident, especially at 239.0 Julian days.

As shown in Table 6.1, the rms difference between modeled currents and the atlas-predicted currents at SSB averaged 1.85 cm/s for the two, 35-day runs. Since the rms of the total current there averaged 33.65 cm/s, 1.85 cm/s represents 5.5% of the total. When all stations are considered, the rms difference averaged 2.6 cm/s. This represents, for an rms of the total current of 20.45 cm/s, 12.7% of the total. Since the results for Runs A and B are nearly the same, the mean current, V_{ijk}, from only Run A will be used hence.

Table 6.1. Mean rms differences (cm/s) between modeled current, v_m, and atlas-predicted current, c, for various values of S_f for (a) the Sunshine Skyway Bridge (SSB) and for (b) all stations for two, 35-day simulations (Runs A and B). For comparison purposes, the rms difference for the case of $S_f = 0.0$ (standard deviation of the modeled current) and $S_f = 1.0$ (standard deviation of the modeled current about the modeled mean current) are included.

S_f	Rms Difference at SSB (cm/s)		Mean rms Difference at All Stations (cm/s)	
	Run A	Run B	Run A	Run B
0.0	33.8	33.5	21.1	19.8
1.0	7.0	8.3	4.5	4.7
(Eq. 6.3)	1.8	1.9	2.9	2.3

For all stations, the rms differences ranged from 0.3 to 5.3 cm/s, with the largest differences occurring at stations C-41 (5.3 cm/s) and C-5 (5.1 cm/s), which is at the entrance to Old Tampa Bay. Differences varied from cycle to cycle, ranging from 1.2 to 6.6 cm/s. In the mean, the largest differences (3.1 cm/s) generally occurred for the ebbs, as compared to the semidiurnal floods (2.5 cm/s) and the diurnal floods (3.0 cm/s).

6.5. ACCURACY OF ATLAS PREDICTION VS. OBSERVED CURRENTS

Scale Factor from Observed Current

Additional accuracy tests were performed to measure the ability of the atlas prediction to reproduce the observed velocity, v_o, when the scale factors S_f and slack water times are computed from the observed velocities at SSB. Therefore, the rms value of the following difference was analyzed:

$$d_2 = v_o - S_f(v_o) V_{ijk} \tag{6.5}$$

Since V is derived from the model and not observations, it is expected that rms differences will be higher than those found in the previous test. The results for five stations (locations are shown in Figure A.1) are shown in Table 6.2. The first line of Table 6.2 shows the rms differences between the atlas-predicted current and the observed current when the scale factor is computed from modeled currents at SSB. The second line of Table 6.2 shows the rms differences between the atlas-predicted current and the observed current when the scale factor is computed from observed currents at SSB. At SSB (C-3), the rms difference is 4.1 cm/s, which as expected is

Table 6.2. Mean rms differences (cm/s) between the atlas-predicted current, c, and the observed current, v_o, using three methods of computing S_f. Results are shown for Run A for various stations and the average for those stations. The S_f basis current at SSB is either the modeled current v_m, the observed current v_o, or the table-predicted maximum and minimum v_p.

Scale Factor	C-2	C-3	C-4	C-5	C-20	Avg
$S_f(v_m)$	3.3	1.8	2.9	5.1	3.7	3.4
$S_f(v_o)$	9.0	4.1	11.5	9.2	8.8	8.5
$S_f(v_p)$	12.0	10.4	13.6	11.7	12.0	11.9

higher that the 1.8 cm/s value obtained when modeled values were used. For the stations considered, the average rms error between the atlas prediction and the observed current averaged 8.5 cm/s.

Scale Factor from Tidal Current Tables

The final accuracy test was performed to measure the ability of the atlas prediction to reproduce the observed velocity, but with the scale factors S_f and slack water times taken from the NOS *Tidal Current Tables* predicted velocities, v_p, at SSB. The rms value of the following difference was computed:

$$d_3 = v_o - S_f(v_p)\, V_{ijk} \tag{6.6}$$

This situation most closely approximates the way the atlas will ultimately be used. Since here S_f is derived from table predictions and not observations, it is expected that rms differences will be higher than those found in the second test. Daily table predictions for SSB in 1990 were developed using the tidal current constituents and methods that were used for producing the daily predictions which were published starting in 1994. The third line in Table 6.2 shows the rms errors between the atlas-predicted current and the observed current at several Tampa Bay stations using this method of generating the S_f values. The table shows that for the stations considered, the difference averages 11.9 cm/s. The difference between using the observations and using the daily table predictions when computing S_f averages approximately 3.4 cm/s.

Plots of the observed current, the atlas-predicted current (using tidal current table values), and the difference at SSB for the same 3-day period are shown in Figure 6.6. In addition to the errors previously discussed, another type of error is evident: prediction of a diurnal flood (at Day 239) when none was observed (incorrect category).

Finally, Figure 6.7 shows the atlas-predicted and observed current at C-5. The error in categorization at Day 239 is also evident at this station.

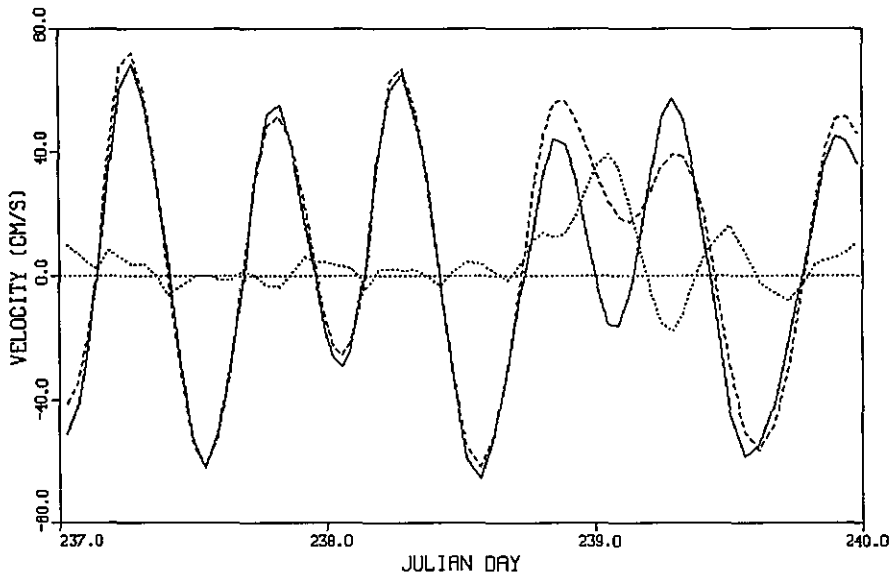

Figure 6.6. The hourly observed current (solid line), the atlas-predicted current (dashed line), and the difference d_3 (dotted line) at SSB (C-3) for 3 days in 1990 using NOS Table values to determine S_f. An error in current categorization caused a large difference around 239.0 Julian days.

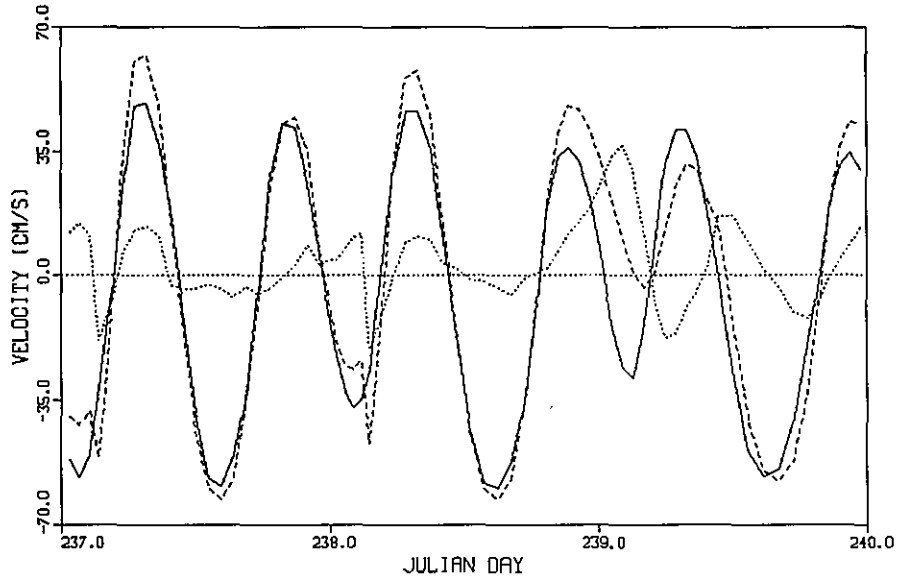

Figure 6.7. The hourly observed current (solid line), the atlas-predicted current (dashed line), and the difference d_3 (dotted line) at the entrance to Old Tampa Bay (C-5) for 3 days in 1990 using NOS Table values to determine S_f. An error in current categorization caused a large difference around 239.0 Julian days.

6.6. CONCLUSIONS

Although this study was based on 70 days of observed currents, it indicated that the proposed approach gives reasonably accurate results. Some specific conclusions are:

The creation of a tidal current atlas based on distinguishing between semidiurnal and diurnal tidal cycles is a practical way to provide information about Bay-wide currents accurately and in a compact form.

The use of three distinct normal cycles gives a mean rms error between atlas predictions and observed current of 11.9 cm/s, which is less than the maximum stated in the NOS prediction standards. The error is comparable to that found for the Long Island Sound atlas (Wei, 1993), 0.35 knots (18.5 cm/s).

There were four types of errors found: (1) shape differences, when the observed currents do not match the shape of the mean curve;, (2) amplitude differences, when the observed peak current does not match the atlas peak; (3) timing differences, when the times of slack water do not match; and (4) category errors, when the improper flood category is chosen.

The mean modeled velocity, V_{ijk}, is generally somewhat smaller than the observed current at the same hour. Therefore, in the atlas all V_{ijk} should be increased by some factor to better represent typical currents.

Although the explanation of the analysis and the prediction methodology contained in this Section may seem straightforward, in reality the implementation is quite complicated and has relied on numerous assumptions whose effect on the overall accuracy needs to be assessed more thoroughly.

7. SUMMARY AND CONCLUSIONS

Application of the Princeton model to Tampa Bay has been successful and the evaluation has shown that the model has skill at reproducing observed variations in currents, water levels, salinities, and temperatures. The major findings of the modeling project are as follows:

- The use of successively-refined grids made a significant difference. Modeled solutions became more realistic with increased grid resolution, especially in cell size across the estuary.

- A new algorithm developed for wetting and drying of cells was successful in that there were few additional computations required and there were no numerical instabilities generated.

- Model evaluation, through calibration and validation, has been extensively explored and a wide variety of statistics (many of which where developed specifically for this study) have been used to demonstrate model skill.

- Because Tampa Bay is relatively shallow, the numerical solution for water levels (especially phase) was sensitive to total water depth. Tidal wave dynamics are strongly influenced by shallow-water wave speed, and since the Bay averages only 4 meters in depth, small differences in total depth (tens of centimeters) make a difference.

- In general, the numerical solutions for current were less accurate than for water level, due to the greater spacial variability of the flow. In Tampa Bay, sub-grid scale features such as submerged dredge spoil mounds (whose bathymetry is poorly mapped), small islands, and channels all contribute to the complexity of the situation. Currents could vary significantly over distances as small as a few tens of meters.

- Extensive comparisons of observed variables to model output indicate that the model could be an important tool in designing additional observational surveys and assist in the placement of sensors.

Overall, model accuracy was good, with the rms errors shown in Table 7.1. In comparison to other modeling results (Table 4.12), water levels were quite accurate and currents had average accuracy. For salinity (Table 5.4), results were better than average and for temperature, results were about average.

Analysis of the proposed method of developing the tidal current atlas, with three categories of current (semidiurnal flood, semidiurnal ebb, and diurnal flood) showed that expected errors would be about 12 cm/s (Table 6.2). It is recommended that the use of fewer diurnal flood hours (i.e., less than 18), to save storage space, be tested for accuracy.

While undergoing final validation, the model was used to enhance the synthesis report (Zervas 1993). It was found that (a) the natural period of Tampa Bay was 10.37 h, (b) the water level

Table 7.1. Summary of Tampa Bay model accuracy (rms errors between modeled and observed) for several variables.

Variable	Rms Error	Source
total currents	10.1 cm/s	Table 4.6
max. flood/ebb currents	14.0 cm/s	"
max. flood/ebb times	36.6 min	Table 4.4
water levels	3.9 cm	Table 4.6
high/low tide	3.7 cm	"
high/low tide time	24.2 min	Table 4.5
salinity	1.10 psu	Table 5.3
temperature	0.88°C	"

is a standing wave in Hillsborough Bay, (c) there are significant westward surface buoyancy-currents just south of the Interbay Peninsula, and (d) net currents over the vertical at SSB for a 10 m/s wind were found to be seaward at 6 cm/s.

Several potential future studies are indicated. A higher-resolution grid should be developed to study flow around the dredged channels. The buoyancy-driven flow at the Interbay Peninsula and along the east side of the Bay where there is substantial fresh water inflow should be studied. Additional study of the heat flux should be conducted, including the effects of cloudiness and the possibility of adding a bottom heat flux. Finally, the model should be used in connection with the PORTS to study wind events with the goal of improving NOS predictions which are based on the astronomical tide.

REFERENCES

American Society of Testing and Materials, 1992: Standard Practice for Evaluating Mathematical Models for the Environmental Fate of Chemicals. **ASTM Designation E 978-92**, ASTM, Philadelphia, PA, pp 7.

Appell, G. F., T. N. Mero, and J. J. Sprenke, 1991: Design of a current, water level, and meteorological information system for Tampa Bay. **Proceedings, IEEE Oceans 91**, 859 - 863.

Berger, R., W. Martin, R. McAdory, and J. Schmidt, 1994: Galveston Bay 3D model study, channel deepening, circulation, and salinity results. **Proceedings, 3rd International Conference on Estuarine and Coastal Modeling**, Oak Brook, IL, September 8-10, 1993, 1 - 13.

Bethem, T. D., and H. R. Frey, 1991: Operational physical oceanographic real-time data dissemination. **Proceedings, IEEE Oceans 91**, 865 - 867.

Blumberg, A. F., and H. J. Herring, 1987: Circulation modeling using orthogonal curvilinear coordinates. in **Three-Dimensional Models of Marine and Estuarine Dynamics** (J. C. J. Nihoul and B. M. Jamart, eds), Elsevier Oceanography Series, 45, 55 - 88.

Blumberg, A. F., and G. L. Mellor, 1987: A description of a three-dimensional coastal ocean circulation model. **Three-Dimensional Coastal Ocean Models**, (ed. Heaps), American Geophysical Union, Washington, DC., 1 - 16.

Boler, R. (editor), 1992: Surface Water Quality, Hillsborough County, Florida: 1988 - 1989. Hillsborough County Environmental Protection Commission, 1900 9th Ave., Tampa, FL.

Clark, P. A., and R. W. MacAuley, 1989: Geography and Economy of Tampa Bay and Sarasota Bay. **Tampa and Sarasota Bays: Issues, Resources, Status, and Management**. NOAA Estuary-of-the-Month Seminar Series No. 11, 1 - 17.

Defant, A., 1958: **Ebb and Flow: the Tides of the Earth, Air, and Water.** University of Michigan Press, Ann Arbor, MI, 121 pp.

Dennis, R. E., and E. E. Long, 1971: A user's guide to a computer program for harmonic analysis of data at tidal frequencies. **NOAA Technical Report** NOS 41. NOAA, National Ocean Service, Office of Oceanography and Marine Assessment, Rockville, MD, 31 pp.

Dinardi, D. A., 1978: Tampa Bay Circulatory Survey 1963. NOS Oceanographic Circulatory Survey Report No. 2, NOAA, National Ocean Service, Office of Oceanography and Marine Assessment, Rockville, MD. 39 pp.

Dragovich, A., and J. E. Sykes, 1967: Oceanographic Atlas for Tampa Bay, Florida, and adjacent waters of the Gulf of Mexico: 1958 - 61. U.S. Department of the Interior, Fish and Wildlife Service, Bureau of Commercial Fisheries, Circular 255, 466 pp.

Flannery, M. S., 1989: Tampa and Sarasota Bays: Watersheds and Tributaries. **Tampa and Sarasota Bays: Issues, Resources, Status, and Management**. NOAA Estuary-of-the-Month Seminar Series No. 11, 18 - 48.

Frey, H. R., 1991: Physical oceanographic real-time systems for operational. **Proceedings, IEEE Oceans 91**, 855 - 858.

Galperin, B., A. F. Blumberg, and R. H. Weisberg, 1991: A time-dependent three-dimensional model of circulation in Tampa Bay. **Proceedings, Tampa BASIS (Bay Area Scientific Symposium) 2**, Tampa, FL, February 27 - March 1, 1991. 67 - 75.

___, 1992: The importance of density driven circulation in well mixed estuaries: the Tampa Bay experience. **Proceedings, Estuarine and Coastal Modeling**, Tampa, FL, November 11 - 13, 1991. 332 - 343.

Goodwin, C. R., 1977: Circulation patterns for historical, existing, and proposed channel configurations in Hillsborough Bay, Florida. **Proceedings, 24th International Navigation Congress**, Leningrad, Subject 4, Section 4, 167 - 179.

___, 1980: Preliminary simulated tidal flow and circulation patterns in Hillsborough Bay, Florida. U.S. Geological Survey Open File Report 80-1021, 25 pp.

___, 1987: Tidal-Flow, Circulation, and Flushing Changes Caused by Dredge and Fill in Tampa Bay, Florida. **U.S. Geological Survey Water-Supply Paper** 2282, 88 pp.

___, 1991: Tidal-Flow, Circulation, and Flushing Changes Caused by Dredge and Fill in Hillsborough Bay, Florida. **U.S. Geological Survey Water-Supply Paper** 2376, 49 pp.

___ and D. M. Michaelis, 1976: Tides in Tampa Bay, Florida: June 1971 to December 1973. U.S. Geological Survey, Tallahassee, FL. Open File Report FL-75004, 338 pp.

___ and B. E. Ross, 1984: Evaluation of changes in circulation, spring tide, and hurricane surge characteristics in Tampa Bay caused by Sunshine Skyway pier protection system, (unpublished manuscript), 35 pp.

Haney, R. L., 1991: On the pressure gradient force over steep topography in sigma coordinate ocean models. **Journal of Physical Oceanography**, 21, 610 - 619.

Hess, K. W., 1989: MECCA Program Documentation. NOAA, National Environmental Satellite, Data, and Information Service, Satellite Applications Laboratory, **NOAA Technical Report NESDIS 46**. 258 pp.

___ (editor), 1990: Tampa Bay Oceanography Project: Progress Report for FY 1990. NOAA, National Ocean Service, Office of Oceanography and Marine Assessment, Rockville, MD. 38 pp.

___, 1991: Numerical circulation model calibration and validation for Tampa Bay using NOS circulation survey data. **Proceedings, Tampa BASIS (Bay Area Scientific Symposium)** 2, Tampa, FL, February 27 - March 1, 1991. 67 - 75.

___ (editor), 1992: Tampa Bay Oceanography Project: Progress Report for FY 1991. NOAA, National Ocean Service, Office of Ocean and Earth Sciences, Rockville, MD. 71 pp.

___, 1993: Modeling astronomical tides and currents in Tampa Bay. **Proceedings, International Conference on HydroScience and Engineering**, Washington, DC, June 8-11, 1993. 1499 - 1506.

___, and K. T. Bosley, 1992: Techniques for validation of a model for Tampa Bay. **Proceedings, 2nd International Conference on Estuarine and Coastal Modeling**, Tampa, FL, November 11-13, 1991. 83 - 94.

Jelesnianski, C. P., J. Chen, W. A. Shaffer, and A. J. Gilad, 1984: SLOSH - a hurricane storm surge forecasting model. **Preprints, Oceans 84**, Washington, DC, Marine Technology Society and IEEE/Oceanic Engineering Society, 314 - 317.

Johnson, B. H., R. E. Heath, B. B. Hsieh, K. W. Kim, and H. L. Butler, 1991: Development and Verification of a Three-Dimensional, Numerical Hydrodynamic, Salinity, and Temperature Model of Chesapeake Bay. **WES Technical Report** HL-91-7, U.S. Army Corps of Engineers, Waterways Experiment Station, Vicksburg, MS, pp 193.

Lardner, R. W., A. H. Al-Rabeh, and N. Gunay, 1993: Optimal estimation of parameters for a two-dimensional hydrodynamical model of the Arabian Gulf. **Journal of Geophysical Research**, 98, 18,229 - 18,242.

Large, W. G., and S. Pond, 1981: Open ocean momentum flux measurements in moderate to strong winds. **Journal of Physical Oceanography** 11, 324 - 336.

Leendertse, J. J. 1967: Aspects of a computational model for long-period water-wave propagation. RAND Technical Memorandum RM-5294-PR, The RAND Corp, Santa Monica, CA, 164 pp.

Mellor, G. L., 1993: User's guide for a three-dimensional, primitive equation, numerical ocean model. Atmospheric and Oceanic Sciences Program, Princeton University, Princeton, NJ, (unpublished manuscript) 35 pp.

___, 1991: An equation of state for numerical models of oceans and estuaries, **Journal of Atmospheric and Oceanic Technology**, v. 8 (4), 609 - 611.

___, and A. F. Blumberg, 1985: Modeling vertical and horizontal diffusivities with the sigma coordinate system. **Monthly Weather Review**, 113, 1379 - 1383.

National Ocean Survey, 1979: Tampa Bay Tidal Current Charts (First Edition). NOAA, U.S. Department of Commerce. 15 pp.

National Ocean Service, 1990: Tampa Bay Oceanography Project: Plan for FY 1990 to FY 1992. NOAA, National Ocean Service, Office of Oceanography and Marine Assessment, Rockville, MD. 68 pp.

Nichols, C. R., 1993: Operational characteristics of the Tampa Bay physical oceanographic real-time system. **Proceedings, International Conference on HydroScience and Engineering,** Washington, DC, June 8-11, 1993. 1491 - 1498.

Nowadly, F., 1992: **NOS Oceanographic Circulation Survey Report** No. 11. Tampa Bay Oceanography project: 1990 - 1991. NOAA, National Ocean Service, Office of Ocean and Earth Sciences, Rockville, MD. 25 pp + Appendices.

Orlanski, I., 1976: A simple boundary condition for unbounded hyperbolic flows. **Journal of Computational Physics**, 21, 251 - 269.

Parker, B. B., and R. C. Patchen, 1987: The circulation and water level forecast atlas: a new product in development at NOS. **Proceedings, Oceans 87**, Halifax, NS, September 28 - October 1, 1987. 857 - 862.

Parkinson, C. L., and W. M. Washington, 1979: A large-scale numerical model of sea ice. **Journal of Geophysical Research**, 84, 311 - 337.

Peene, S. J., and Y. P. Sheng, 1992: Modeling tide and wind driven circulation in Sarasota and Tampa Bay. **Proceedings, 2nd International Conference on Estuarine and Coastal Modeling,** Tampa, FL, November 11-13, 1991. 357 - 369.

Reid, R. O., and B. R. Bodine, 1968: Numerical model for storm surges in Galveston Bay. **Journal of the Waterways and Harbors Division**, ASCE, 94, No. WW1, Proceedings Paper 5805, 33 - 57.

Roig, L. C., and I. P. King, 1992: Continuum model for flows in emergent marsh vegetation. **Proceedings, 2nd International Conference on Estuarine and Coastal Modeling**, Tampa, FL, November 11-13, 1991. 268 - 279.

Schmalz, R. A., 1994: Long Island Sound Oceanography Project, Summary Report, Volume 1: Application and Documentation of the Long Island Sound Three-Dimensional Circulation Model. NOAA, National Ocean Service, Office of Ocean and Earth Sciences, Silver Spring, MD. 77 pp.

___, M. F. Devine, and P. H. Richardson, 1994: Long Island Sound Oceanography Project, Summary Report, Volume 3: Residual Circulation and Thermohaline Structure. NOAA, National Ocean Service, Office of Ocean and Earth Sciences, Silver Spring, MD. 279 pp.

Schureman, P., 1958: **Manual of Harmonic Analysis and Prediction of Tides.** U.S. Department of Commerce, Coast and Geodetic Survey, Special Publication No. 98 [revised 1940 edition, reprinted 1988], 317 pp.

Schwiderski, E. W., 1980: On charting global ocean tides. **Reviews of Geophysics and Space Physics** 18 (1), 243 - 268.

Shaffer, W. A., C. P. Jelesnianski, and J. Chen, 1986: Hurricane storm surge forecasting. **Preprints, Oceans 86**, Washington, DC, Marine Technology Society and IEEE/Oceanic Engineering Society, 1379 - 1385.

Sheng, Y. P., 1983: Mathematical modeling of three-dimensional coastal currents and sediment dispersion: model development and application. Technical Report CERC-83-2. U.S. Army Engineer Waterways Experiment Station, Vicksburg, MS. 228 pp.

___, H.-K. Lee, and K. H. Wang, 1990: On numerical strategies of estuarine and coastal modeling. **Proceedings, 1st International Conference on Estuarine and Coastal Modeling**, Newport, RI, November 15-17, 1989. 291 - 301.

___, and J.-K. Choi, 1992: Three dimensional numerical modeling of tidal circulation and salinity transport in James River estuary. **Proceedings, 2nd International Conference on Estuarine and Coastal Modeling**, Tampa, FL, November 11-13, 1991. 209 - 218.

Spaulding, M. L, D. P. French, and H. Rines, 1989: A review of the Tampa Bay water quality model system. Applied Science Associates, Inc., Narragansett, RI, Report ASA 88-58. 137 pp.

Wei, E. J., 1993: Development of a Long Island Sound Tidal Circulation and Water Level Atlas. **Proceedings, International Conference on Hydroscience and Engineering**, Washington, DC, June 8-11, 1993. 1483 - 1490.

Williams, R. G., T. D. Bethem, and H. R. Frey, 1989: Tampa Bay Current Prediction Quality Assurance Miniproject. **NOAA Technical Memorandum** NOS OMA 50, National Ocean Service, Office of Oceanography and Marine Assessment, Rockville, MD, 11 pp + figures.

Willmott, C. J., S. G. Ackleson, R. E. Davis, J. J. Feddema, K. M. Klink, D. R. Legates, J. O'Donnell, and C. M. Rowe, 1985: Statistics for the evaluation and comparison of models. **Journal of Geophysical Research**, 90, 8995 - 9005.

Wurtele, M. G., J. Paegle, and A. Sielecki, 1971: The use of open boundary conditions with the storm-surge equations. **Monthly Weather Review**, v. 99 (6), 537 - 544.

Zervas, C. (editor), 1993: **Tampa Bay Oceanography Project: Physical Oceanographic Synthesis.** NOAA, National Ocean Service, Office of Ocean and Earth Sciences, Silver Spring, MD. 175 pp + appendices.

Zetler, B. D., 1982: **Computer Applications to Tides in the National Ocean Survey. Supplement to Manual of Harmonic Analysis and Prediction of Tides** (Special Publication No. 98). National Ocean Service, Rockville, MD. 85 pp.

ACKNOWLEDGEMENTS

The following people made important contributions to the completion of this report. Dr. Henry R. Frey, former Chief of the Coastal and Estuarine Oceanography Branch, conceived of and organized TOP and provided leadership and critical resources for the Project. Dr. Richard Schmalz provided the initial version of the Princeton model code and, along with Dr. Charles Sun, supplied a wealth of information on the code and modeling in general. Drs. Chris Zervas and Kathryn Bosley, in their effort analyzing and displaying the TOP data, provided crucial oceanographic insights and established a high standard for scientific achievement. Drs. Boris Galperin, Alan Blumberg, and George Mellor provided important further insights about the Princeton model. Finally, numerous people in the State of Florida also contributed data, insights, and other information and resources that advanced TOP and the modeling effort.

APPENDIX A. OBSERVATIONAL DATA

An intensive 16-month circulation survey of currents, water levels, water temperature, salinity, winds, and other meteorological parameters began in June 1990 and was successfully completed in September 1991. The TOP circulation survey resulted in the greatest volume of circulation measurements acquired from one estuary in the 100-year history of NOAA's Coastal Ocean Circulation Program; details of the measurement program, instrument locations, and data availability can be found in Nowadly (1992). Data from the circulation survey are being used to revise and expand NOAA's tide and current prediction tables, beginning with the 1994 tables. The new data will also be used to estimate prediction uncertainties due to wind and river effects. The current data are also important for the calibration and validation of the numerical model.

The extensive oceanographic data set collected in Tampa Bay during TOP consists of

- current meter data from 40 fixed stations, including both acoustic Doppler current profilers (ADCPs) and electromagnetic current meters;
- current meter data from a downward-facing towed ADCP at five transects in the Bay;
- water levels from 16 stations along the shore of the Bay and Gulf;
- wind, temperature, and atmospheric pressure measurements at five meteorological stations in the Bay and additional temperature, solar radiation, and humidity measurements at one station;
- time series of salinity and temperature data from conductivity-temperature (CT) sensors at three mooring sites with near-bottom and near-surface measurements;
- near-bottom CT measurements at 33 of the fixed current meter sites; and
- salinity and temperature profiles over depth at 684 stations along six transects from conductivity-temperature-depth (CTD) sensors.

Locations of the fixed stations are shown in Figure A.1.

Current Meters

Two types of current meters were used: the ADCP manufactured by RD Instruments and the InterOcean S4 electromagnetic current meter. The ADCP acoustically measures current velocity in a number of vertical bins chosen for this survey to be 1 m thick. These current meters were deployed on the seafloor in an upward-facing configuration. The S4 electromagnetic current meters were deployed in shallow areas of Tampa Bay and measured currents at only one level (1 to 3 m above bottom). Current velocity cross sections were obtained from a downward-facing ADCP mounted on a catamaran towed along a number of selected transects.

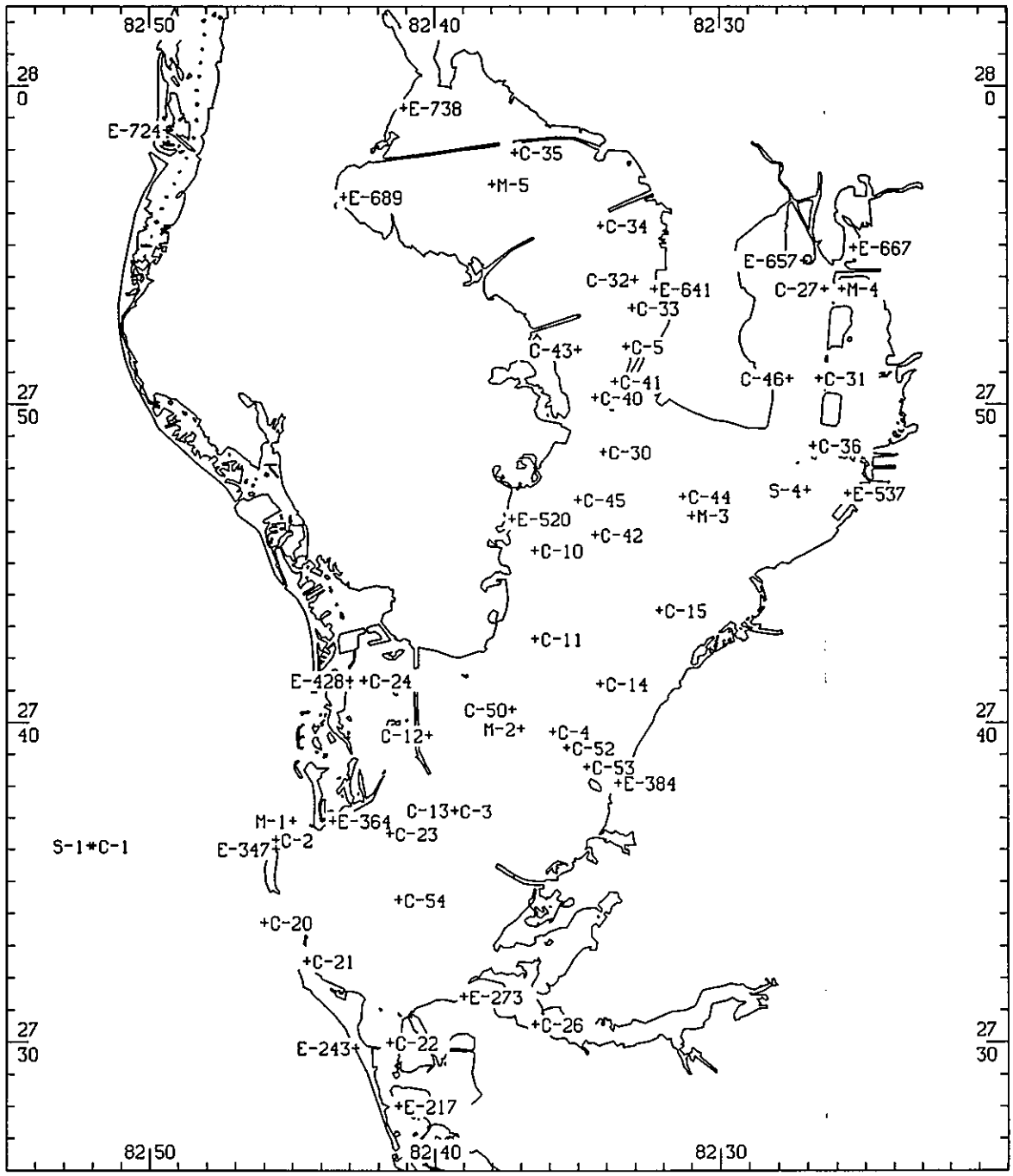

Figure A.1. Location of TOP survey stations (denoted by '+'), where C denotes a current meter, E a water level gage, M a meteorological station, and S a CT. Not shown are:

C-6 (located appx. 50 km west of C-1),
C-51 (located between C-50 and C-52),
C-55 (located near C-4),
C-56 (located near C-2),
C-60 (co-located with C-1),
S-2 (co-located with M-2),
S-3 (co-located with C-31), and
E-858 (at Venice Pier, located to the south at 27° 35.0' N, 83° 15.7' W.

Current meter deployments were for long-term (over a year) and short-term (60 days) time periods. There were six long-term stations (C-1 to C-6). C-1 was located 10 km offshore to provide a boundary condition for numerical modeling. C-2 was in Egmont Channel, the main entrance to Tampa Bay, and is the reference station presently used in the NOS Tidal Current Tables. C-3 was located in the main shipping channel near the Sunshine Skyway, while C-4 was further up the channel near the turn to Port Manatee. C-5 was at the entrance to Old Tampa Bay near Port Tampa and C-6 was about 50 km offshore on the continental shelf. Acceptable data for the planned periods were not obtained for all instruments.

The short-term instrument deployments (C-10 to C-60) were grouped into a series of five periods concentrating on different sections of the Bay. The first and second periods covered middle and lower Tampa Bay, respectively. During the third period, the focus was on Old Tampa Bay and Hillsborough Bay. Periods 4 and 5 were planned to examine small-scale processes near Port Tampa and Port Manatee, respectively.

The towed ADCP transects were planned to delineate the small-scale velocity structure in the vicinity of the shipping channels. CT-1 was a transect across the entrance to Tampa Bay. CT-2 crossed the Bay parallel to the Sunshine Skyway. CT-3 was oriented along the channel to Port Manatee while CT-4 was along the channel to Port Tampa. CT-5 was a transect along the main shipping channel from below the Sunshine Skyway to the turn to Port Manatee. Locations of transects are shown in Zervas (1993), Figure 2.2.

Water Level Gages

Water level data were collected concurrently with the current data in order to update the Tide Tables. Water level measurements were collected from 16 stations throughout Tampa Bay and along the Gulf Coast. The stations at St. Petersburg (E-520) and Clearwater Beach (E-724) are permanent NOS tide stations while the other 14 were temporary stations occupied during TOP (Figure A.1). The permanent station at Clearwater Beach and the temporary stations at Venice Pier (E-858) and Anna Maria Island (E-243) were on the Gulf Coast north and south of Tampa Bay, while the remaining stations were inside the Bay. St. Petersburg is the reference station for Tampa Bay in the NOS Tide Tables. The acquisition of water level data for TOP was conducted in two phases to minimize the number of instruments required to complete the project.

Meteorological Sensors

Meteorological data in support of TOP were collected from five meteorological sensor packages deployed from the mouth to the upper reaches of Tampa Bay (Figure A.1). Measurement parameters include wind speed and direction, air temperature, and barometric pressure. Additionally, relative humidity and solar radiation were measured at M-2 as part of the Tampa Bay PORTS and were provided to the National Weather Service (Hess, 1992). Meteorological data collected from December 1989 through June 1991 at Tampa International Airport (TPA) were obtained from NOAA's National Climatic Data Center (NCDC).

Hydrologic Data

The Tampa Bay watershed, which includes rivers, tidal creeks, mangrove swamps, marshes, canals, springs, and streams, encompasses an area of approximately 5000 km^2 (Clark and MacAuley, 1989). Hydrological data from the main rivers were available from the USGS at eleven waterway discharge stations (Figure A.2).

Salinity and Temperature Sensors

Moored CTDs and CTs provided salinity and temperature time series of varying length at 36 locations throughout the Bay. Four mooring locations (S-1, S-2, S-3, and S-4) had a near-surface and a near-bottom CT. The remaining CTs and CTDs were moored at the fixed current meter stations (except stations C-10 through C-15). The locations of these moorings are shown on Figure A.1

Another component of the oceanographic survey consisted of five hydrographic cruises conducted from August 1990 to August 1991. These five seasonal cruises were performed in summer (August 1990 and 1991), fall (November 1990), winter (February/March 1991), and spring (May/June 1991). During these cruises, 684 individual conductivity-temperature-depth (CTD) casts were taken at stations along six transects. Transect 1 extended south-southeastward from just off Mullet Key across Egmont and Southwest Channels. Transect 2 ran northwest-southeast parallel to the Sunshine Skyway. Transect 3 extended east-west south of the Y Cut. The Outer Egmont transect, Transect 4, began outside the Tampa Bay entrance and continued east along the channel between Egmont and Mullet Keys. Running from the Sunshine Skyway to the Y Cut, Transect 5 covered the main navigation channel. Finally, Transect 6 extended north from the Y Cut to the head of Hillsborough Bay. Locations of transects are shown in Zervas (1993), Figure 5.1.

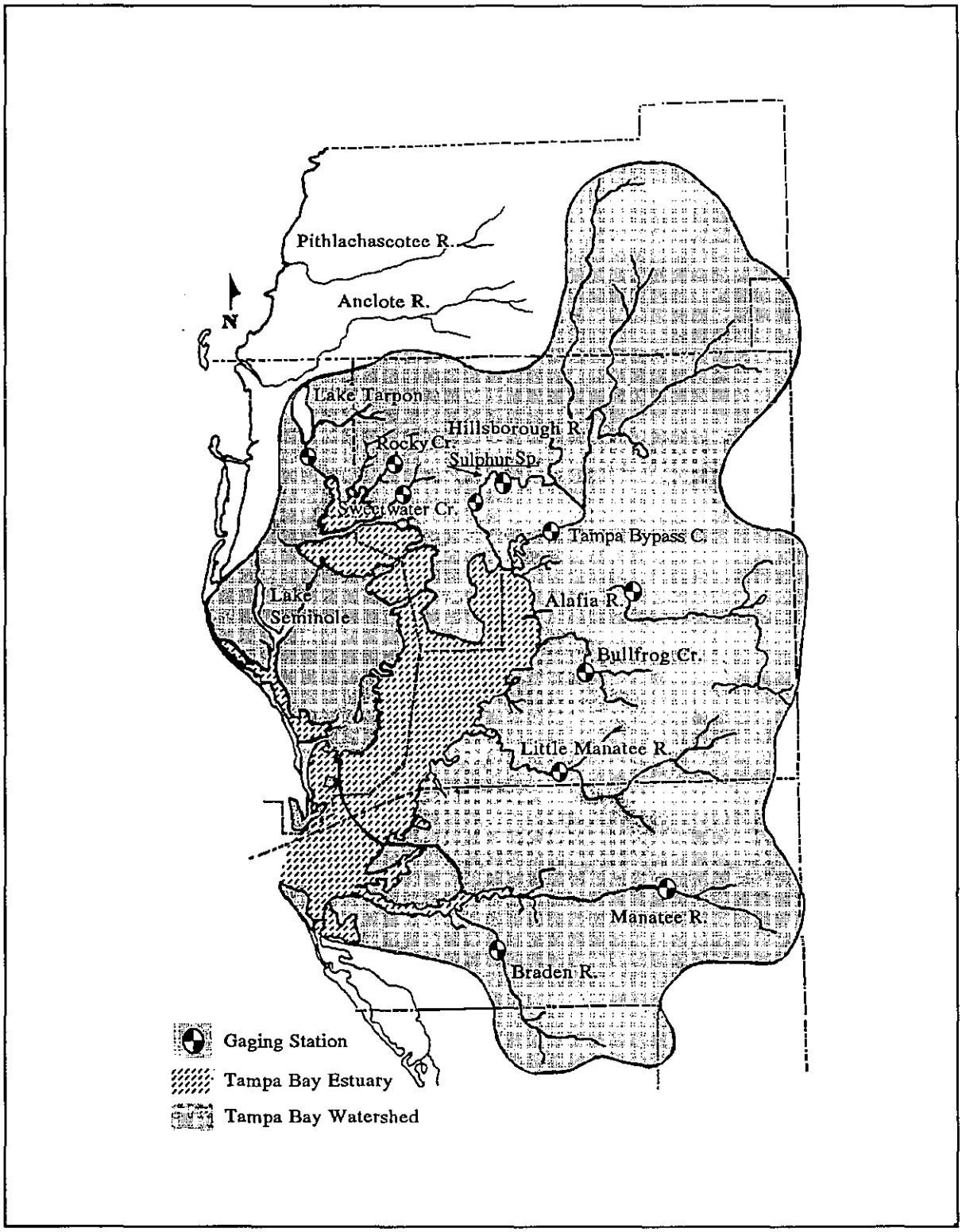

Figure A.2. The Tampa Bay estuary and watershed (adapted from Clark and MacAuley, 1989). The eleven USGS waterway discharge gaging stations used in this study are indicated.

APPENDIX B. FORMULATION OF ATMOSPHERIC HEAT EXCHANGE

The total downward specific heat flux at the air-water interface, Q_T (W/m^2) (Parkinson and Washington, 1979; Hess, 1989), is

$$Q_T = Q_1 + Q_2 \tag{B.1}$$

where Q_1 is the solar shortwave component that penetrates several meters into the water column below the surface, and Q_2 is the longwave flux that is absorbed at the surface. These components are treated separately.

The Solar Shortwave Component

The shortwave specific flux, Q_1 (W/m^2), is used in the internal heating term R_θ (°C/s) for a layer (Eq. 2.5) as follows

$$R_\theta = \frac{Q_1}{\rho_w c_w}\left[\frac{\exp(\alpha z_a) - \exp(\alpha z_b)}{z_a - z_b}\right] \tag{B.2}$$

$$\alpha = \frac{2.3}{D_{10}} \tag{B.3}$$

where ρ_w is water density, c_w is the specific heat capacity of water (4186 J/kg/°K), z_a is the z-coordinate of the top of the layer, z_b is the z-coordinate of the bottom of the layer, and D_{10} is the depth to which only 10 percent of the surface flux penetrates (assuming exponential decrease with depth from the surface). The quantity α (m^{-1}) is known as the diffuse attenuation coefficient.

The solar shortwave component of specific heat flux is defined as

$$Q_1 = Q_{ss}(1 - A_{ss})F_{cc}(C_c) \tag{B.4}$$

where Q_{ss} is the flux at the sea surface under cloudless conditions, A_s is the albedo of the sea surface, F_c is a cloudiness function, and C_c is the fraction of sky covered by clouds. The cloudiness function used here (there are many in the literature) is

$$F_c = 1 - C_c \tag{B.5}$$

Here the sea surface flux (Parkinson and Washington, 1979) is

$$Q_{ss} = \frac{C_{sol}\cos^2\zeta}{0.10 + 1.085\cos\zeta + 10^{-5}(\cos\zeta + 2.7)e_v} \tag{B.6}$$

where C_{sol} is the solar constant (1353 W/m^2), e_v is the atmospheric vapor pressure at the surface, and ζ is the solar zenith angle defined by

$$\cos\zeta = \sin\phi\sin\psi + \cos\phi\cos\psi\cos\nu \tag{B.7}$$

where ϕ is geographic latitude, ψ is the solar declination approximated by

$$\psi = 23.44^{o}\cos[2\pi(\frac{172 - day}{365})] \tag{B.8}$$

and ν is the hour angle of the sun

$$\nu = 2\pi(\frac{12 - solar\ hour}{24}) \tag{B.9}$$

The solar hour is the hour of the day on a 24-hour clock. The atmospheric vapor pressure, e_v (mb), is found by

$$e_v = R_h e_s(\Theta) \tag{B.10}$$

$$e_s = 611 \times 10^{7.5\left(\frac{\Theta - 273.16}{\Theta - 35.86}\right)} \tag{B.11}$$

where R_h is the relative humidity and Θ is the air temperature. In Eq. B.6, e_v is evaluated at an elevation just above the water surface; the effective air temperature there, Θ_0, is defined as

$$\Theta_0 = \beta\theta_s + (1 - \beta)\Theta_{10} \tag{B.12}$$

and is calculated using θ_s, the water temperature at the surface and Θ_{10}, the air temperature at 10 meters above the water. All temperatures are in °K. Here β is taken to be 0.9.

The Flux at the Skin Layer

The heat flux at the surface skin layer is the sum of several terms (Parkinson and Washington, 1979):

$$Q_2 = Q_L + Q_B + Q_E + Q_S \tag{B.13}$$

where Q_L is the longwave radiation from the atmosphere to the sea, Q_B is the negative of the black body radiation from the water surface, Q_E is the net downward evaporative (or latent) heat flux, and Q_S is the net downward sensible heat flux. Taking the terms one at a time, the longwave radiation is

$$Q_L = C_{sb}\Theta_{10}^4\{1 - 0.26\exp(-0.000777[273 - \Theta_{10}]^2)\} \tag{B.14}$$

where C_{sb} is the Stefan-Boltzman constant (5.670 x 10^{-8} W/m^2 °K^4).

The downward black body radiation from the sea is

$$Q_B = -E_s C_{sb} \theta_s^4 \tag{B.15}$$

where E_s (taken to be 0.97) is the surface emissivity.

The net downward evaporative heat flux is

$$Q_E = C_d \rho_a L_v W_{10} (\gamma_{10} - \gamma_0) \tag{B.16}$$

where ρ_a is the air density, C_d is the transfer coefficient, W_{10} is the wind speed at 10 meters above the water, γ_{10} is the specific humidity of the air at 10 meters, γ_0 is the specific humidity at the surface (where saturation is assumed), and L_v is the latent heat of vaporization (2.5 x 10^6 J/kg). Specific humidity is related to vapor pressure by

$$\gamma = \frac{\epsilon e_v}{p_a - (1 - \epsilon) e_v} \tag{B.17}$$

where ϵ is the ratio of the molecular weights of dry air and water vapor (0.622) and p_a is the atmospheric pressure (mb).

The sensible heat flux is approximated by the bulk formula

$$Q_S = \rho_a c_p C_d W_{10} (\Theta_{10} - \Theta_0) \tag{B.18}$$

where c_p is the specific heat capacity of dry air (1004 J/kg/°K).

Input Variables

Besides using the water temperature, θ_s, the heat flux model needs values throughout the day and year for atmospheric temperature, Θ_{10}, and wind speed, W_{10}. We assume that other variables, such as atmospheric pressure, p_a, relative humidity, R_h, and cloud cover, C_c, can be taken as constants without adversely effecting heat balance. Additional parameters used are the depth to which 10 percent of light penetrates, D_{10}, albedo, A_s, emissivity, E_s, and bulk transfer coefficient, C_d. The following values are used:

$$(p_a, R_h, C_c, D_{10}, A_s, E_s, C_d) = (1014.0, 0.80, 0.10, 1.0, 0.10, 0.97, 0.003) \tag{B.19}$$

APPENDIX C. MODEL GRID FILE

```
TAMPA CURVILINEAR GRID
27.80  -82.80      2      ALAT0,ALON0,INDEX
40  60 .1  1.00            IMAX,JMAX,DMIN1,DMIN2
 1  0.00  0.002     ICURVE,H0(old=.35, new=.0),Z0(old=.003, new=.002)
   I     J      H1          H2          DEPTH     ANGLE       COR         Z0
   6     2     674.73     2640.44      10.67     278.24      27.70      0.0020
   7     2     758.38     2630.06      10.67     277.12      27.70      0.0020
   8     2     854.53     2625.33      11.28     278.08      27.69      0.0020
   9     2     642.24     2619.82      10.06     277.69      27.68      0.0020
  10     2     459.06     2614.57       9.45     277.82      27.68      0.0020
  11     2     486.89     2615.26       8.84     277.48      27.68      0.0020
  12     2     837.38     2608.72       9.45     278.87      27.67      0.0020
  13     2    1252.43     2585.56      10.67     278.40      27.66      0.0020
  14     2    1571.03     2574.01      10.06     278.96      27.65      0.0020
  15     2    1331.69     2563.52       9.45     279.78      27.63      0.0020
  16     2    1548.21     2561.10      10.67     279.69      27.62      0.0020
  17     2    1799.80     2586.42       9.45     280.86      27.61      0.0020
  18     2    1769.07     2616.80      11.58     282.69      27.59      0.0020
  19     2     942.20     2624.44      10.67     285.52      27.58      0.0020
  20     2     952.89     2605.94      10.67     286.76      27.57      0.0020
  21     2    1487.03     2601.34      10.67     288.06      27.56      0.0020
  22     2    1050.26     2610.20      11.28     289.62      27.55      0.0020
  23     2    1008.81     2609.53      11.28     291.73      27.54      0.0020
  24     2    1143.78     2618.76      11.58     292.23      27.53      0.0020
  25     2    1147.46     2605.24      10.67     290.27      27.52      0.0020
  26     2    1152.40     2545.78      10.36     291.46      27.51      0.0020
  27     2    1095.84     2530.36      10.36     295.23      27.50      0.0020
  28     2    1943.97     2572.00      11.28     296.13      27.49      0.0020
  29     2    1365.62     2598.44      10.06     296.87      27.48      0.0020
  30     2    1396.79     2603.80      10.06     296.96      27.47      0.0020
  31     2    1061.74     2602.18      10.06     296.50      27.46      0.0020
   5     3    1097.80     2362.98      10.97     277.45      27.72      0.0020
   6     3     682.60     2350.29      10.97     277.25      27.71      0.0020
   .     .     ......      ......        ...       ...       ....       ......
   .     .     ......      ......        ...       ...       ....       ......
   7    57    1154.52     1438.04       1.47      4.75      27.99      0.0020
   8    57    1111.19     1401.84       1.00      2.90      27.99      0.0020
   9    57     650.12     1375.51       1.00      2.96      27.99      0.0020
  11    57    1136.24      697.36       1.65    359.44      27.98      0.0020
   5    58    1548.72     1784.76       4.16      3.31      28.00      0.0020
   7    58    1187.34     1735.84       1.47      3.96      28.00      0.0020
   5    59    1777.89     2276.72       3.16      1.67      28.02      0.0020
   7    59    1207.46      708.42       1.00      4.71      28.01      0.0020
   0     0       0.00        0.00       0.00      0.00       0.00       0.00
  13          NUMBER OF BARRIERS
  31    41        1.0         0.0
  32    41        1.0         0.0
  33    41        1.0         0.0
  31    22        1.0         0.0
  27    22        1.0         0.0
  29    22        1.0         1.0
  27    23        1.0         1.0
  29    23        1.0         0.0
  29    36        0.0         1.0
  31    37        1.0         0.0
  16    18        0.0         0.0
  12    20        0.0         0.0
  25     7        1.0         0.0
```

APPENDIX D. RMS DIFFERENCE ESTIMATES FOR CONSTITUENT SERIES

The following method produces the rms difference between two tidal series from amplitude and phase differences for each constituent. Let η_1 and η_2 be two tidal signals whose constituents differ in amplitude by δ_n and in phase by ϵ_n

$$\eta_1 = \sum_{n=1}^{N} A_n \exp[i(\omega_n t - \phi_n)] \tag{D.1}$$

$$\eta_2 = \sum_{n=1}^{N} (A_n + \delta_n) \exp[i(\omega_n t - \phi_n - \epsilon_n)] \tag{D.2}$$

where $i = \sqrt{-1}$. Let $E_n = \exp[i(\omega_n t - \phi_n)]$. Then the difference between the two series is

$$\eta_d \equiv \eta_1 - \eta_2 = \sum_{n=1}^{N} [A_n E_n - (A_n + \delta_n)\exp(-i\epsilon_n)E_n] = \sum_{n=1}^{N} [1 - (1 + \frac{\delta_n}{A_n})\exp(-i\epsilon_n)]A_n E_n \tag{D.3}$$

Defining

$$Z_n = 1 - (1 + \frac{\delta_n}{A_n})\exp(-i\epsilon_n) = 1 - (1 + \frac{\delta_n}{A_n})(\cos\epsilon_n - i\sin\epsilon_n) \tag{D.4}$$

gives

$$\eta_d = \sum_{n=1}^{N} Z_n A_n E_n \tag{D.5}$$

The rms amplitude of a sine series in which each term has an amplitude of a_n is

$$r = \left[\frac{1}{2}\sum_{n=1}^{N} a_n^2\right]^{1/2} \tag{D.6}$$

so, by analogy, the rms amplitude of η_d is

$$r = \left[\frac{1}{2}\sum_{n=1}^{N} (Z_n A_n)^2\right]^{1/2} \tag{D.7}$$

Computing the magnitude of the complex number gives the estimate of total rms difference

$$r = \left[\frac{1}{2}\sum_{n=1}^{N} A_n^2 \left[[1 - (1 + \frac{\delta_n}{A_n})\cos\epsilon_n]^2 + [(1 + \frac{\delta_n}{A_n})\sin\epsilon_n]^2\right]\right]^{1/2} \tag{D.8}$$

APPENDIX E. MODEL EVALUATION STATISTICS

The following set of statistics were originally derived by Hess and Bosley (1992).

Time Series Statistics

To quantify the model's performance, first consider a series of de-meaned, observed values a uniform time (e.g., hourly) intervals, y_i (for i = 1,...n), and an equal-length series of de-meaned model output values, $\hat{y}_i$, with the same starting time and number of values. For the entire series, the rms difference is

$$D_{rms} = [\frac{1}{n} \sum_{i=1}^{n} (\hat{y}_i - y_i)^2]^{1/2} \quad \text{(E.1)}$$

This and other potentially useful measures are described by Willmott et al. (1985). However, since observed water level and current ranges can vary widely from station to station, a more meaningful statistic is the ratio of the rms difference to the mean observed range (i.e., a relative difference)

$$D' = \frac{D_{rms}}{R} \quad \text{(E.2)}$$

where the range, R, is defined by Eq. E.3.

Statistics for Tidal Extrema

Since tidal variation is important in most estuaries, the next logical step in the analysis is to find the times and amplitudes of the extrema (highs and lows or floods and ebbs) for both the observed and the modeled time series. This is done by first finding the zero crossing (or slack) times, then finding the time and value of the extrema between each pair of crossing times. Since the data are evenly spaced in time, interpolation is used to determine the times and amplitudes of extrema more accurately. The resulting set of extrema is then analyzed so that in each series, extrema closer than 2 hours are excluded. This process yields two sets of values: the observed extrema Y_j at times T_j for j = 1, 2.. N, and the modeled extrema $\hat{Y}_j$ at times $\hat{T}_j$ for j = 1, 2.. $\hat{N}$. In general, N is unequal to $\hat{N}$.

The mean observed tidal range at a station, R, and the modeled range, $\hat{R}$, can be computed as

$$R = \frac{2}{N} \sum_{j=1}^{N} |Y_j| \quad \text{(E.3)}$$

$$\hat{R} = \frac{2}{\hat{N}} \sum_{j=1}^{\hat{N}} |\hat{Y}_j| \quad \text{(E.4)}$$

A weighted gain, G_w, characterizes the modeled range, $\hat{R}$, relative to the observed range

$$G_w = \frac{\frac{1}{N}\sum_{j=1}^{N} |Y_j| \left|\frac{\hat{Y}_j}{Y_j}\right|}{\frac{1}{N}\sum_{j=1}^{N} |Y_j|} = \frac{\frac{1}{N}\sum_{j=1}^{N} |\hat{Y}_j|}{\frac{1}{N}\sum_{j=1}^{N} |Y_j|} = \frac{\hat{R}}{R} \tag{E.5}$$

for N equaling $\hat{N}$ (i.e., the same number of extrema from each set are used). The observed and modeled extrema are then compared by selecting, for each extremum j, the closest modeled extrema [denoted by subscript j'] that (1) has the same sign and (2) is within 3 hours (one-quarter of a semidiurnal period); observed extrema that have no modeled extrema within 3 hours are ignored. As a result of this comparison, there will be M pairs. Although the weighted gain describes a characteristic of the entire series, it has no information on individual extrema differences; the rms difference for extrema, A_{rms}, has this information

$$A_{rms} = \left[\frac{1}{M} \sum_{j=1}^{M} (\hat{Y}_{j'} - Y_j)^2 \right]^{1/2} \tag{E.6}$$

Finally, a description of phase differences is needed. The mean time lag, L_m, for the extrema is defined as

$$L_m = \frac{1}{M} \sum_{j=1}^{M} (\hat{T}_{j'} - T_j) \tag{E.7}$$

The mean lag is valuable because modeled wave speed errors, if they exist, will be manifest as a lag (or lead) at all stations. However, the rms lag, L_{rms}, is also useful:

$$L_{rms} = \left[\frac{1}{M} \sum_{j=1}^{M} (\hat{T}_{j'} - T_j)^2 \right]^{1/2} \tag{E.8}$$

When summing the results from several stations, values must be weighted by the number of data pairs (M_s) for each station. Letting the subscript s denote the station and F the mean or rms statistic, the "global" statistic, $\langle F \rangle$, for all S stations is

$$\langle F \rangle = \frac{\sum_{s=1}^{S} M_s F_s}{\sum_{s=1}^{S} M_s} \tag{E.9}$$

Skill Assessment Parameters

It is one of the primary goals to have some objective measure of the model's skill at reproducing the observed variability. To obtain such a measure for individual stations, first define the

relative rms differences for peak and lag values, by analogy to Eq. E.2, as

$$A' = \frac{A_{rms}}{R} \qquad L' = \frac{L_{rms}}{6.21\,hours} \tag{E.10}$$

where 6.21 hours (one-half an M_2 tidal period) approximates the mean time between extrema. Finally, three skill parameters are constructed from the global quantities as follows:

$$S_D = 1 - \langle D' \rangle \qquad \text{(hourly difference skill)} \tag{E.11}$$

$$S_A = 1 - \langle A' \rangle \qquad \text{(extrema amplitude skill)} \tag{E.12}$$

$$S_L = 1 - \langle L' \rangle \qquad \text{(extrema time skill)} \tag{E.13}$$

These skill parameters, along with weighted gain (Eq. E.5) and mean lag (Eq. E.7), are the primary parameters used to quantify model accuracy.

Previous Results

The model was run for the period August 30 to September 9, 1990, for validation purposes (Hess and Bosley, 1992). The results for currents are shown in Table E.1 and for water level in Table E.2. Modeled currents were for mid-depth and interpolated to the cell center. Comparisons are based on 10-minute values at mid-depth. In general, model gain for currents is significantly less than unity (G_w = 0.805), and the mean lag is significantly worse (L_m = -24 minutes) than for water levels. The rms time difference (L_{rms} = 46 minutes) is larger than for water levels. Model skill parameters vary from 87% to 94%.

Table E.1. Results of the Hess and Bosley (1992) validation run for currents.

Sta.	n	R (m/s)	D_{rms} (m/s)	D'	N	G_w	A_{rms} (m/s)	L_m (hr)	L_{rms} (hr)
C-2	1152	1.624	.172	.106	31	.789	.233	-.532	.714
C-3	1062	1.400	.162	.116	31	.771	.213	-.436	.662
C-4	1152	1.124	.130	.116	31	.688	.187	-.457	.713
C-5	1152	1.241	.067	.054	31	.958	.058	-.179	.496
C-20	1152	1.100	.150	.136	29	.620	.224	.151	.643
C-21	1152	.948	.112	.119	32	.909	.104	-.564	1.075
C-23	1152	.954	.088	.092	32	1.101	.071	-.537	.759
Global Values			.126	.106		.837	.154	-.371	.726
Skill Parameters			S_D=89.4%				S_A=87.3%		S_L=88.3%

Table E.2. Results of the Hess and Bosley (1992) validation run for water levels.

	Station	n	R (m)	D_{rms} (m)	D′	N	G_w	A_{rms} (m)	L_m (hr)	L_{rms} (hr)
1	Ec01	193	.530	.014	.026	30	1.043	.012	-.034	.125
2	e217	193	.509	.042	.083	27	1.119	.042	-.323	.672
3	e243	193	.573	.043	.074	25	1.027	.049	-.159	.748
4	e273	193	.541	.030	.056	27	1.070	.026	-.197	.402
5	e347	193	.554	.027	.048	25	1.077	.032	.077	.489
6	e364	193	.506	.024	.047	23	1.085	.028	.020	.212
7	e384	193	.503	.030	.060	25	1.097	.033	-.148	.221
8	e428	193	.575	.048	.083	25	.997	.024	.374	.483
9	e520	193	.520	.040	.076	28	1.099	.043	-.086	.505
10	e537	193	.584	.044	.075	29	1.052	.033	-.293	.381
11	e657	193	.643	.053	.083	28	1.062	.051	-.218	.564
12	e689	193	.688	.038	.055	29	.930	.038	-.109	.293
Global Values				.036	.064		1.054	.034	-.097	.423
Skill Parameters				S_D=93.6%				S_A=93.9%		S_L=93.1%